Chapter 1
The EEM in Ultrathin Films (UFs) of Nonparabolic Semiconductors

1.1 Introduction

The concept of the effective mass of the carriers in semiconductors is one of the basic pillars in the realm of solid state and related sciences [1]. It must be noted that among the various definitions of the effective electron mass (e.g effective acceleration mass, density-of-state effective mass, concentration effective mass, conductivity effective mass, Faraday rotation effective mass, etc) [2], it is the effective momentum mass that should be regarded as the basic quantity [3]. This is due to the fact that it is this mass which appears in the description of transport phenomena and all other properties of the conduction electrons in a semiconductor with arbitrary band nonparabolicity [3]. It can be shown that it is the effective momentum mass which enters in various transport coefficients and plays the most dominant role in explaining the experimental results of different scattering mechanisms through Boltzmann's transport equation [4, 5]. The carrier degeneracy in semiconductors influences the effective mass when it is energy dependent. Under degenerate conditions, only the electrons at the Fermi surface of n-type semiconductors participate in the conduction process and hence, the effective momentum mass of the electrons (EEM) corresponding to the Fermi level would be of interest in electron transport under such conditions. The Fermi energy is again determined by the carrier energy spectrum and the electron statistics and therefore, these two features would determine the dependence of the EEM in degenerate n-type semiconductors under the degree of carrier degeneracy. In recent years, various energy wave vector dispersion relations have been proposed [6–38] which have created the interest in studying the EEM in such materials under external conditions. The nature of these variations has been investigated in the literature [39–85]. Some of the significant features, which have emerged from these studies, are:

(a) The EEM increases monotonically with electron concentration.
(b) The EEM increases with doping in heavily doped materials in the presence of band tails.

S. Bhattacharya and K. P. Ghatak, *Effective Electron Mass in Low-Dimensional Semiconductors*, Springer Series in Materials Science 167,
DOI: 10.1007/978-3-642-31248-9_1, © Springer-Verlag Berlin Heidelberg 2013

(c) The nature of variations is significantly influenced by the energy band constants of various materials having different band structures.
(d) The EEM oscillates with inverse quantizing magnetic field due to SdH effect. The EEM in Bismuth under magnetic quantization depends both on the Fermi energy and on the magnetic quantum number due to the presence of band nonparabolicity only.
(e) The EEM increases with the magnitude of the quantizing electric field in n-channel inversion layers of III-V semiconductors and depend on the subband index for both low and high electric field limits.
(f) The EEM in ultrathin films of nonlinear optical materials depends on the Fermi energy and size quantum numbers due to the specific dispersion relations.
(g) The EEM has significantly different values in superlattices and also in the presence of quantum confined superlattices of small gap semiconductors with graded interfaces.

In recent years, with the advent of fine lithographical methods [86, 87] molecular beam epitaxy [88], organometallic vapor-phase epitaxy [89], and other experimental techniques, the restriction of the motion of the carriers of bulk materials in one (ultrathin films, NIPI structures, inversion, and accumulation layers), two (nanowires) and three (quantum dots, magnetosize quantized systems, magneto accumulation layers, magneto inversion layers, quantum dot superlattices, magneto ultrathin film superlattices, and magneto NIPI structures) dimensions have in the last few years, attracted much attention not only for their potential in uncovering new phenomena in nanoscience but also for their interesting quantum device applications [90–93]. In ultrathin films (UFs), the restriction of the motion of the carriers in the direction normal to the film (say, the z direction) may be viewed as carrier confinement in an infinitely deep 1D rectangular potential well, leading to quantization [known as quantum size effect (QSE)] of the wave vector of the carrier along the direction of the potential well, allowing 2D carrier transport parallel to the surface of the film representing new physical features not exhibited in bulk semiconductors [94–98]. The low-dimensional heterostructures based on various materials are widely investigated because of the enhancement of carrier mobility [99].These properties make such structures suitable for applications in ultrathin film lasers [100], heterojunction FETs [101, 102], high-speed digital networks [103–106], high-frequency microwave circuits [107], optical modulators [108], optical switching systems [109], and other devices. The constant energy 3D wave-vector space of bulk semiconductors becomes 2D wave-vector surface in UFs due to dimensional quantization. Thus, the concept of reduction of symmetry of the wave-vector space and its consequence can unlock the physics of low-dimensional structures.

In this chapter, we study the EEM in UFs of nonparabolic semiconductors having different band structures. At first we shall investigate the EEM in UFs of nonlinear optical compounds which are being used in nonlinear optics and light emitting diodes [110]. The quasi-cubic model can be used to investigate the symmetric properties of both the bands at the zone center of wave vector space of the same compound. Including the anisotropic crystal potential in the Hamiltonian, and special features

of the nonlinear optical compounds, Kildal [111] formulated the electron dispersion law under the assumptions of isotropic momentum matrix element and the isotropic spin-orbit splitting constant, respectively, although the anisotropies in the two aforementioned band constants are the significant physical features of the said materials [112–114]. In Sect. 1.2.1, the EEM in UFs of nonlinear optical semiconductors has been investigated by considering the combined influence of the anisotropies of the said energy band constants together with the inclusion of the crystal field splitting respectively within the framework of *k.p* formalism. The III-V compounds find applications in infrared detectors [115], quantum dot light emitting diodes [116], quantum cascade lasers [117], ultrathin film wires [118], optoelectronic sensors [119], high electron mobility transistors [120], etc. The electron energy spectrum of III-V semiconductors can be described by the three- and two-band models of Kane [121, 122], together with the models of Stillman et al. [123], Newson and Kurobe [124] and, Palik et al. [125] respectively. In this context it may be noted that the ternary and quaternary compounds enjoy the singular position in the entire spectrum of optoelectronic materials. The ternary alloy $Hg_{1-x}Cd_xTe$ is a classic narrow gap compound. The band gap of this ternary alloy can be varied to cover the spectral range from 0.8 to over 30 μm [126] by adjusting the alloy composition. $Hg_{1-x}Cd_xTe$ finds extensive applications in infrared detector materials and photovoltaic detector arrays in the 8–12 μm wave bands [127]. The above uses have generated the $Hg_{1-x}Cd_xTe$ technology for the experimental realization of high mobility single crystal with specially prepared surfaces. The same compound has emerged to be the optimum choice for illuminating the narrow subband physics because the relevant material constants can easily be experimentally measured [128]. Besides, the quaternary alloy $In_{1-x}Ga_xAs_yP_{1-y}$ lattice matched to InP, also finds wide use in the fabrication of avalanche photodetectors [129], hetero-junction lasers [130], light emitting diodes [131] and avalanche photodiodes[132], field effect transistors, detectors, switches, modulators, solar cells, filters, and new types of integrated optical devices are made from the quaternary systems [133]. It may be noted that all types of band models as discussed for III-V semiconductors are also applicable for ternary and quaternary compounds. In Sect. 1.2.2, the EEM in UFs of III-V, ternary and quaternary semiconductors has been studied in accordance with the said band models and the simplified results for wide gap materials having parabolic energy bands under certain limiting conditions have further been demonstrated as a special case and thus confirming the compatibility test.

The II-VI semiconductors are being used in nanoribbons, blue green diode lasers, photosensitive thin films, infrared detectors, ultra high-speed bipolar transistors, fiber optic communications, microwave devices, solar cells, semiconductor gamma-ray detector arrays, semiconductor detector gamma camera and allow for a greater density of data storage on optically addressed compact discs [134–141]. The carrier energy spectra in II-VI compounds are defined by the Hopfield model [142] where the splitting of the two-spin states by the spin-orbit coupling and the crystalline field has been taken into account. The Sect. 1.2.3 contains the investigation of the EEM in UFs of II-VI compounds.

In recent years, Bismuth (Bi) nanolines have been fabricated and Bi also finds use in array of antennas which leads to the interaction of electromagnetic waves

with such Bi-nanowires [143, 144]. Several dispersion relations of the carriers have been proposed for Bi. Shoenberg [145, 146] experimentally verified that the de Haas-Van Alphen and cyclotron resonance experiments supported the ellipsoidal parabolic model of Bi, although, the magnetic field dependence of many physical properties of Bi supports the two-band model [147].The experimental investigations on the magneto-optical and the ultrasonic quantum oscillations support the Lax ellipsoidal nonparabolic model [147]. Kao [148], Dinger and Lawson [149] and Koch and Jensen [150] demonstrated that the Cohen model [151] is in conformity with the experimental results in a better way. Besides, the hybrid model of bismuth, as developed by Takoka et al., also finds use in the literature [152]. McClure and Choi [153] derived a new model of Bi and they showed that it can explain the data for a large number of magneto-oscillatory and resonance experiments.

In Sect. 1.2.4, the EEM in UFs of Bi has been formulated in accordance with the aforementioned energy band models for the purpose of relative assessment. Besides, under certain limiting conditions all the results for all the models of 2D systems are reduced to the well-known result of the EEM in UFs of wide gap materials. This above statement exhibits the compatibility test of our theoretical analysis.

Lead chalcogenides (PbTe, PbSe, and PbS) are IV-VI nonparabolic semiconductors whose studies over several decades have been motivated by their importance in infrared IR detectors, lasers, light-emitting devices, photovoltaics, and high temperature thermoelectrics [154–158]. PbTe, in particular, is the end compound of several ternary and quaternary high performance high temperature thermoelectric materials [159–163]. It has been used not only as bulk but also as films [164–167], ultrathin films [168] superlattices [169, 170] nanowires [171] and colloidal and embedded nanocrystals [172–175], and PbTe films doped with various impurities have also been investigated [176–183] These studies revealed some of the interesting features that had been seen in bulk PbTe, such as Fermi level pinning and, in the case of superconductivity [184]. In Sect. 1.2.5, the EEM in UFs of IV-VI semiconductors has been studied taking PbTe, PbSe, and PbS as examples.

The stressed semiconductors are being investigated for strained silicon transistors, quantum cascade lasers, semiconductor strain gages, thermal detectors, and strained-layer structures [185–188]. The EEM in UFs of stressed compounds (taking stressed n-InSb as an example) has been investigated in Sect. 1.2.6 The vacuum deposited Tellurium (Te) has been used as the semiconductor layer in thin-body transistors (TFT) [189] which is being used in CO_2 laser detectors [190], electronic imaging, strain sensitive devices [191, 192], and multichannel Bragg cell [193]. Section 1.2.7 contains the investigation of EEM in UFs of Tellurium.

The n-Gallium Phosphide (n-GaP) is being used in quantum dot light emitting diode [194], high efficiency yellow solid state lamps, light sources, high peak current pulse for high gain tubes. The green and yellow light emitting diodes made of nitrogen-doped n-GaP possess a longer device life at high drive currents [195–197]. In Sect. 1.2.8, the EEM in UFs of n-GaP has been studied. The Platinum Antimonide ($PtSb_2$) finds application in device miniaturization, colloidal nanoparticle synthesis, sensors and detector materials and thermo-photovoltaic devices [198–200]. Section 1.2.9 explores the EEM in UFs of $PtSb_2$.Bismuth telluride

(Bi_2Te_3) was first identified as a material for thermoelectric refrigeration in 1954 [201] and its physical properties were later improved by the addition of bismuth selenide and antimony telluride to form solid solutions [202–206]. The alloys of Bi_2Te_3 are useful compounds for the thermoelectric industry and have been investigated in the literature [202–206]. In Sect. 1.2.10, the EEM in UFs of Bi_2Te_3 has been considered.

The usefulness of elemental semiconductor Germanium is already well known since the inception of transistor technology and, it is also being used in memory circuits, single photon detectors, single photon avalanche diode, ultrafast optical switch, THz lasers and THz spectrometers [207–210]. In Sect. 1.2.11, the EEM has been studied in UFs of Ge. Gallium Antimonide (GaSb) finds applications in the fiber optic transmission window, heterojunctions, and ultrathin films. A complementary heterojunction field effect transistor in which the channels for the p-FET device and the n-FET device forming the complementary FET are formed from GaSb. The band gap energy of GaSb makes it suitable for low power operation [211–216]. In Sect. 1.2.12, the EEM in UFs of GaSb has been studied. Section 1.3 contains the result and discussions pertaining to this chapter. The last Sect. 1.4 contains open research problems.

1.2 Theoretical Background

1.2.1 The EEM in UFs of Nonlinear Optical Semiconductors

The form of *k.p* matrix for nonlinear optical compounds can be expressed extending Bodnar [112] as

$$H = \begin{bmatrix} H_1 & H_2 \\ H_2^+ & H_1 \end{bmatrix} \tag{1.1}$$

where,

$$H_1 \equiv \begin{bmatrix} E_{g0} & 0 & P_{\|}k_z & 0 \\ 0 & \left(-2\Delta_{\|}/3\right) & \left(\sqrt{2}\Delta_{\perp}/3\right) & 0 \\ P_{\|}k_z & \left(\sqrt{2}\Delta_{\perp}/3\right) & -\left(\delta + \frac{1}{3}\Delta_{\|}\right) & 0 \\ 0 & 0 & 0 & 0 \end{bmatrix}$$

$$H_2 \equiv \begin{bmatrix} 0 & -f_{,+} & 0 & f_{,-} \\ f_{,+} & 0 & 0 & 0 \\ 0 & 0 & 0 & 0 \\ f_{,+} & 0 & 0 & 0 \end{bmatrix}$$

in which E_{g_0} is the band gap in the absence of any field, $P_{\|}$ and $P_{\perp}$ are the momentum matrix elements parallel and perpendicular to the direction of crystal axis respectively,

δ is the crystal-field splitting constant, $\Delta_{\parallel}$ and $\Delta_{\perp}$ are the spin-orbit splitting constants parallel and perpendicular to the C-axis respectively, $f_{,\pm} \equiv \left(P_{\perp}/\sqrt{2}\right)\left(k_x \pm ik_y\right)$ and $i = \sqrt{-1}$. Thus, neglecting the contribution of the higher bands and the free electron term, the diagonalization of the above matrix leads to the dispersion relation of the conduction electrons in bulk specimens of nonlinear optical semiconductors as

$$\gamma(E) = f_1(E)k_s^2 + f_2(E)k_z^2 \tag{1.2}$$

where,

$$\gamma(E) \equiv E(E+E_{g0})\left[(E+E_{g0})(E+E_{g0}+\Delta_{\parallel}) + \delta\left(E+E_{g_o}+\frac{2}{3}\Delta_{\parallel}\right) + \frac{2}{9}(\Delta_{\parallel}^2 - \Delta_{\perp}^2)\right],$$

E is the total energy of the electron as measured from the edge of the conduction band in the vertically upward direction in the absence of any quantization, $k_s^2 = k_x^2 + k_y^2$,

$$f_1(E) \equiv \frac{\hbar^2 E_{g0}\left(E_{g0}+\Delta_{\perp}\right)}{\left[2m_{\perp}^*\left(E_{g0}+\frac{2}{3}\Delta_{\parallel}\right)\right]} \times \left[\delta\left(E+E_{g0}+\frac{1}{3}\Delta_{\parallel}\right) + (E+E_{g0})\left(E+E_{g0}+\frac{2}{3}\Delta_{\parallel}\right) + \frac{1}{9}(\Delta_{\parallel}^2 - \Delta_{\parallel}^2)\right]$$

$$f_2(E) \equiv \frac{\hbar^2 E_{g0}\left(E_{g0}+\Delta_{\parallel}\right)}{\left[2m_{\parallel}^*\left(E_{g0}+\frac{2}{3}\Delta_{\parallel}\right)\right]}\left[(E+E_{g0})\left(E+E_{g0}+\frac{2}{3}\Delta_{\parallel}\right)\right], \quad \hbar = h/2\pi,$$

h is *Planck's constant* and $m_{\parallel}^*$ and $m_{\perp}^*$ are the *longitudinal and transverse effective electron masses* at the edge of the *conduction band respectively*.

For dimensional quantization along z-direction, the dispersion relation of the 2D electrons in this case can be written following (1.2) as

$$\psi_1(E) = \psi_2(E)k_s^2 + \psi_3(E)(n_z\pi/d_z)^2 \tag{1.3}$$

where $\psi_1(E) = \gamma(E)$, $\psi_2(E) = f_1(E)$, $\psi_3(E) = f_2(E)$, $n_z(= 1, 2, 3, \ldots)$ and d_z are the size quantum number and the nano-thickness along the z-direction respectively.

The EEM is defined as the ratio of the electron momentum to the group velocity.

The EEM at the Fermi level in the xy-plane can be written as

$$m^*(E_F, n_z) = \hbar^2 k_s \left.\frac{\partial k_s}{\partial E}\right|_{E=E_{Fs}} \tag{1.4}$$

where E_{Fs} is the Fermi energy in the presence of size quantization as measured from the edge of the conduction band in the vertically upward direction in the absence of any quantization. From (1.3) and (1.4), the EEM in this case can be written as

$$m^*(E_{Fs}, n_z) = \left(\frac{\hbar^2}{2}\right)[\psi_2(E_{Fs})]^{-2}\left[\psi_2(E_{Fs})\left\{\{\psi_1(E_{Fs})\}' - \{\psi_3(E_{Fs})\}'\left(\frac{n_z\pi}{d_z}\right)^2\right\} - \left\{\psi_1(E_{Fs}) - \psi_3(E_{Fs})\left(\frac{n_z\pi}{d_z}\right)^2\right\}\{\psi_2(E_{Fs})\}'\right] \tag{1.5}$$

where, the primes denote the differentiation of the differentiable functions with respect to Fermi energy. Thus, we observe that the EEM is the function of size quantum number and the Fermi energy due to the combined influence of the crystal-field splitting constant and the anisotropic spin-orbit splitting constants respectively. To study the dependence of the EEM as a function of electron concentration per unit area we have to formulate the corresponding density-of-states function (DOS).

The general expression of the total 2D DOS ($N_{2DT}(E)$)in this case is given by

$$N_{2DT}(E) = \frac{2g_v}{(2\pi)^2}\sum_{n_z=1}^{n_{zmax}}\frac{\partial A(E, n_z)}{\partial E}H\left(E - E_{n_z}\right) \tag{1.6}$$

where, g_v is the valley degeneracy, $A(E, n_z)$ is the area of the constant energy 2D wave vector space for UFs, $H(E - E_{n_z})$is the Heaviside step function and (E_{n_z}) is the corresponding subband energy. Using (1.3) and (1.6), the expression of the $N_{2DT}(E)$ for UFs of nonlinear optical semiconductors can be written as

$$N_{2DT}(E) = \left(\frac{g_v}{2\pi}\right)\sum_{n_z=1}^{n_{zmax}}[\psi_2(E)]^{-2}\left[\psi_2(E)\left\{\{\psi_1(E)\}' - \{\psi_3(E)\}'\left(\frac{n_z\pi}{d_z}\right)^2\right\} - \left\{\psi_1(E) - \psi_3(E)\left(\frac{n_z\pi}{d_z}\right)^2\right\}\{\psi_2(E)\}'\right]H(E - E_{n_{z_1}}) \tag{1.7}$$

where, the subband energies $(E_{n_{z_1}})$ in this case is given by

$$\psi_1(E_{n_{z_1}}) = \psi_2(E_{n_{z_1}})(n_z\pi/d_z)^2 \tag{1.8}$$

Combining (1.7) with the Fermi-Dirac occupation probability factor, integrating between $E_{n_{z_1}}$ to infinity and applying the generalized Somerfeld's lemma, the 2D carrier statistics in this case assumes the form

$$n_{2D} = \frac{g_v}{2\pi}\sum_{n_x=1}^{n_{xmax}}\left[T_{51}\left(E_{Fs}, n_z\right) + T_{52}\left(E_{Fs}, n_z\right)\right] \tag{1.9}$$

where,

$$T_{51}\left(E_{Fs}, n_z\right) \equiv \left[\frac{\psi_1(E_{Fs}) - \psi_3(E_{Fs})(n_z\pi/d_z)^2}{\psi_2(E_{Fs})}\right],$$

$$T_{52}\left(E_{Fs}, n_z\right) \equiv \sum_{r=1}^{s} L(r)[T_{51}\left(E_{Fs}, n_z\right)],$$

$L(r) = 2(k_BT)^{2r}(1 - 2^{1-2r})\xi(2r)\frac{\partial^{2r}}{\partial E_f^{2r}}$, k_B is the Boltzmann constant, T is the temperature, r is the set of real positive integers whose upper limit is s, $\xi(2r)$ is the Zeta function of order 2r [217].

1.2.2 The EEM in UFs of III–V Semiconductors

The dispersion relation of the conduction electrons of III-V compounds are described by the models of Kane (both three and two bands) [121, 122], Stillman et al. [123], Newson and Kurobe [124] and Palik et al. [125] respectively. For the purpose of complete and coherent presentation, the EEM in UFs of III-V semiconductors have also been investigated in accordance with the aforementioned different dispersion relations for the purpose of relative comparison as follows:

(a) The three-band model of Kane
Under the conditions, $\delta = 0, \Delta_{\parallel} = \Delta_{\perp} = \Delta$ (isotropic spin orbit splitting constant) and $m_{\perp}^* = m_{\perp}^* = m_c$ (isotropic effective electron mass at the edge of the conduction band), (1.2) gets simplified into the form

$$\frac{\hbar^2k^2}{2m_c} = I_{11}(E), I_{11}(E) \equiv \frac{E(E + E_{g0})(E + E_{g0} + \Delta)(E_{g0} + \frac{2}{3}\Delta)}{E_{g0}(E_{g0} + \Delta)(E + E_{g0} + \frac{2}{3}\Delta)} \tag{1.10}$$

which is known as the three-band model of Kane [121, 122] and is often used to study the electronic properties of III-V materials.
Thus, under the conditions $\delta = 0, \Delta_{\parallel} = \Delta_{\perp} = \Delta$ and $m_{\parallel}^* = m_{\perp}^* = m_c$, (1.3) assumes the form

$$\frac{\hbar^2k_s^2}{2m_c} + \frac{\hbar^2}{2m_c}(n_z\pi/d_z)^2 = I_{11}(E) \tag{1.11}$$

Using (1.11) and (1.4), the EEM in x–y plane for this case can be written as

$$m^*(E_{Fs}) = m_c\{I_{11}(E_{Fs})\}' \tag{1.12}$$

It is worth noting that the EEM in this case is a function of Fermi energy alone and is independent of size quantum number.
The total 2D DOS function can be written as

$$N_{2DT}(E) = \left(\frac{m_c g_v}{\pi \hbar^2}\right) \sum_{n_z=1}^{n_{zmax}} \left\{ [I_{11}(E)]' H\left(E - E_{n_{z_2}}\right) \right\} \tag{1.13}$$

where, the subband energies $E_{n_{z_2}}$ can be expressed as

$$I_{11}(E_{n_{z_2}}) = \frac{\hbar^2}{2m_c}(n_z \pi / d_z)^2 \tag{1.14}$$

The 2D carrier concentration assumes the form

$$n_{2D} = \frac{m_c g_v}{\pi \hbar^2} \sum_{n_z=1}^{n_{zmax}} [T_{53}(E_{Fs}, n_z) + T_{54}(E_{Fs}, n_z)] \tag{1.15}$$

where

$$T_{53}(E_{Fs}, n_z) \equiv \left[I_{11}(E_{Fs}) - \frac{\hbar^2}{2m_c}\left(\frac{n_z \pi}{d_z}\right)^2 \right] \text{ and}$$

$$T_{54}(E_{Fs}, n_z) \equiv \sum_{r=1}^{s} L(r) T_{53}(E_{Fs}, n_z).$$

Under the inequalities $\Delta \gg E_{g0}$ or $\Delta \ll E_{g0}$ (1.10) can be expressed as

$$E(1 + \alpha E) = \frac{\hbar^2 k^2}{2m_c} \tag{1.16}$$

where, $\alpha \equiv 1/E_{g0}$ and is known as band nonparabolicity.
It may be noted that (1.16) is the well-known two-band model of Kane and is used in the literature to study the physical properties of those III-V and optoelectronic materials whose energy band structures obey the aforementioned inequalities.
Under the said inequalities (1.11) assumes the form

$$E(1 + \alpha E) = \frac{\hbar^2 k_s^2}{2m_c} + \frac{\hbar^2}{2m_c}\left(\frac{n_z \pi}{d_z}\right)^2 \tag{1.17}$$

The EEM in this case can be written as

$$m^*(E_{Fs}) = m_c(1 + 2\alpha E_{Fs}) \tag{1.18}$$

Thus, we observe that the EEM in the present case is a function of Fermi energy only due to the presence of band nonparabolicity.
The total 2D DOS function assumes the form

$$N_{2DT}(E) = \frac{m_c g_v}{\pi \hbar^2} \sum_{n_z=1}^{n_{zmax}} (1 + 2\alpha E) H\left(E - E_{n_{z_3}}\right) \tag{1.19}$$

where, the subband energy ($E_{n_{z_3}}$) can be expressed as

$$\frac{\hbar^2}{2m_c}(n_z \pi / d_z)^2 = E_{n_{z_3}}\left(1 + \alpha E_{n_{z_3}}\right) \tag{1.20}$$

The 2D electron statistics can be written as

$$n_{2D} = \frac{m_c g_v}{\pi \hbar^2} \sum_{n_z=1}^{n_{zmax}} \int_{E_{n_{z_3}}}^{\infty} \frac{(1 + 2\alpha E) dE}{1 + exp\left(\frac{E - E_{Fs}}{k_B T}\right)}$$

$$= \frac{m_c k_B T g_v}{\pi \hbar^2} \sum_{n_z=1}^{n_{zmax}} \left[(1 + 2\alpha E_{n_{z_3}}) F_0(\eta_{n_1}) + 2\alpha k_B T F_1(\eta_{n_1})\right] \tag{1.21}$$

where, $\eta_{n_1} \equiv (E_{Fs} - E_{n_{z_3}})/k_B T$ and $F_j(\eta)$ is the one-parameter Fermi-Dirac integral of order j which can be written [218, 219] as

$$F_j(\eta) = \left(\frac{1}{\Gamma(j+1)}\right) \int_0^{\infty} \frac{x^j dx}{1 + \exp(x - \eta)}, \quad j > -1 \tag{1.22}$$

or for all j, analytically continued as a complex contour integral around the negative *x-axis*

$$F_j(\eta) = \left(\frac{\Gamma(-j)}{2\pi\sqrt{-1}}\right) \int_{-\infty}^{+0} \frac{x^j dx}{1 + \exp(-x - \eta)} \tag{1.23}$$

where η is the dimensionless x independent variable.
Under the condition $\alpha \to 0$, the expressions of total 2D DOS, for UFs whose bulk electrons are defined by the isotropic parabolic energy bands can, be written as

$$N_{2DT}(E) = \frac{m_c g_v}{\pi \hbar^2} \sum_{n_z=1}^{n_{zmax}} H\left(E - E_{n_{z_p}}\right) \tag{1.24}$$

The subband energy ($E_{n_{z_p}}$), the EEM, and the n_{2D} can respectively be expressed as

$$E_{n_{z_p}} = \frac{\hbar^2}{2m_c}\left(\frac{n_z \pi}{d_z}\right)^2 \tag{1.25}$$

$$m^*(E_{Fs}) = m_c \tag{1.26}$$

and

$$n_{2D} = \frac{m_c k_b T g_v}{\pi \hbar^2} \sum_{n_z=1}^{n_{zmax}} F_0(\eta_{n_2}) \tag{1.27}$$

where, $\eta_{n_2} \equiv \frac{1}{k_B T}\left[E_{Fs} - \frac{\hbar^2}{2m_c}\left(\frac{n_z \pi}{d_z}\right)^2\right]$

It may be noted that the results of this section are already well known in the literature [220].

(b) The model of Stillman et al.

In accordance with the model of Stillman et al. [123], the electron dispersion law of III-V materials assumes the form

$$E = \bar{t}_{11}k^2 - \bar{t}_{12}k^4 \tag{1.28}$$

where,

$$\bar{t}_{11} \equiv \frac{\hbar^2}{2m_c}; \bar{t}_{12} \equiv \left(1 - \frac{m_c}{m_0}\right)^2 \left(\frac{\hbar^2}{2m_c}\right)^2 \times \left[\left(3E_{g0} + 4\Delta + \frac{2\Delta^2}{E_{g0}}\right).\{(E_{g0} + \Delta)(2\Delta + 3E_{g0})\}^{-1}\right]$$

and m_0 is the free electron mass.

Equation (1.28) can be expressed as

$$\frac{\hbar^2 k^2}{2m_c} = I_{12}(E) \tag{1.29}$$

where, $I_{12}(E) \equiv a_{11}\left[1 - (1 - a_{12}E)^{1/2}\right]$, $a_{11} \equiv \left(\frac{\hbar^2 \bar{t}_{11}}{4m_c \bar{t}_{12}}\right)$ and $a_{12} \equiv \frac{4\bar{t}_{12}}{\bar{t}_{11}^2}$.

The 2D electron dispersion relation in this case assumes the form

$$\frac{\hbar^2 k_s^2}{2m_c} + \frac{\hbar^2}{2m_c}(n_z \pi / d_z)^2 = I_{12}(E) \tag{1.30}$$

Using (1.30) and (1.4), the EEM in x–y plane for this case can be written as

$$m^*(E_{Fs}) = m_c\{I_{12}(E_{Fs})\}' \tag{1.31}$$

It appears that the EEM in this case is a function of Fermi energy alone and is independent of size quantum number.

The total 2D DOS function can be written as

$$N_{2DT}(E) = \left(\frac{m_c g_v}{\pi \hbar^2}\right) \sum_{n_z=1}^{n_{zmax}} \left\{ [I_{12}(E)]' H(E - E_{n_{z_3}}) \right\} \tag{1.32}$$

where, the subband energies $E_{n_{z_3}}$ can be expressed as

$$I_{12}(E_{n_{z_3}}) = \frac{\hbar}{2m_c}(n_z \pi / d_z)^2 \tag{1.33}$$

The 2D carrier concentration assumes the form

$$n_{2D} = \frac{m_c g_v}{\pi \hbar^2} \sum_{n_z=1}^{n_{zmax}} \left[T_{55}(E_{Fs}, n_z) + T_{56}(E_{Fs}, n_z) \right] \tag{1.34}$$

where

$$T_{55}(E_{Fs}, n_z) \equiv \left[I_{12}(E_{Fs}) - \frac{\hbar^2}{2m_c} \left(\frac{n_z \pi}{d_z}\right)^2 \right] \text{ and}$$

$$T_{56}(E_{Fs}, n_z) \equiv \sum_{r=1}^{s} L(r) T_{55}(E_{Fs}, n_z)$$

(c) Model of Palik et al.
The energy spectrum of the conduction electrons in III-V semiconductors up to the fourth order in effective mass theory, taking into account the interactions of heavy hole, light hole and the split-off holes can be expressed in accordance with the model of Palik et al. [125] as

$$E = \frac{\hbar^2 k^2}{2m_c} - \bar{B}_{11} k^4 \tag{1.35}$$

where

$$\bar{B}_{11} = \left[\frac{\hbar^4}{4E_{g0}(m_c)^2} \right] \left[\frac{1 + \frac{x_{11}^2}{2}}{1 + \frac{x_{11}}{2}} \right] (1 - y_{11})^2,$$

$$x_{11} = \left[1 + \left(\frac{\Delta}{E_{g0}} \right) \right]^{-1} \text{ and } y_{11} = \frac{m_c}{m_o}$$

The (1.35) gets simplified as

$$\frac{\hbar^2 k^2}{2m_c} = I_{13}(E) \tag{1.36}$$

where

$$I_{13}(E) = \bar{b}_{12}\left[\bar{a}_{12} - ((\bar{a}_{12})^2 - 4E\bar{B}_{11})^{1/2}\right],$$
$$\bar{a}_{12} = \left(\frac{\hbar^2}{2m_c}\right) \text{ and } \bar{b}_{12} = \left[\frac{\bar{a}_{12}}{2\bar{B}_{11}}\right]$$

The 2D electron dispersion relation in this case assumes the form

$$\frac{\hbar^2 k_s^2}{2m_c} + \frac{\hbar^2}{2m_c}(n_z\pi/d_z)^2 = I_{13}(E) \tag{1.37}$$

Using (1.37) and (1.4), the EEM in *x*–*y* plane for this case can be written as

$$m^*(E_{Fs}) = m_c\{I_{13}(E_{Fs})\}' \tag{1.38}$$

It appears that the EEM in this case is a function of Fermi energy alone and is independent of size quantum number.
The total 2D DOS function can be written as

$$N_{2DT}(E) = \left(\frac{m_c g_v}{\pi\hbar^2}\right)\sum_{n_z=1}^{n_{z_{max}}}\left\{[I_{13}(E)]' H(E - E_{n_{z_4}})\right\} \tag{1.39}$$

where, the subband energies $E_{n_{z_4}}$ can be expressed as

$$I_{13}(E_{n_{z_4}}) = \frac{\hbar}{2m_c}(n_z\pi/d_z)^2 \tag{1.40}$$

The 2D carrier concentration assumes the form

$$n_{2D} = \frac{m_c g_v}{\pi\hbar^2}\sum_{n_z=1}^{n_{z_{max}}}\left[T_{57}(E_{Fs}, n_z) + T_{58}(E_{Fs}, n_z)\right] \tag{1.41}$$

where

$$T_{57}(E_{Fs}, n_z) \equiv \left[I_{13}(E_{Fs}) - \frac{\hbar^2}{2m_c}\left(\frac{n_z\pi}{d_z}\right)^2\right] \text{ and}$$
$$T_{58}(E_{Fs}, n_z) \equiv \sum_{r=1}^{s} L(r)T_{57}(E_{Fs}, n_z)$$

1.2.3 The EEM in UFs of II–VI Semiconductors

The carrier energy spectra in bulk specimens of II-VI compounds in accordance with Hopfield model [142] can be written as

$$E = a'_o k_s^2 + b'_o k_z^2 \pm \bar{\lambda}_o k_s \tag{1.42}$$

where $a'_o \equiv \hbar^2/2m^*_\perp$, $b'_o \equiv \hbar^2/2m^*_\perp$, and $\bar{\lambda}_o$ represents the splitting of the two-spin states by the spin-orbit coupling and the crystalline field.

The dispersion relation of the conduction electrons of UFs of II-VI materials for dimensional quantization along z-direction can be written following (1.42) as

$$E = a'_o k_s^2 + b'_o \left(\frac{n_z \pi}{d_z}\right)^2 \pm \bar{\lambda}_o k_s \tag{1.43}$$

Using (1.43), the EEM in this case can be written as

$$m^*(E_{Fs}, n_z) = m^*_\perp \left[1 \mp \frac{(\bar{\lambda}_o)}{\left[(\bar{\lambda}_o)^2 - 4a'_o b'_o \left(\frac{n_z \pi}{d_z}\right)^2 + 4a'_o E_{Fs}\right]^{1/2}}\right] \tag{1.44}$$

Thus, we can infer that the EEM in the UFs of II-VI compounds is a function of both the size quantum number and the Fermi energy due to the presence of the term $\bar{\lambda}_o$.

The subband energy $E_{n_{z_5}}$ assumes the form

$$E_{n_{z_5}} = b'_o (n_z \pi / d_z)^2 \tag{1.45}$$

The area of constant energy 2D quantized surface in this case is given by

$$A_\pm (E, n_z) = \left[\frac{\pi}{2\left(a'_0\right)^2}\left[\left(\overline{\lambda_0}\right)^2 + 2a'_0\left(E - E_{n_{z_5}}\right) \pm \overline{\lambda_0}\left[\left(\overline{\lambda_0}\right)^2 + 4a'_0\left(E - E_{n_{z5}}\right)\right]^{1/2}\right]\right] \tag{1.46}$$

The surface electron concentration under the condition of extreme carrier degeneracy can be expressed in this case as

$$n_{2D} = \frac{2g_v}{2(2\pi)^2} \sum_{n_z=1}^{n_{z\max}} \left[A_+\left(E_{Fs}, n_z\right) + A_-\left(E_{Fs}, n_z\right)\right] \tag{1.47}$$

Using (1.46) and (1.47) we get

$$n_{2D} = \frac{g_v m_\perp^*}{\pi \hbar^2} \sum_{n_z=1}^{n_{z\max}} \left(E_{Fs} - E_{n_{z_5}} + \left(\bar{\lambda}\right)^2 m_\perp^* \hbar^{-2} \right) \tag{1.48}$$

1.2.4 The EEM in UFs of Bismuth

(a) The McClure and Choi model
The dispersion relation of the carriers in Bi can be written, following the McClure and Choi [153], as

$$E(1+\alpha E) = \frac{p_x^2}{2m_1} + \frac{p_y^2}{2m_2} + \frac{p_z^2}{2m_3} + \frac{p_y^2}{2m_2}\alpha E \left\{ 1 - \left(\frac{m_2}{m_2'} \right) \right\} + \frac{p_y^4 \alpha}{4m_2 m_2'} - \frac{\alpha p_x^2 p_y^2}{4m_1 m_2} - \frac{\alpha p_y^2 p_z^2}{4m_2 m_3} \tag{1.49}$$

where $p_i \equiv \hbar k_i$, $i = x, y, z$, m_1, m_2 and m_3 are the effective carrier masses at the band-edge along x, y and z directions respectively and m_2' is the effective-mass tensor component at the top of the valence band (for electrons) or at the bottom of the conduction band (for holes).
The dispersion relation of the conduction electrons in UFs of Bi for dimensional quantization along k_z direction can be written following (1.49) for this model as

$$E(1+\alpha E) = \frac{p_x^2}{2m_1} + \frac{p_y^2}{2m_2} + \frac{\hbar^2}{2m_3}\left(\frac{n_z \pi}{d_z} \right)^2 + \frac{p_y^2}{2m_2}\alpha E \left\{ 1 - \left(\frac{m_2}{m_2'} \right) \right\} + \frac{p_y^4 \alpha}{4m_2 m_2'} - \frac{\alpha p_x^2 p_y^2}{4m_1 m_2} - \frac{\alpha p_y^2 \hbar^2}{4m_2 m_3}\left(\frac{n_z \pi}{d_z} \right)^2 \tag{1.50}$$

Equation (1.50) can, approximately, be expressed as

$$\gamma_1(E, n_z) = p_1 k_x^2 + q_1(E) k_y^2 + R_1(E, n_z) k_y^4 \tag{1.51}$$

where,

$$\gamma_1(E, n_z) \equiv \left[E(1+\alpha E) - \frac{\hbar^2}{2m_3}\left(\frac{n_z \pi}{d_z} \right)^2 \right], \quad p_1 \equiv \frac{\hbar^2}{2m_1},$$

$$q_1(E) \equiv \frac{\hbar^2}{2m_2}\left[1 + \alpha E \left(1 - \frac{m_2}{m_2'} \right) - \alpha E(1+\alpha E) \right]$$

and

$$R_1(E,n_z) \equiv \left[\frac{\alpha\hbar^4}{4m_2m_2'} + \alpha\left(\frac{\hbar^2}{2m_2}\right)^2\left\{1+\alpha E\left(1-\frac{m_2}{m_2'}\right) - \frac{\alpha\hbar^2}{2m_3}\left(\frac{n_z\pi}{d_z}\right)^2\right\}\right]$$

The area enclosed by (1.51) is defined by the following integral:

$$A\left(E,n_z\right) = 4\left[\frac{R_1\left(E,n_z\right)}{p_1}\right]^{1/2}\cdot J_1\left(E,n_z\right) \tag{1.52}$$

where,

$$J_1(E,n_z) \equiv \int_0^{u_o(E,n_z)}\left[\frac{\gamma_1(E,n_z)}{R_1(E,n_z)} - \frac{q_1(E)k_y^2}{R_1(E,n_z)} - k_y^4\right]^{1/2} dk_y$$

and

$$u_0(E,n_z) \equiv \left[\sqrt{\frac{q_1^2(E)}{4R_1^2(E,n_z)} + \frac{\gamma_1(E,n_z)}{R_1(E,n_z)}} - q_1(E)\right]^{1/2}$$

Thus, the area enclosed can be written as

$$A(E,n_z) = \frac{4}{3}\left[\frac{R_1(E,n_z)}{p_1}\right]^{1/2}\left[a^2(E,n_z)+b^2(E,n_z)\right]^{1/2}$$

$$\left[a^2(E,n_z)F\left[\frac{\pi}{2},l(E,n_z)\right] - \left[a^2(E,n_z)-b^2(E,n_z)\right]E\left[\frac{\pi}{2},l(E,n_z)\right]\right] \tag{1.53}$$

where,

$$a^2(E,n_z) \equiv \frac{q_1(E)}{2R_1(E,n_z)} + \frac{1}{2}\left[\frac{q_1^2(E)}{R_1^2(E,n_z)} + \frac{4\gamma_1(E,n_z)}{R_1(E,n_z)}\right]^{1/2},$$

$$b^2(E,n_z) \equiv \frac{1}{2}\left[\frac{q_1^2(E)}{R_1^2(E,n_z)} + \frac{4\gamma_1(E,n_z)}{R_1(E,n_z)}\right]^{1/2} - \left(\frac{q_1(E)}{2R_1(E,n_z)}\right),$$

$$l(E,n_z) \equiv \frac{b(E,n_z)}{\sqrt{a^2(E,n_z)+b^2(E,n_z)}},\ F\left[\frac{\pi}{2},l(E,n_z)\right] \text{ and } E\left[\frac{\pi}{2},l(E,n_z)\right]$$

are the complete elliptic integral of the first and second kinds respectively [217] Using (1.53), the EEM can be written as

$$m^*(E_{Fs}, n_z) = \left(\frac{2\hbar^2}{3\pi\sqrt{p_1}}\right)[R_3(E, n_z)]|_{E=E_{Fs}} \tag{1.54}$$

where,

$$\begin{aligned}
&R_3(E_{Fs}, n_z)\\
&\equiv \frac{1}{2}\left[R_1(E_{Fs}, n_z)\right]^{-1/2}[R_1(E_{Fs}, n_z)]'[a^2(E_{Fs}, n_z) + p^2(E_{Fs}, n_z)]^{1/2}\\
&\times\left[a^2(E_{Fs}, n_z)F\left(\frac{\pi}{2}, l(E_{Fs}, n_z)\right) - [a^2(E_{Fs}, n_z)\right.\\
&\left.- b^2(E_{Fs}, n_z)]E\left(\frac{\pi}{2}, l(E_{Fs}, n_z)\right)\right]\\
&+\sqrt{R_1(E_{Fs}, n_z)}\left[a^2(E_{Fs}, n_z) + b^2(E_{Fs}, n_z)\right]^{-1/2}\\
&\times\left[a(E_{Fs}, n_z)(a(E_{Fs}, n_z))' + b(E_{Fs}, n_z)(b(E_{Fs}, n_z))'\right]\\
&\times\left[a^2(E_{Fs}, n_z)F\left(\frac{\pi}{2}, l(E_{Fs}, n_z)\right) - [a^2(E_{Fs}, n_z)\right.\\
&\left.-b^2(E_{Fs}, n_z)]E\left(\frac{\pi}{2}, l(E_{Fs}, n_z)\right)\right]\\
&+\sqrt{R_1(E_{Fs}, n_z)}[a^2(E_{Fs}, n_z) + b^2(E_{Fs}, n_z)]^{1/2}\\
&\times\left[2a(E_{Fs}, n_z)(a(E_{Fs}, n_z))'F\left(\frac{\pi}{2}, l(E_{Fs}, n_z)\right)\right.\\
&+a^2(E_{Fs}, n_z)\left\{F\left(\frac{\pi}{2}, l(E_{Fs}, n_z)\right)\right\}' - [2a(E_{Fs}, n_z)[a(E_{Fs}, n_z)]'\\
&-2b(E_{Fs}, n_z)(b(E_{Fs}, n_z))']E\left(\frac{\pi}{2}, l(E_{Fs}, n_z)\right)\\
&\left.-\left[a^2(E_{Fs}, n_z) - b^2(E_{Fs}, n_z)\right]\left(E\left(\frac{\pi}{2}, l(E_{Fs}, n_z)\right)\right)'\right]
\end{aligned}$$

Thus, the EEM in this case is a function of both the Fermi energy and the size quantum number due to the presence of band nonparabolicity only.
The total 2D DOS function can be written following (1.53), as

$$N_{2DT}(E) = \left(\frac{2g_v}{3\pi^2\sqrt{p_1}}\right)\sum_{n_z=1}^{n_{zmax}} R_3(E, n_z)H(E - E_{n_{z6}}) \tag{1.55}$$

where, the subband energies $E_{n_{z6}}$ assume the form

$$E_{n_{z6}}(1 + \alpha E_{n_{z6}}) = \frac{\hbar^2}{2m_3}\left(\frac{n_2\pi}{d_z}\right)' \tag{1.56}$$

Combining (1.55) with the Fermi-Dirac occupation probability factor, the 2D electron statistics in UFs of Bi in accordance with the McClure and Choi model can be expressed as

$$n_{2D} = \left(\frac{2g_v}{3\pi^2\sqrt{p_1}}\right)\sum_{n_z=1}^{n_{zmax}}[\theta_1(E_{Fs}, n_z) + \theta_2(E_{Fs}, n_z) \tag{1.57}$$

where,

$$\theta_1(E_{Fs}, n_z) \equiv \left\{\sqrt{R_1(E_{Fs}, n_z)}[a^2(E_{Fs}, n_z) + b^2(E_{Fs}, n_z)]^{1/2} \times \left[a^2(E_{Fs}, n_z)F\left(\frac{\pi}{2}, l(E_{Fs}, n_z)\right) - [a^2(E_{Fs}, n_z) - b^2(E_{Fs}, n_z)]F\left(\frac{\pi}{2}, l(E_{Fs}, n_z)\right)\right]\right\}$$

and $\theta_2(E_{Fs}, n_z) \equiv \sum_{r=1}^{s} L(r)[\theta_1(E_{Fs}, n_z)]$.

(b) The Hybrid Model

The dispersion relation of the carriers in bulk specimens of Bi in accordance with the Hybrid model can be represented as [152]

$$E(1 + \alpha E) = \frac{\theta_0(E)(\hbar k_y^2)}{2M_2} + \frac{\alpha\gamma_0\hbar^4 k_y^4}{4M_2^2} + \frac{\hbar^2 k_x^2}{2m_1} + \frac{\hbar^2 k_z^2}{2m_3} \tag{1.58}$$

in which $\theta_0(E) \equiv [1 + \alpha E(1 - \gamma_0) + \overline{\delta}_0]$, $\gamma_0 \equiv \frac{M_2}{m_2}$, $\overline{\delta}_0 \equiv \frac{M_2}{M_2'}$ and the other notations are defined in [152].

In the presence of size quantization along y-direction, the 2D electron dispersion relation can be written as

$$\frac{\hbar^2 k_x^2}{2m_1} + \frac{\hbar^2 k_z^2}{2m_3} = E(1 + \alpha E) - \frac{\theta_0(E)\hbar^2}{2M_2}\left(\frac{\pi n_y}{d_y}\right)^2 - \frac{\alpha\gamma_0\hbar^4}{4M_2^2}\left(\frac{\pi n_y}{d_y}\right)^4 \tag{1.59}$$

The 2D area is given by

$$A(E, n_y) = \frac{2\pi\sqrt{m_1 m_3}}{\hbar_2} t_{29}(E, n_y) \tag{1.60}$$

$$t_{29}(E, n_y) = \left[E(1 + \alpha E) - \frac{\theta_0(E)\hbar^2}{2M_2}\left(\frac{\pi n_y}{d_y}\right)^2 - \frac{\alpha\gamma_0\hbar^4}{4M_2^4}\left(\frac{\pi n_y}{d_y}\right)^4\right]$$

The effective mass in the X–Z plane can be written as

$$m^*(E_{Fs}, n_y) = [\sqrt{m_1 m_3}]t_{29}'(E_{Fs}, n_y) \tag{1.61}$$

Therefore, the effective mass in UFs of Bi in accordance with Hybrid model is a function of Fermi energy and the size quantum number due to the presence of band nonparabolicity only.

The subband energy are given as

$$E_{n_y}(1+\alpha E)-\frac{\theta_0(E_{n_y})\hbar^2}{2M_2}\left(\frac{\pi n_y}{d_y}\right)^2-\frac{\alpha\gamma_0\hbar^4}{4M_2^2}\left(\frac{\pi n_y}{d_y}\right)^4=0 \tag{1.62}$$

The total DOS function in this case can be written as

$$N_{2DT}(E)=\frac{g_v\sqrt{m_1m_3}}{\pi\hbar^2}\sum_{n_y=1}^{n_{ymax}}\left\{t_{29}(E,n_y)\right\}'H(E-E_{n_y}) \tag{1.63}$$

The use of (1.63) leads to the 2D electron statistics in UFs of Bi in this case as

$$N_{2D}=\frac{g_v\sqrt{m_1m_3}}{\pi\hbar^2}\sum_{n_y=1}^{n_{ymax}}\left[t_{29}(E_{Fs},n_y)+t_{30}(E_{Fs},n_y)\right] \tag{1.64}$$

in which $t_{30}(E_{Fs},n_y)=\sum_{r=1}^{s_o}L(r)[t_{29}(E_{Fs},n_y)]$

(c) The Cohen model

In accordance with the Cohen model [151], the dispersion law of the carriers in Bi is given by

$$E(1+\alpha E)=\frac{p_x^2}{2m_1}+\frac{p_z^2}{2m_3}-\frac{\alpha Ep_y^2}{2m_2'}+\frac{p_y^2(1+\alpha E)}{2m_2}+\frac{\alpha p_y^4}{4m_2m_2'} \tag{1.65}$$

The 2D electron dispersion law in UFs of Bi in accordance with this model can be written following (1.65) as

$$E(1+\alpha E)=\frac{p_x^2}{2m_1}+\frac{\hbar^2}{2m_3}\left(\frac{n_z\pi}{d_z}\right)^2-\frac{\alpha Ep_y^2}{2m_2'}+\left(\frac{\alpha p_y^4}{4m_2m_2'}\right)+\frac{p_y^2}{2m_2}(1+\alpha E) \tag{1.66}$$

The (1.66) can be written as

$$\gamma_1(E,n_z)=p_1k_x^z+q_2(E)k_y^2+R_2k_y^4 \tag{1.67}$$

where, $q_2(E)\equiv\left[\frac{\hbar^2}{2m_2}(1+\alpha E)-\frac{\alpha E\hbar^2}{2m_2'}\right]$ and $R_2\equiv\left(\frac{\alpha\hbar^4}{4m_2m_2'}\right)$.

The EEM in this case can be written as

$$m^*(E_{Fs},n_z)=\left(\frac{2\hbar^2}{3\pi\sqrt{p_1}}\right)\left[R_4(E,n_z)\right]|_{E=E_{Fs}} \tag{1.68}$$

in which,

$$
\begin{aligned}
&R_4(E_{Fs}, n_z)\\
&\equiv \sqrt{R_2}[a_1^2(E_{Fs}, n_z) + b^2(E_{Fs}, n_z)]^{-1/2}[a_1(E_{Fs}, n_z)(a_1(E_{Fs}, n_z))'\\
&\quad + b_1(E_{Fs}, n_z)(b_1(E_{Fs}, n_z))'\left[a_1^2(E_{Fs}, n_z)F\left(\frac{\pi}{2}, l(E_{Fs}, n_z)\right)\right.\\
&\quad \left. - [a_1^2(E_{Fs}, n_z) - b_1^2(E_{Fs}, n_z)]E\left(\frac{\pi}{2}, l_1(E_{Fs}, n_z)\right)\right]\\
&\quad + \sqrt{R_2}\left[a_1^2(E_{Fs}, n_z) + b_1^2(E_{Fs}, n_z)\right]^{1/2}\left[2a_1(E_{Fs}, n_z)(a_1(E_{Fs}, n_z))'\right.\\
&\quad \times F\left(\frac{\pi}{2}, l_1(E_{Fs}, n_z)\right) + a_1^2(E_{Fs}, n_z)\left\{F\left(\frac{\pi}{2}, l_1(E_{Fs}, n_z)\right)\right\}'\\
&\quad \times \left[2a_1(E_{Fs}, n_z)(a_1(E_{Fs}, n_z))' - 2b_1(E_{Fs}, n_z)(b_1(E_{Fs}, n_z))'\right]E\left(\frac{\pi}{2}, l_1(E_{Fs}, n_z)\right)\\
&\quad \left. - \left[a_1^2(E_{Fs}, n_z) - b_1^2(E_{Fs}, n_z)\right]\left(E\left(\frac{\pi}{2}, l_1(E_{Fs}, n_z)\right)\right)'\right]\Bigg],
\end{aligned}
$$

$$
a_1^2(E_{Fs}, n_z) \equiv \frac{q_2(E_{Fs})}{2R_2} + \frac{1}{2}\left[\frac{q_2^2(E_{Fs})}{R_2^2} + \frac{4\gamma_1(E_{FS}, n_z)}{R_2}\right]^{1/2},
$$

$$
b_1^2(E_{Fs}, n_z \equiv \frac{1}{2}\left[\frac{q_2^2(E_{Fs})}{R_2^2} + \frac{4\gamma_1(E_{Fs}, n_z)}{R_2}\right]^{1/2} - \left(\frac{q_2(E_{Fs})}{2R_2}\right)
$$

$$
\text{and } l_1(E_{Fs}, n_z) \equiv \frac{b_1(E_{Fs}, n_z)}{\sqrt{a_1^2(E_{Fs}, n_z) + b_1^2(E_{Fs}, n_z)}}.
$$

which shows that the EEM in this present case is again a function of both the size quantum number and the Fermi energy due to the presence of the band nonparabolicity only.
The total DOS is given by

$$
N_{2DT}(E) = \left(\frac{2g_v}{3\pi^2\sqrt{p_1}}\right)\sum_{n_z=1}^{n_{zmax}} R_4(E, n_z)H(E - E_{nz7}) \tag{1.69a}
$$

where, $E_{n_{z7}}$ is the lowest positive root of the equation

$$
\gamma_1\left(E_{n_{z7}}, n_z\right) = 0 \tag{1.69b}
$$

Combining (1.69a) with the Fermi-Dirac occupation probability factor, the 2D electron statistics in UFs of Bi in accordance with the Cohen model can be written as

$$
n_{2D} = \left(\frac{2g_v}{3\pi^2\sqrt{p_1}}\right)\sum_{n_z=1}^{n_{z_{max}}}\left[\theta_3(E_{Fs}, n_z) + \theta_4(E_{Fs}, n_z)\right] \tag{1.70}
$$

where,

$$\theta_3(E_{Fs}, n_z) \equiv \left\{\sqrt{R_2}\left[a_1^2(E_{Fs}, n_z) - b_1^2(E_{Fs}, n_z)\right]^{1/2}\left[a_1^2(E_{Fs}, n_z)F\left(\frac{\pi}{2}, l_1(E_{Fs}, n_z)\right)\right.\right.$$
$$\left.\left. - \left[a_1^2(E_{Fs}, n_z) - b_1^2(E_{Fs}, n_z)\right]F\left(\frac{\pi}{2}, l_1(E_{Fs}, n_z)\right)\right]\right],$$

and $\theta_4(E_{Fs}, n_z) \equiv \sum_{r=1}^{s} L(r)\left[\theta_3(E_{Fs}, n_z)\right]$.

(d) The Lax model
The electron energy spectra in bulk specimens of Bi in accordance with the Lax model can be written as [147]

$$E(1 + \alpha E) = \frac{p_x^2}{2m_1} + \frac{p_y^2}{2m_2} + \frac{p_z^2}{2m_3} \tag{1.71}$$

The 2D electron dispersion law in this case can be written as

$$E(1 + \alpha E) = \frac{\hbar^2 k_x^2}{2m_1} + \frac{\hbar^2 k_y}{2m_2} + \frac{\hbar^2}{2m_3}\left(\frac{n_z\pi}{d_z}\right)^2 \tag{1.72}$$

The EEM in this case assumes the form

$$m^*(E_{Fs}) = \sqrt{m_1 m_2}(1 + 2\alpha E_{Fs}) \tag{1.73}$$

Thus, we see that the EEM for the Lax model is a function of the Fermi energy alone due to the band nonparabolicity.
The subband energy, the total DOS function and the 2D electron statistics for this model can, respectively, be expressed as

$$E_{n_{z8}}(1 + \alpha E_{n_{z8}}) = \frac{\hbar^2}{2m_3}(n_z\pi/d_z)^2 \tag{1.74}$$

$$N_{2DT}(E) = \frac{g_v\sqrt{m_1 m_2}}{\pi\hbar^2}\sum_{n_z=1}^{n_{zmax}}(1 + 2\alpha E)H(E - E_{n_{z8}}) \tag{1.75}$$

$$n_{2D} = \frac{g_v\sqrt{m_1 m_2}k_B T}{\pi\hbar^2}\sum_{n_z=1}^{n_{zmax}}\left[(1 + 2\alpha E_{n_{z8}})F_0(\eta_{y2}) + 2\alpha k_B T F_1(\eta_{y2})\right] \tag{1.76}$$

where, $\eta_{y_2} = \dfrac{E_{Fs} - E_{n_{z8}}}{k_B T}$.

(e) The ellipsoidal parabolic model
The 2D dispersion relation, the EEM, the subband energy ($E_{n_{z9}}$), the total DOS,

and the 2D electron statistics for this model can respectively be written as

$$E = \left(\frac{\hbar^2 k_x^2}{2m_1}\right) + \left(\frac{\hbar^2 k_y^2}{2m_2}\right) + \left(\frac{\hbar^2}{2m_3}\right)\left(\frac{n_z \pi}{d_z}\right)^2 \tag{1.77}$$

$$m^*(E_{Fs}) = \left(\sqrt{m_1 m_2}\right) \tag{1.78}$$

$$N_{2DT}(E) = \frac{g_v \sqrt{m_1 m_2}}{\pi \hbar^2} \sum_{n_z=1}^{n_{zmax}} H(E - E_{n_{z9}}) \tag{1.79}$$

$$E_{n_{z9}} = \left(\frac{\hbar^2}{2m_3}\right)\left(\frac{n_z \pi}{d_z}\right)^2 \tag{1.80}$$

$$N_{2D} = \left[\frac{k_B T g_v \sqrt{m_1 m_2}}{\pi \hbar^2}\right] \sum_{n_z=1}^{n_{zmax}} F_0(\eta_{y3}) \tag{1.81}$$

where, $\eta_{y3} \equiv (k_B T)^{-1}\left[E_{Fs} - E_{n_{z9}}\right]$

1.2.5 The EEM in UFs of IV–VI Semiconductors

The dispersion relation of the conduction electrons in IV-VI semiconductors can be expressed in accordance with Dimmock [221] as

$$\left[\overline{\varepsilon} - \frac{E_{g0}}{2} - \frac{\hbar^2 k_s^2}{2m_t^-} - \frac{\hbar^2 k_z^2}{2m_l^-}\right]\left[\overline{\varepsilon} + \frac{E_{g0}}{2} + \frac{\hbar^2 k_s^2}{2m_t^-} + \frac{\hbar^2 k_z^2}{2m_l^-}\right] = P_\perp^2 k_s^2 + P_\parallel^2 k_z^2 \tag{1.82}$$

where $\overline{\varepsilon}$ is the energy as measured from the center of the band gap E_{g0}, $m_t^{\pm}$ and $m_l^{\pm}$ represent the contributions to the transverse and longitudinal effective masses of the external L_6^+ and L_6^- bands arising from the $\vec{k}.\vec{p}$ perturbations with the other bands taken to the second order. Using $\varepsilon = E + \left(E_{g0}/2\right)$, $P_\perp^2 = \frac{\hbar^2 E_{g0}}{2m_t^*}$, $P_\parallel^2 = \frac{\hbar^2 E_{g0}}{2m_l^*}$ (m_t^* and m_l^* are the transverse and longitudinal effective electron masses at $k = 0$) in (1.82), we can write

$$\left[E - \frac{\hbar^2 k_s^2}{2m_t^-} - \frac{\hbar^2 k_z^2}{2m_l^-}\right]\left[1 + \alpha E + \alpha + \frac{\hbar^2 k_s^2}{2m_t^+} + \alpha + \frac{\hbar^2 k_z^2}{2m_l^+}\right] = \frac{\hbar^2 k_s^2}{2m_t^*} + \frac{\hbar^2 k_z^2}{2m_l^*} \tag{1.83}$$

The 2D dispersion relation of the conduction electrons in IV-VI materials in UFs for the dimensional quantization along z direction can be expressed as

$$E(1+\alpha E)+\alpha E\left(\frac{\hbar^2k_x^2}{2x_4}+\frac{\hbar^2k_y^2}{2x_5}\right)+\alpha E\frac{\hbar^2}{2x_6}\left(\frac{n_z\pi}{d_z}\right)^2-(1+\alpha E)\left(\frac{\hbar^2k_x^2}{2x_1}+\frac{\hbar^2k_y^2}{2x_2}\right)$$
$$-\alpha\left(\frac{\hbar^2k_x^2}{2x_1}+\frac{\hbar^2k_y^2}{2x_2}\right)\left(\frac{\hbar^2k_x^2}{2x_4}+\frac{\hbar^2k_y^2}{2x_5}\right)-\alpha\left(\frac{\hbar^2k_x^2}{2x_1}+\frac{\hbar^2k_y^2}{2x_2}\right)\frac{\hbar^2}{2x_6}\left(\frac{n_z\pi}{d_z}\right)^2$$
$$-(1+\alpha E)\frac{\hbar^2}{2x_3}\left(\frac{n_z\pi}{d_z}\right)^2-\alpha\frac{\hbar^2}{2x_3}\left(\frac{n_z\pi}{d_z}\right)^2\left(\frac{\hbar^2k_x^2}{2x_4}+\frac{\hbar^2k_y^2}{2x_5}\right)-\alpha\frac{\hbar^2}{2x_3}\left(\frac{n_z\pi}{d_z}\right)^2\frac{\hbar^2}{2x_6}\left(\frac{n_z\pi}{d_z}\right)^2$$
$$=\frac{\hbar^2k_x^2}{2m_1}+\frac{\hbar^2k_y^2}{2m_2}+\frac{\hbar^2}{2m_3}\left(\frac{n_z\pi}{d_z}\right)^2 \tag{1.84}$$

where

$$x_4=m_t^+,\ x_5=\frac{m_t^++2m_l^+}{3},\ x_6=\frac{3m_t^+m_l^+}{2m_l^++m_t^+},\ x_1=m_t^-,\ x_2=\frac{m_t^-+2m_l^-}{3},$$

$$x_3=\frac{3m_t^-m_l^-}{2m_l^-+m_t^-},\ m_1=m_t^*,\ m_2=\frac{m_t^++2m_l^*}{3}\text{ and }m_3=\frac{3m_l^*m_t^*}{m_t^*+2m_l^*}.$$

Substituting $k_x=r\mathrm{Cos}\theta$ and $k_y=r\mathrm{Sin}\theta$ (where r and θ are 2D polar coordinates in 2D wave vector space) in (1.84), we can write

$$r_4\left[\alpha\frac{1}{4}\left(\frac{\hbar^2Cos^2\theta}{x_1}+\frac{\hbar^2Sin^2\theta}{x_2}\right)\left(\frac{\hbar^2Cos^2\theta}{x_4}+\frac{\hbar^2Sin^2\theta}{x_5}\right)\right]+r^2\frac{1}{2}\left[\left(\frac{\hbar^2Cos^2\theta}{m_1}+\frac{\hbar^2Sin^2\theta}{m_2}\right)\right.$$
$$+\alpha\frac{\hbar^2}{2x_3}\left(\frac{n_z\pi}{d_z}\right)^2\left(\frac{\hbar^2Cos^2\theta}{x_4}+\frac{\hbar^2Sin^2\theta}{x_5}\right)+\alpha\left(\frac{\hbar^2Cos^2\theta}{x_1}+\frac{\hbar^2Sin^2\theta}{x_2}\right)\frac{\hbar^2}{2x_6}\left(\frac{n_z\pi}{d_z}\right)^2$$
$$+\hbar^2(1+\alpha E)\left(\frac{Cos^2\theta}{x_1}+\frac{Sin^2\theta}{x_2}\right)-\hbar^2\alpha E\left(\frac{Cos^2\theta}{x_4}+\frac{Sin^2\theta}{x_5}\right)\Bigg]-[E(1+\alpha E)$$
$$\left.+\alpha E\frac{\hbar^2}{2x_6}\left(\frac{n_z\pi}{d_z}\right)^2-(1+\alpha E)\frac{\hbar^2}{2x_3}\left(\frac{n_z\pi}{d_z}\right)^2-\alpha\left(\frac{\hbar^4}{4x_3x_6}\left(\frac{n_z\pi}{d_z}^4\right)\right)\right]=0 \tag{1.85}$$

The area $A(E,n_z)$ of the 2D wave vector space can be expressed as

$$A(E,n_z)=\overline{J}_1-\overline{J}_2 \tag{1.86}$$

where

$$\overline{J}_1\equiv 2\int_0^{\pi/2}\frac{c}{b}d\theta \tag{1.87}$$

and

$$\overline{J}_2\equiv 2\int_0^{\pi/2}\frac{ac^2}{b^3}d\theta \tag{1.88}$$

in which

$$\alpha \equiv \left[\alpha\left(\frac{\hbar^4}{4}\right)\left(\frac{Cos^2\theta}{x_1}+\frac{Sin^2\theta}{x_2}\right)\left(\frac{Cos^2\theta}{x_4}+\frac{Sin^2\theta}{x_3}\right)\right],$$

$$b \equiv \left(\frac{\hbar^2}{2}\right)\left[\left(\frac{Cos^2\theta}{m_1}+\frac{Sin^2\theta}{m_2}\right)+\alpha\left(\frac{\hbar^2}{2x_3}\right)\left(\frac{n_2\pi}{d_z}\right)^2\left(\frac{Cos^2\theta}{x_4}+\frac{Sin^2\theta}{x_5}\right)\right.$$
$$+\alpha\left(\frac{\hbar^2}{2x_6}\right)\left(\frac{n_2\pi}{d_z}\right)^2\left(\frac{Cos^2\theta}{m_1}+\frac{Sin^2\theta}{m_2}\right)+(1+\alpha E)\left(\frac{Cos^2\theta}{x_1}+\frac{Sin^2\theta}{x_2}\right)$$
$$\left.-\alpha E\left(\frac{Cos^2\theta}{x_4}+\frac{Sin^2\theta}{x_5}\right)\right]$$

and

$$c \equiv \left[E(1+\alpha E)+\alpha E\left(\frac{\hbar^2}{2x_6}\right)\left(\frac{n_z\pi}{d_z}\right)^2-(1+\alpha E)\left(\frac{\hbar^2}{2x_3}\right)\left(\frac{n_z\pi}{d_z}\right)^2\right.$$
$$\left.-\alpha\left(\frac{\hbar^4}{4x_3x_6}\right)\left(\frac{n_z\pi}{d_z}^4\right)\right]$$

(1.87) can be expressed as $\overline{J}_1 = 2\int_0^{\pi/2}\frac{t_3(E,n_z)d\theta}{A_1(E,n_z)Cos^2\theta+B_1(E,n_z)Sin^2\theta}$ where, $t_3(E,n_z) \equiv c$, $A_1(E,n_z) \equiv \frac{\hbar^2}{2m_1}t_1(E,n_z)$,

$$t_1(E,n_z) \equiv \left[1+m_1\left[\frac{1}{x_4}\frac{\alpha\hbar^2}{2x_3}\left(\frac{n_z\pi}{d_z}\right)^2+\frac{\alpha\hbar^2}{2x_1x_6}\left(\frac{n_z\pi}{d_z}\right)^2+\frac{1+\alpha E}{x_1}-\frac{\alpha E}{x_4}\right]\right]$$

$B_1(E,n_z) \equiv \frac{\hbar^2}{2m_2}t_2(E,n_z)$ and

$$t_2(E,n_z) \equiv \left[1+m_2\left[\frac{\alpha\hbar^2}{2x_3x_5}\left(\frac{n_z\pi}{d_z}\right)^2+\frac{\alpha\hbar^2}{2x_2x_6}\left(\frac{n_z\pi}{d_z}\right)^2+\frac{1+\alpha E}{d_z}-\frac{\alpha E}{x_5}\right]\right].$$

Performing the integration, we get

$$\overline{J}_1 = \pi t_3(E,n_z)[A_1(E,n_z)B_1(E,n_z)]^{-1/2} \tag{1.89}$$

From (1.88) we can write

$$\overline{J}_2 = \frac{\alpha t_3^2(E,n_z)\hbar^4}{2B_1^3(E,n_z)}I \tag{1.90}$$

where

$$I \equiv \int_0^{\infty} \frac{(a_1 + a_2 z^2)(a_3 + a_4 z^2) dz}{[(\overline{a})^2 + z^2]^3} \tag{1.91}$$

in which $a_1 \equiv \frac{1}{x_1}, a_2 \equiv \frac{1}{x_2}, z = \tan\theta, \theta$ is a new variable, $a_3 \equiv \frac{1}{x_4}, a_4 \equiv \frac{1}{x_5}$ and $(\overline{a})^2 \equiv \left(\frac{A_1(E,n_z)}{B_1(E,n_z)}\right)$. The use of the Residue theorem leads to the evaluation of the integral in (1.91) as

$$I \equiv \frac{\pi}{4\overline{a}}[a_1 a_4 + 3a_2 a_4] \tag{1.92}$$

Therefore, the 2D area of the 2D wave vector space can be written as

$$A(E, n_z) = \frac{\pi t_3(E, n_z)}{\sqrt{A_1(E, n_z) B_1(E, n_z)}} \left[1 - \frac{1}{x_5}\left(\frac{1}{x_1} + \frac{3}{x_2}\right) \frac{\alpha t_3(E, n_z)\hbar^4}{8B_1^2(E, n_z)}\right] \tag{1.93}$$

The EEM for the UFs of IV-VI materials can thus be written as

$$m^*(E, n_z) = \frac{\hbar^2}{2}[\theta_5(E, n_z)]\Big|_{E=E_{Fs}} \tag{1.94}$$

where,

$$\begin{aligned}
\theta_5(E, n_z) \equiv & \left[1 - \frac{1}{x_5}\left(\frac{1}{x_1} + \frac{3}{x_2}\right) \frac{\alpha t_3(E, n_z)\hbar^4}{8[B_1(E, n_z)]^2}\right] [A_1(E, n_z) B_1(E, n_z)]^{-1} \\
& \times \left[\sqrt{A_1(E, n_z) B_1(E, n_z)}\{t_3(E, n_z)\}' - t_3(E, n_z)\right. \\
& \times \left.\left\{\frac{1}{2}\{A_1(E, n_z)\}'\left[\frac{B_1(E, n_z)}{A_1(E, n_z)}\right]^{-1/2} + \frac{1}{2}\{B_1(E, n_z)\}'\left[\frac{A_1(E, n_z)}{B_1(E, n_z)}\right]^{-1/2}\right\}\right] \\
& - \frac{1}{8}\frac{t_3(E, n_z)\alpha\hbar^4}{\sqrt{A_1(E, n_z) B_1(E, n_z)}} \frac{1}{x_5}\left(\frac{1}{x_1} + \frac{3}{x_2}\right) [B_1(E, n_z)]^{-4} \\
& \times \left[\{B_1(E, n_z)\}^2\{t_3(E, n_z)\}' - 2B_1(E, n_z)\{B_1(E, n_z)\}' t_3(E, n_z)\right]
\end{aligned}$$

Thus, the EEM is a function of Fermi energy and the quantum number due to the band nonparabolicity.

The total DOS function can be written as

$$N_{2DT}(E) = \left(\frac{g_v}{2\pi}\right) \sum_{n_z=1}^{n_{zmax}} \theta_5(E, n_z) H(E - E_{n_{z10}}) \tag{1.95}$$

where the subband energy ($E_{n_{z10}}$) in this case can be written as

$$E_{n_{z10}}\left(1+\alpha E_{n_{z10}}\right)+\alpha E_{n_{z10}}\frac{\hbar^2}{2x_6}\left(\frac{n_z\pi}{d_z}\right)^2-\left(1+\alpha E_{n_{z10}}\right)\frac{\hbar^2}{2x_3}\left(\frac{n_z\pi}{d_z}\right)^2$$
$$-\alpha\frac{\hbar^2}{2x_3}\left(\frac{n_z\pi}{d_z}\right)^2\frac{\hbar^2}{2x_6}\left(\frac{n_z\pi}{d_z}\right)^2-\left[\frac{\hbar^2}{2m_3}\left(\frac{n_z\pi}{d_z}\right)^2\right]=0 \tag{1.96}$$

The use of (1.95) leads to the expression of 2D electron statistics as

$$n_{2D}=\frac{g_v}{2\pi}\sum_{n_z=1}^{n_{zmax}}\left[T_{59}(E_{Fs},n_z)+T_{60}(E_{Fs},n_z)\right] \tag{1.97}$$

where $T_{59}(E_{Fs},n_z)\equiv\frac{A(E_{Fs},n_z)}{\pi}$ and $T_{60}(E_{Fs},n_z)\equiv\sum_{r=1}^{s}L(r)T_{59}(E_{Fs},n_z)$.

1.2.6 The EEM in UFs of Stressed Semiconductors

The electron energy spectrum in stressed Kane-type semiconductors can be written [222–225] as

$$\left(\frac{k_x}{\overline{a}_0(E)}\right)^2+\left(\frac{k_y}{\overline{b}_0(E)}\right)^2+\left(\frac{k_z}{\overline{c}_0(E)}\right)^2=1 \tag{1.98}$$

where

$$[\overline{a}_0(E)]^2\equiv\frac{\overline{K}_0(E)}{\overline{A}_0(E)+\frac{1}{2}\overline{D}_0(E)},\ \overline{K}_0(E)\equiv\left[E-C_1\varepsilon-\frac{2C_2^2\varepsilon_{xy}^2}{3E_g'}\right]\left(\frac{3E_g'}{2B_2^2}\right),$$

C_1 is the conduction band deformation potential, ε is the trace of the strain tensor $\hat{\varepsilon}$ which can be written as $\hat{\varepsilon}=\begin{bmatrix}\varepsilon_{xx}&\varepsilon_{xy}&0\\ \varepsilon_{xy}&\varepsilon_{yy}&0\\ 0&0&\varepsilon_{zz}\end{bmatrix}$, C_2 is a constant which describes the strain interaction between the conduction and valance bands, $E_g'\equiv E_g+E-C_1\varepsilon$, B_2 is the momentum matrix element,

$$\overline{A}_0(E)\equiv\left[1-\frac{(\overline{a}_0+C_1)}{E_g'}+\frac{3\overline{b}_0\varepsilon_{xx}}{2E_g'}-\frac{\overline{b}_0\varepsilon}{2E_g'}\right],$$
$$\overline{a}_0\equiv-\frac{1}{3}(\overline{b}_0+2\overline{m}),\overline{b}_0\equiv\frac{1}{3}(\overline{l}-\overline{m}),\overline{d}_0\equiv\frac{2\overline{n}}{\sqrt{3}},$$

$\overline{l},\overline{m},\overline{n}$ are the matrix elements of the strain perturbation operator, $\overline{D}_0(E)\equiv(\overline{d}_0\sqrt{3})\frac{\varepsilon_{xy}}{E_g'}$,

$$[\bar{b}_0(E)]^2 \equiv \frac{\overline{K}_0(E)}{\overline{A}_0(E) - \frac{1}{2}\overline{D}_0(E)}, \quad [\bar{c}_0(E)]^2 \equiv \frac{\overline{K}_0(E)}{\overline{L}_0(E)},$$
$$\text{and } \overline{L}_0(E) \equiv \left[1 - \frac{(\bar{a}_0 + C_1)}{E_g'} + \frac{3\bar{b}_0\varepsilon_{zz}}{E_g'} - \frac{\bar{b}_0\varepsilon}{2E_g'}\right]$$

The 2D electron energy spectrum in UFs of stressed materials assumes the form

$$\frac{K_x^2}{[\bar{a}_0(E)]^2} + \frac{K_y^2}{[\bar{b}_0(E)]^2} + \frac{1}{[\bar{c}_0(E)]^2}(n_z\pi/d_z) = 1 \tag{1.99}$$

The area of 2D wave vector space enclosed by (1.99) can be written as

$$A(E, n_z) = \pi P^2(E, n_z)\bar{a}_0(E)\bar{b}_0(E) \tag{1.100}$$

where $P^2(E, n_z) = [1 - [n_z\pi/d_z\bar{c}_0(E)]^2]$.

The expression of the surface EEM in this case can be written as

$$m^*(E_{Fs}, n_z) = \frac{\hbar^2}{2}[\theta_6(E, n_z)]\Big|_{E=E_{Fs}} \tag{1.101}$$

in which,

$$\theta_6(E, n_z) = \Big[2P(E, n_z)\{P(E, n_z)\}'\bar{a}_0(E)\bar{b}_0(E) + \{P(E, n_z)\}^2\{\bar{a}_0(E)\}'\bar{b}_0(E) + \{P(E, n_z)\}^2\{\bar{b}_0(E)\}'\bar{a}_0(E)\Big]$$

The EEM in this case is the function of Fermi energy and the size quantization number due to the presence of stress only.

Thus, the total 2D DOS function can be expressed as

$$N_{2DT}(E) = \left(\frac{g_v}{2\pi}\right)\sum_{n_z=1}^{n_{zmax}} \theta_6(E, n_z)H(E - E_{n_{z11}}) \tag{1.102}$$

The subband energies ($E_{n_{z11}}$) are given by

$$\bar{c}_0(E_{n_{z11}}) = n_z\pi/d_z \tag{1.103}$$

The 2D surface electron concentration per unit area for UFs of stressed Kane-type compounds can be written as

$$n_{2D} = \frac{g_v}{2\pi}\sum_{n_z=1}^{n_{zmax}} [T_{61}(E_{Fs}, n_z) + T_{62}(E_{Fs}, n_z)] \tag{1.104}$$

where

$$T_{61}(E_{Fs}, n_z) \equiv [P^2(E_{Fs}, n_z)\bar{a}_0(E_{Fs})\bar{b}_0(E_{Fs})]$$
$$\text{and } T_{62}(E_{Fs}, n_z) \equiv \sum_{r=1}^{s} L(r)T_{61}(E_{Fs}, n_z).$$

In the absence of stress together with the substitution, $B_2^2 \equiv 3\hbar^2(E_g/4m_c)$, (1.98) assumes the same form as given by (1.16).

1.2.7 The EEM in UFs of Tellurium

The dispersion relation of the conduction electrons in Te can be expressed as [226]

$$E = \psi_1 k_z^2 + \psi_2 k_s^2 \pm [\psi_3^2 k_s^2 + \psi_2^4 k_s^2]^{1/2} \tag{1.105}$$

where, $\psi_1 = 6.7\times10^{-16}$ mev.m^2, $\psi_2 = 4.2\times10^{-16}$ mev.m^2, $\psi_3 = 6\times10^{-8}$, mev.m and $\psi_4 = 3.6 \times 10^{-8}$ mev.m

The 2D electron energy spectrum in ultrathin films of Te assumes the form

$$k_s^2 = \psi_5(E) - \psi_6\left(\frac{\pi n_z}{d_z}\right)^2 \pm \psi_7\left[\psi_8^2(E) - \left(\frac{\pi n_z}{d_z}\right)^2\right]^{\frac{1}{2}} \tag{1.106}$$

where, $\psi_5(E) = \left[\frac{E}{\psi_2} + \frac{\psi_4^2}{2\psi_2^2}\right]$, $\psi_6 = \frac{\psi_1}{\psi_2}$, $\psi_7 = \frac{\psi_4\sqrt{\psi_1}}{\psi_2^{\frac{3}{2}}}$, $\psi_8^2(E) = \frac{\psi_4^4 + 4E\psi_2\psi_4^2 + 4\psi_2^2\psi_3^2}{4\psi_1\psi_2\psi_4^2}$

The EEM in this case is given by

$$m^*(E_{Fs}, n_z) = \frac{\hbar^2}{2}\left[t'_{40}(E, n_z)\right]\Big|_{E=E_{Fs}} \tag{1.107}$$

where, $t_{40}(E, n_z) = \left[\psi_5(E) - \psi_6\left(\frac{\pi n_z}{d_z}\right)^2 \pm \psi_7\left[\psi_8^2(E) - \left(\frac{\pi n_z}{d_z}\right)^2\right]^{1/2}\right]^{1/2}$

It appears that the EEM in UFs of Te is a function of Fermi energy and size quantum number which are the characteristics of such systems.

Thus, the total 2D DOS function can be expressed as

$$N_{2DT}(E) = \left(\frac{g_v}{\pi}\right)\sum_{n_z=1}^{n_{zmax}} t'_{40}(E, n_2)H(E - E_{n_{z12}}) \tag{1.108}$$

The subband energies ($E_{n_{z12}}$) are given by

$$E_{n_{z12}} = \psi_1 (n_z \pi / d_z)^2 \pm \psi_3 (n_z \pi / d_z) \tag{1.109}$$

The 2D surface electron concentration per unit area for UFs of Te can be written as

$$n_{2D} = \frac{g_v}{\pi} \sum_{n_z=1}^{n_{zmax}} [t_{40}(E_{Fs}, n_2) + t_{41}(E_{Fs}, n_2)] \tag{1.110}$$

where $t_{41}(E_{Fs}, n_2) \equiv \sum_{r=1}^{s} L(r) t_{40}(E_{Fs}, n_z)$.

1.2.8 The EEM in UFs of Gallium Phosphide

The energy spectrum of the conduction electrons in n-GaP can be written as [227]

$$E = \frac{\hbar^2 k_s^2}{2m_\perp^*} + \frac{\hbar^2}{2m_{||}^*}[\overline{A}' k_s^2 + k_z^2] - \left[\frac{\hbar^4 k_0^2}{m_{||}^{*2}}(k_s^2 + k_z^2) + |V_G|^2\right]^{1/2} + |V_G| \tag{1.111}$$

where, K_0 and $|V_G|$ are constants of the energy spectrum and $\overline{A}' = 1$.

The 2D electron dispersion relation in size quantized n-GaP can be expressed as

$$E = a k_s^2 + C(n_z \pi / d_z)^2 + |V_G| - \left[D k_s^2 + |V_G|^2 + D(n_z \pi / d_z)^2\right]^{1/2} \tag{1.112}$$

in which, $a \equiv \frac{\hbar^2}{2m_\perp^*} + \frac{\hbar^2}{2m_{||}^*}$, $C \equiv \frac{\hbar^2}{2m_{||}^*}$ and $D \equiv (\hbar^2 k_0 / m_{||}^*)^2$

The subband energy ($E_{n_{z13}}$) are given by

$$E_{n_{z13}} = C(\pi n_z / d_z)^2 + |V_G| - \left[|V_G|^2 + D(\pi n_z / d_z)^2\right]^{1/2} \tag{1.113}$$

Equation (1.112) can be expressed as

$$k_s^2 = t_{42}(E, n_z) \tag{1.114}$$

in which, $t_{42}(E, n_z) \equiv [\{2a(E - t_1) + D\} - \{[2a(E - t_1) + D]^2 - 4a^2[(E - t_1)^2 - t_2]\}^{1/2}]$, $t_1 \equiv |V_G| + C(\pi n_z / d_z)^2$ and $t_2 \equiv |V_G|^2 + D(\pi n_z / d_z)^2$

The EEM can be expressed from (1.114) as

$$m^*(E_{Fs}, n_z) = \frac{\hbar^2}{2} t'_{42}(E_{Fs}, n_z) \tag{1.115}$$

It appears that the EEM in UFs of GaP is a function of Fermi energy and size quantum number due to the presence of the system constant k_0 .

The total DOS function is given by

$$N_{2DT}(E) = \frac{g_v}{4\pi a^2} \sum_{n_z=1}^{n_{z_{max}}} \left[t'_{42}(E, n_z)\right] H(E - E_{n_{z13}}) \tag{1.116}$$

The electron statistics in UFs in n-GaP assumes the form

$$n_{2D} = \frac{g_v}{4\pi a^2} \sum_{n_z=1}^{n_{z_{max}}} \left[t_{42}(E_{Fs}, n_z) + t_{43}(E_{Fs}, n_z)\right] \tag{1.117}$$

where, $t_{43}(E_{Fs}, n_z) \equiv \sum_{r=1}^{s} L(r) \left[t_{42}(E_{Fs}, n_z)\right]$

1.2.9 The EEM in UFs of Platinum Antimonide

The dispersion relation for the n-type $PtSb_2$ can be written as [228]

$$\left(E + \lambda_0 \frac{(\bar{\bar{a}})^2}{4} k^2 - l k_s^2 \frac{(\bar{\bar{a}})^2}{4}\right)\left(E + \delta_0 - \nu \frac{(\bar{\bar{a}})^2}{4} k^2 - \bar{\bar{n}} \frac{(\bar{\bar{a}})^2}{4} k_s^2\right) = I \frac{(\bar{\bar{a}})^4}{16} k^4 \tag{1.118}$$

where $\omega_1 \equiv \left(\lambda_0 \frac{(\bar{\bar{a}})^2}{4} - l \frac{(\bar{\bar{a}})^2}{4}\right), \omega_2 \equiv \lambda_0 \frac{(\bar{\bar{a}})^2}{4}, \omega_3 \equiv \left((\bar{\bar{n}}) \frac{(\bar{\bar{a}})^2}{4} + \nu \frac{(\bar{\bar{a}})^2}{4}\right), \omega_4 \equiv \nu \frac{(\bar{\bar{a}})^2}{4}, I_1 \equiv I \left(\frac{(\bar{\bar{a}})^2}{4}\right)^2$, $\lambda_0, l, \delta_0, \nu$ and $\bar{\bar{n}}$ are the band constants and $\bar{\bar{a}}$ is the lattice constant.

The (1.118) can be expressed as

$$\left[E + \omega_1 k_s^2 + \omega_2 k_z^2\right]\left[E + \delta_0 - \omega_3 k_s^2 - \omega_4 k_z^2\right] = I_1 (k_z^2 + k_s^2)^2 \tag{1.119}$$

The use of (1.119) leads to the expression of the 2D dispersion law in UFs of n-$PtSb_2$ as

$$k_s^2 = t_{44}(E, n_z) \tag{1.120}$$

where,

$$t_{44}(E, n_z) = [2A_9]^{-1}\left[-A_{10}(E, n_z) + \sqrt{A_{10}^2(E, n_z) + 4A_9 A_{11}(E, n_z)}\right] \tag{1.121}$$

$A_9 = [I_1 + \omega_1 \omega_3]$, $A_{10}(E, n_z)$

$$= \left[\omega_3 E + \omega_1 \left\{E + \delta_0 - \omega_4 \left(\frac{\pi n_z}{d_z}\right)^2\right\} + \omega_2\omega_3 \left(\frac{\pi n_z}{d_z}\right)^2 + 2I_1 \left(\frac{\pi n_z}{d_z}\right)^2\right]$$

and

$$A_{11}(E, n_z) \equiv \left[E\left[E + \delta_0 - \omega_4 \left(\frac{\pi n_z}{d_z}\right)^2\right] + \omega_2 \left(\frac{\pi n_z}{d_z}\right)^2 \left[E + \delta_0 - \omega_4 \left(\frac{\pi n_z}{d_z}\right)^2\right] - I_1 \left(\frac{\pi n_z}{d_z}\right)^4\right]$$

The area of k_s space can be expressed as

$$A(E, n_z) = \frac{\pi}{2A_9} t_{44}(E, n_z) \tag{1.122}$$

The EEM can be written as

$$m^*(E_{Fs}, n_z) = \frac{\hbar^2}{4A_9} t'_{44}(E_{Fs}, n_z) \tag{1.123}$$

It appears that the EEM in UFs of $PtSb_2$ is a function of Fermi energy and size quantum number which is the characteristic features of such systems.

The total DOS function assumes the form

$$N_{2DT}(E) = \frac{g_v}{4\pi A_9} \sum_{n_z=1}^{n_{zmax}} [t'_{44}(E, n_z)] H(E - E_{n_{z14}}) \tag{1.124}$$

where the quantized levels $E_{n_{z14}}$ can be expressed through the equation

$$E_{n_{z14}} = (2)^{-1}\left[-\left[\omega_2 \left(\frac{\pi n_z}{d_z}\right)^2 + \delta_0 - \omega_4 \left(\frac{\pi n_z}{d_z}\right)^2\right] + \left\{\left[\omega_2 \left(\frac{\pi n_z}{d_z}\right)^2 + \delta_0 - \omega_4 \left(\frac{\pi n_z}{d_z}\right)^2\right]^2 + 4\left[I_1 \left(\frac{\pi n_z}{d_z}\right)^4 + \omega_2\omega_4 \left(\frac{\pi n_z}{d_z}\right)^4 - \omega_2\delta_0 \left(\frac{\pi n_z}{d_z}\right)^2\right]\right\}^{1/2}\right] \tag{1.125}$$

The electron statistics can be written as

$$n_{2D} = \frac{2g_v}{(2\pi)^2}\frac{\pi}{2A_9}\sum_{n_z=1}^{n_{zmax}}\int_{E_{nz}}^{\infty}\frac{\partial}{\partial E}[t_{44}(E,n_z)]f(E)dE$$

$$n_{2D} = \frac{g_v}{4\pi A_9}\sum_{n_z=1}^{n_{zmax}}[t_{44}(E_{Fs},n_z)+t_{45}(E_{Fs},n_z)] \tag{1.126}$$

where $t_{45}(E_{Fs},n_z) \equiv \sum_{r=1}^{s} L(r)[t_{44}(E_{Fs},n_z)]$

1.2.10 The EEM in UFs of Bismuth Telluride

The dispersion relation of the conduction electron Bi_2Te_3 can be written as [229–231]

$$E(1+\alpha E) = \overline{\omega}_1 k_x^2 + \overline{\omega}_2 k_y^2 + \overline{\omega}_3 k_z^2 + 2\overline{\omega}_4 k_z k_y \tag{1.127}$$

where

$$\overline{\omega}_1 = \frac{\hbar^2}{2m_0}\overline{\alpha}_{11}, \overline{\omega}_2 = \frac{\hbar 2}{2m_0}\overline{\alpha}_{22}, \overline{\omega}_3 = \frac{\hbar^2}{2m_0}\overline{\alpha}_{33}, \overline{\omega}_4 = \frac{\hbar^2}{2m_0}\overline{\alpha}_{23}$$

in which $\overline{\alpha}_{11}, \overline{\alpha}_{22}, \overline{\alpha}_{33}$ and $\overline{\alpha}_{23}$ are system constants.

The 2D electron dispersion law in UFs of $Bi_2\ Te_3$ assumes the form

$$E(1+\alpha E) = \overline{\omega}_1(\frac{n_x\pi}{d_x})^2 + \overline{\omega}_2 k_y^2 + \overline{\omega}_3 k_z^2 + 2\overline{\omega}_4 k_z k_y \tag{1.128}$$

The area of the ellipse is given by

$$A_n(E,n_z) = \frac{\pi}{\sqrt{\overline{\alpha}_{22}\overline{\alpha}_{33}-4\overline{\alpha}_{23}^2}}\left[\frac{2m_0E(1+\alpha E)}{\hbar^2} - \overline{\alpha}_{11}(\frac{n_x\pi}{d_x})^2\right] \tag{1.129}$$

The EEM can be expressed as

$$m^*(E_{Fs}) = \frac{m_0(1+2\alpha E_{Fs})}{\sqrt{\overline{\alpha}_{22}\overline{\alpha}_{33}-4\overline{\alpha}_{23}^2}} \tag{1.130}$$

It appears that the EEM in UFs of Bi_2Te_3 is a function of Fermi energy due to the presence of the band nonparabolicity.

The total DOS function assumes the form

$$N_{2DT}(E) = \frac{g_v m_0}{\pi\hbar^2\sqrt{\overline{\alpha}_{22}\overline{\alpha}_{33} - 4\overline{\alpha}_{23}{}^2}} \sum_{n_z=1}^{n_x max} (1 + 2\alpha E) H(E - E_{n_{z15}}) \tag{1.131}$$

where, $(E_{n_{z15}})$ can be expressed through the equation

$$E_{n_{z15}}(1 + \alpha E_{n_{z15}}) = \overline{\omega}_1 \left(\frac{n_x \pi}{d_x}\right)^2 \tag{1.132}$$

The electron concentration can be written as

$$n_{2D} = \frac{k_B T g_v}{\pi\hbar^2} \left(\frac{m_0}{\sqrt{\overline{\alpha}_{22}\overline{\alpha}_{33} - 4\overline{\alpha}_{23}{}^2}}\right) \sum_{n_z=1}^{n_{zmax}} [(1 + 2\alpha E_{n_{z15}}) F_0(\eta_{n_{15}}) + 2\alpha k_B T F_1(\eta_{n15})] \tag{1.133}$$

where, $\eta_{n_{15}} = \frac{E_{Fs} - E_{n_{z15}}}{k_B T}$.

1.2.11 The EEM in UFs of Germanium

It is well known that the conduction electrons $n-Ge$ obey two different types of dispersion laws since band nonparabolicity has been included in two different ways as given in the literature [232, 234].

a. The energy spectrum of the conduction electrons in bulk specimens of $n-Ge$ can be expressed in accordance with Cardona et al. [232, 233] as

$$E = -\frac{E_{g0}}{2} + \frac{\hbar^2 k_z^2}{2m_{\parallel}^*} + \left[\frac{E_{g0}^2}{4} + E_{g0} k_s^2 \left(\frac{\hbar^2}{2m_{\perp}^*}\right)\right]^{\frac{1}{2}} \tag{1.134}$$

where in this case $m_{\parallel}^*$ and $m_{\perp}^*$ are the longitudinal and transverse effective masses along <111> direction at the edge of the conduction band respectively.
Equation (1.134) can be written as

$$\frac{\hbar^2 k_s^2}{2m_{\perp}^*} = E(1 + \alpha E) + \alpha \left(\frac{\hbar^2 k_z^2}{2m_{\parallel}^*}\right) - (1 + 2\alpha E)\left(\frac{\hbar^2 k_z^2}{2m_{\parallel}^*}\right) \tag{1.135}$$

In the presence of size quantization along k_z direction, the 2D dispersion relation of the conduction relations in UFs of n-Ge can be written by extending the method as given in [235] as

$$\frac{\hbar^2 k_x^2}{2m_1^*} + \frac{\hbar^2 k_y^2}{2m_2^*} = \gamma(E, n_z) \tag{1.136}$$

where, $m_1^* \equiv m_\perp^*, \quad m_2^* = \frac{m_\perp^* + 2m_\parallel^*}{3}$,

$$\gamma(E, n_z) \equiv \left[E(1+\alpha E) - (1+2\alpha E)\frac{\hbar^2}{2m_3^*}\left(\frac{n_z\pi}{d_z}\right)^2 + \alpha\left[\frac{\hbar^2}{2m_3^*}\left(\frac{n_z\pi}{d_z}\right)^2\right]^2\right]$$

and $m_3^* = \frac{3m_\parallel^* m_\parallel^*}{2m_\parallel^* + m_\perp^*}$

The area of ellipse of the 2D surface as given by (1.136) can be written as

$$A(E, n_z) = \frac{2\pi\sqrt{m_1^* m_2^*}}{\hbar^2}\gamma(E, n_z) \tag{1.137}$$

The EEM can be expressed using (1.137) as

$$m^*(E_{Fs}, n_z) \equiv \sqrt{m_1^* m_2^*}\left[(1+2\alpha E_{Fs}) - (2\alpha)\frac{\hbar^2}{2m_3^*}\left(\frac{n_z\pi}{d_z}\right)^2\right] \tag{1.138}$$

Therefore, the EEM is a function of Fermi energy and size quantum number due to the presence of band nonparabolicity only.

The DOS function per subband can be expressed as

$$N_{2D}(E) = \frac{4\sqrt{m_1^* m_2^*}}{\pi\hbar^2}\left[1 + 2\alpha E - 2\alpha\left(\frac{\hbar^2}{2m_3^*}\left(\frac{\pi n_z}{d_z}\right)^2\right)\right] \tag{1.139}$$

The total DOS function is given by

$$N_{2DT}(E) = \frac{4}{\pi\hbar^2}\sqrt{m_1^* m_2^*}\sum_{n_z=1}^{n_{zmax}} \times\left[1 + 2\alpha E - 2\alpha\left(\frac{\hbar^2}{2m_3^*}\left(\frac{\pi n_z}{d_z}\right)^2\right)\right] H(E - E_{n_z 16}) \tag{1.140}$$

where, $E_{n_{z16}}$ is the positive root of the following equation

$$E_{n_{z16}}(1+\alpha E_{n_{z16}}) - (1+2\alpha E_{n_{z16}})\left(\frac{\hbar^2}{2m_3^*}\left(\frac{\pi n_z}{d_z}\right)^2\right) + \alpha\left(\frac{\hbar^2}{2m_3^*}\left(\frac{\pi n_z}{d_z}\right)^2\right)^2 = 0 \tag{1.141}$$

Thus combining (1.140) with the Fermi Dirac occupation probability factor, the electron statistics in this case can be written as

$$n_{2D} = \frac{4\sqrt{m_1^* m_2^*} k_B T}{\pi \hbar^2} \sum_{n_z=1}^{n_{zmax}} \left[(A_1(n_z) + 2\alpha E_{n_{z16}}) F_0(E_{n_{z16}}) + 2\alpha k_B T F_1(E_{n_{z16}}) \right] \tag{1.142}$$

where $A_1(n_z) \equiv \left[1 + 2\alpha(\hbar^2/2m_3^*)(\pi n_z/d_z)^2\right]$ and $\eta_{n_{z16}} \equiv \frac{1}{K_B T}[E_{F2D} - E_{n_{z16}}]$

b. The dispersion relation of the conduction electron in bulk specimens of $n-Ge$ can be expressed in accordance with the model of Wang and Ressier [234] and can be written as

$$E = \frac{\hbar^2 k_z^2}{2m_\parallel^*} + \frac{\hbar^2 k_s^2}{2m_\perp^*} - \overline{c}_1 \left(\frac{\hbar^2 k_s^2}{2m_\perp^*}\right)^2 - \overline{d}_1 \left(\frac{\hbar^2 k_s^2}{2m_\perp^*}\right)\left(\frac{\hbar^2 k_z^2}{2m_\parallel^*}\right) - \overline{e}_1 \left(\frac{\hbar^2 k_z^2}{2m_\parallel^*}\right)^2 \tag{1.143}$$

where $\overline{c}_1 = \overline{C}(2m_\perp^*/\hbar^2)^2, \overline{C} = 1.4\overline{A}, \overline{A} = \frac{1}{4}(\hbar^4/E_{g0}m_\perp^{*2})\left(1 - \frac{m_\perp^*}{m_0}\right)^2, \overline{d}_1 = \overline{d}\left(\frac{4m_\perp^* m_\parallel^*}{\hbar^4}\right), \overline{d} = 0.8\overline{A}, \overline{e}_1 = \overline{e}_0(2m_\parallel^*/\hbar^2)^2$ and $\overline{e}_0 = 0.005\overline{A}$.

Therefore the 2D dispersion law can be expressed as

$$E = A_5(n_z) + A_6(n_z)\beta - \overline{c}_1\beta^2 \tag{1.144}$$

where $A_5(n_z) \equiv \frac{\hbar^2}{2m_3^*}\left(\frac{\pi n_z}{d_z}\right)^2 \left[1 - \overline{e}_1\left(\frac{\hbar^2}{2m_3^*}\right)\left(\frac{\pi n_z}{d_z}\right)^2\right]$,

$A_6(n_z) \equiv \left[1 - \overline{d}_1\left(\frac{\hbar^2}{2m_3^*}\right)\left(\frac{n_z\pi}{d_z}\right)^2\right]$ and $\beta \equiv \frac{\hbar^2 k_x^2}{2m_1^*} + \frac{\hbar^2 k_y^2}{2m_2^*}$.

Equation (1.144) can be written as

$$\frac{\hbar^2 k_x^2}{2m_1^*} + \frac{\hbar^2 k_y^2}{2m_2^*} = I_1(E, n_z) \tag{1.145}$$

where $I_1(E, n_z) \equiv (2\overline{c}_1)^{-1}\left[A_6(n_z) - \left[A_6^2(n_z) - 4\overline{c}_1 E + 4\overline{c}_1 A_5(n_z)\right]^{1/2}\right]$

From (1.145), the area of the 2D k_s -space is given by

$$A(E, n_z) = \frac{2\pi\sqrt{m_1^* m_2^*}}{\hbar^2} I_1(E, n_z) \tag{1.146}$$

The EEm can be expressed using (1.146) as

$$m^*(E_{Fs}, n_z) \equiv \sqrt{m_1^* m_2^*}[I_1(E_{Fs}, n_z)]' \tag{1.147}$$

where $\{I_1(E, n_z)\}' \equiv \frac{\partial}{\partial E}[I_1(E, n_z)]$

Therefore, the EEM according to this model is a function of Fermi energy and size quantum number due to the presence of band nonparabolicity only

The DOS function per subband can be written as

$$N_{2D}(E) = \frac{4}{\pi}\frac{\sqrt{m_1^* m_2^*}}{\hbar^2}\{I_1(E, n_z)\}' \tag{1.148}$$

The total DOS function assumes the form

$$N_{2DT}(E) = \frac{4\sqrt{m_1^* m_2^*}}{\pi\hbar^2}\sum_{n_z=1}^{n_{zmax}}\{I_1(E, n_z)\}' H(E - E_{n_{z17}}) \tag{1.149}$$

where, the subband energy $E_{n_{z17}}$ are given by

$$E_{n_{z17}} = \frac{\hbar^2}{2m_3^*}\left(\frac{\pi n_z}{d_z}\right)^2\left[1 - \bar{e_1}\left(\frac{\hbar^2}{2m_3^*}\right)\left(\frac{\pi n_z}{d_z}\right)^2\right] \tag{1.150}$$

The electron statistics can be written as

$$n_{2D} = \frac{4\sqrt{m_1^* m_2^*}}{\pi\hbar^2}\sum_{n_z=1}^{n_{zmax}}[t_{46}(E_{Fs}, n_z) + t_{47}(E_{Fs}, n_z)] \tag{1.151}$$

where $t_{46}(E_{Fs}, n_z) \equiv I_1(E_{Fs}, n_z)$, $t_{47}(E_{Fs}, n_z) \equiv \sum_{r=1}^{S} L(r)(t_{46}(E_{Fs}, n_z))$.

1.2.12 The EEM in UFs of Gallium Antimonide

The dispersion relation of the conduction electrons in n-GaSb can be written as [236]

$$E = \frac{\hbar^2 k^2}{2m_0} - \frac{\bar{E}'_{g0}}{2} + \frac{\bar{E}'_{g0}}{2}\left[1 + \frac{2\hbar^2 k^2}{\bar{E}'_{g0}}\left(\frac{1}{m_c} - \frac{1}{m_0}\right)\right]^{\frac{1}{2}} \tag{1.152}$$

where $\overline{E}'_{g0} = \left[E_{g0} + \frac{5.10^{-5}T^2}{2(112+T)}\right]$ eV

Equation (1.152) can be expressed as

$$\frac{\hbar^2 k^2}{2m_c} = I_{36}(E) \tag{1.153}$$

where

$$I_{36}(E) = [E + \bar{E}'_{g0} - (m_c/m_o)(\bar{E}'_{g0}/2) - [(\bar{E}'_{g0}/2)^2 + [((\bar{E}'_{g0})^2/2)(1 - (m_c/m_0))] + [(\bar{E}'_{g0}/2)(1 - (m_c/m_0))]^2 + E\bar{E}'_{g0}(1 - (m_c/m_0))]^{1/2}]$$

The 2D electron dispersion relation in this case assumes the form

$$\frac{\hbar^2 k_s^2}{2m_c} + \frac{\hbar^2}{2m_c}(n_z\pi/d_z)^2 = I_{36}(E) \tag{1.154}$$

Using (1.154) , the EEM in x–y plane for this case can be written as

$$m^*(E_{Fs}) = m_c\{I_{36}(E_{Fs})\}' \tag{1.155}$$

It appears that the EEM in this case is a function of Fermi energy alone and is independent of size quantum number.

The total 2D DOS function can be written as

$$N_{2DT}(E) = \left(\frac{m_c g_v}{\pi\hbar^2}\right)\sum_{n_z=1}^{n_{zmax}}\left\{[I_{36}(E)]' H(E - E_{n_{z17}})\right\} \tag{1.156}$$

where, the subband energies $E_{n_{z17}}$ can be expressed as $\overset{\circ}{u}$

$$I_{36}(E_{n_{z17}}) = \frac{\hbar^2}{2m_c}(n_z\pi/d_z)^2 \tag{1.157}$$

The 2D carrier concentration assumes the form

$$n_{2D} = \left(\frac{m_c g_v}{\pi\hbar^2}\right)\sum_{n_z=1}^{n_{zmax}}[t_{55}(E_{Fs}, n_z) + t_{56}(E_{Fs}, n_z)] \tag{1.158}$$

where $t_{55}(E_{Fs}, n_z) \equiv \left[I_{36}(E_{Fs}) - \frac{\hbar^2}{2m_c}\left(\frac{n_z\pi}{d_z}\right)^2\right]$

and $t_{56}(E_{Fs}, n_z) \equiv \sum_{r=1}^{s} L(r)t_{55}(E_{Fs}, n_z)$

1.3 Results and Discussions

Using (1.5) and (1.9) and taking the energy band constants as given in Table 1.1, we have plotted Fig. 1.1. The EEM in UFs of Cd_3As_2 as a function of film thickness and have been shown in Fig 1.1. For comparison, we have also plotted the EEM in the absence of the crystal-field splitting for the three- and the two-band models of Kane. Figure 1.1 exhibits the effect of size quantization on the EEM in general, and bears a good amount of discussion. It appears that the effect of van Hove singularity makes the EEM to suffer severe discontinuities. Assuming a carrier degeneracy of 10^{15} m^{-2}, Fig. 1.1a shows that the EEM can reach upto about 10% of its free

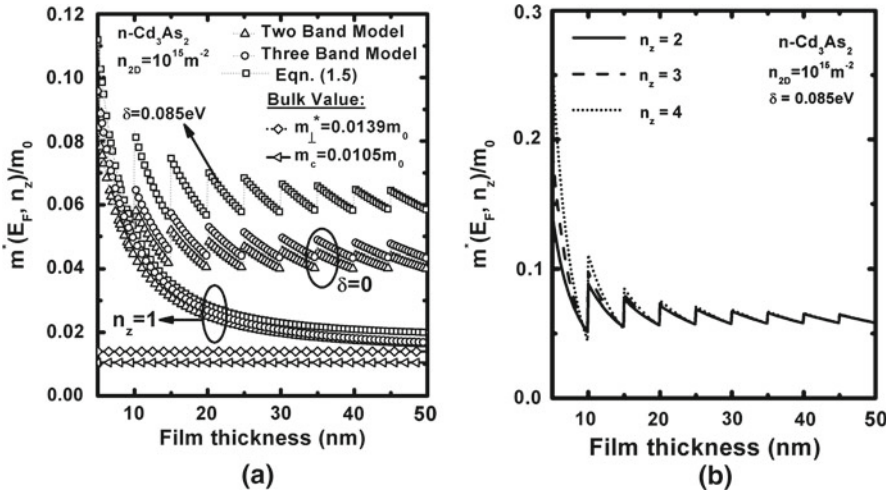

Fig. 1.1 **a** Plot of the EEM as function of film thickness for UFs of n-Cd_3As_2 considering (1.5). The *plots* for three-and two-band models of Kane have also been exhibited in which, $m_{\perp}^{*} = 0.0139m_0$ and $m_c = \frac{1}{2}(m_{11}^{*} + m_{\perp}^{*})m_0 = 0.0105m_0$ are the corresponding bulk values. **b** Plot of the EEM as function of film thickness for UFs of n-Cd_3As_2 for all cases of Fig. 1.1a at different three subband levels

mass at a film thickness of 5 nm, which is quite high from its bulk value and may degrade the carrier mobility to a great extent. In the same figure, we have also demonstrated the effect of assuming only the lowest level subband. It appears that with this approximation, the EEM approaches to the bulk value $m_{\perp}^{*} = 0.0139m_0$ more quickly than that by considering the subbands. With this, it is now more obvious to note that the assumption of a single subband occupancy throughout leads to the practical approach to the determination of EEM. All the models of the single subband occupied curves tend to merge with the bulk value near 50 nm thickness. The increase in the EEM with the reduction of film thickness is due to the increased Fermi energy of the material. It must be noted that with such a highly doped system, the Fermi energy is determined by the carrier statistics equation. It is this Fermi energy which should be used in the determination of the EEM. This is not the case in an intrinsic material. In such a case, the Fermi energy coincides with the intrinsic energy level, which is very near to the energy band gap of the material and thus the variation of the energy band gap with the film thickness needs great concern. The variation of the energy band gap however is significant at extremely narrow film thickness, more in the region below sub-4 nm, a context which shall be highlighted in Chap. 8, where Applications and brief review of experimental results have been discussed. Thus, all the curves below such thickness are expected to suffer deviation with our existing theoretical model, if plotted. In all the subsequent geometry dependent curves, we have restricted ourselves above sub-4 nm regime. Since Cd_3As_2 crystals are usually grown as degenerate n-type specimens, the Fermi level mass will be the effective

mass of consideration for transport in Cd_3As_2. Hence in the quantum limit, the effective mass at the Fermi level corresponding to the lowest electric sub-band will be the effective conductivity mass for electron transport in Cd_3As_2. It appears from these figures that the Fermi level mass is significantly influenced by the effects of size quantization particularly in tetragonal semiconductors like n- Cd_3As_2 having crystalline field effects and energy-dependent anisotropy of the effective mass. It has been found that the effective mass at the Fermi level depends on the size quantum number due to the combined influence of crystal-field splitting and the anisotropic spin-orbit splitting constant, resulting in different effective masses at the Fermi level corresponding to different electric subbands (the different effective masses being the same in the absence of field splitting as can be seen from Fig. 1.1a and b). It has further been observed that the different effective masses corresponding to different electric subbands closely approach each other, for a given film thickness, with increasing electron concentration and for a given electron concentration, with increasing film thickness. These are in conformity with expectations since both with increasing electron concentration at a given film thickness and with increasing film thickness for a given electron concentration, the effects of size quantization gradually become less and less significant. As in bulk specimens, the Fermi level mass increases with increasing carrier concentration at a given value of the film thickness. Besides, for particular values of the film thickness and electron concentration, the combined effect of $\delta \neq 0$ and $\Delta_{11} \neq \Delta_{\perp}$effect of crystal-field splitting is to reduce the effective mass corresponding to any particular subband. It may further be noted that if the direction normal to the film is taken as one of the transverse directions of the single ellipsoid at the zone center and not as the longitudinal direction as assumed in the present chapter, the effective mass at the Fermi level corresponding to any given subband would be somewhat different. Nevertheless, since the mass anisotropy in $Cd_3As_2$is indeed small as can be seen from the values of $P_{11}$and $P_{\perp}$ which are very close to each other, the arbitrary choice of the direction normal to the film with respect to the major axis of the ellipsoid would not result in a significant change in the effective mass at the Fermi level corresponding to a particular subband. The Fermi level mass should gradually become closer to that of bulk specimens with increasing film thickness since, for such thicknesses, the effects of size quantization are greatly diminished. This has also been confirmed in our present work. Furthermore, the general features of the effects of size quantization on the effective mass as discussed here would also be valid with the only exception that the effective mass at the Fermi level will be independent of the size quantum number in the absence of crystal-field splitting and anisotropic spin-orbit splitting constant for the III-V small-gap semiconductors since these semiconductors have nonparabolic energy bands obeying Kane's dispersion relation and the present chapter is based on the generalized Kane's model.

Figure 1.2 exhibits the plot EEM in UFs of n-$CdGeAs_2$ as a function of film thickness in accordance with the three- and two-band models of Kane together with the incorporation of the crystal-field parameter. It appears that the effect of the crystal-field splitting increases the EEM sharply below sub-20 nm. The EEM also increases about 7 % at 5 nm and converges to its bulk value beyond 20 nm at the same value of electron degeneracy. The effect of film thickness on the EEM of III-V semiconduc-

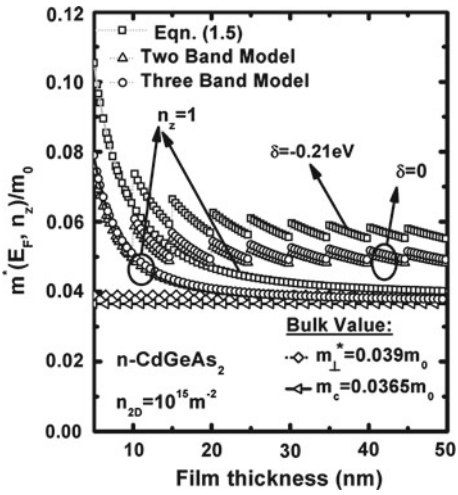

Fig. 1.2 Plot of the EEM as function of film thickness for UFs of n-$CdGeAs_2$ for all the cases of Fig. 1.1 in which, $m_{\perp}^{*} = 0.039m_0$ and $m_c = \frac{1}{2}\left(m_{11}^{*} + m_{\perp}^{*}\right)m_0 = 0.0105m_0$ are the corresponding bulk values

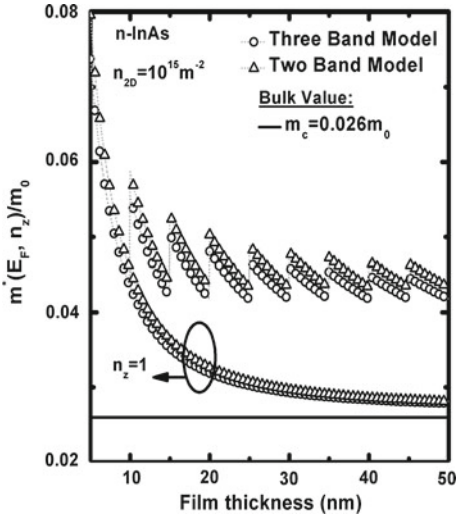

Fig. 1.3 Plot of the EEM as function of film thickness for UFs of n-InAs in accordance with the three- and the two-band model of Kane

tors, most important with respect to extremely low field high mobility of which are n-InAs, n-InSb, and n-GaAs has been exhibited in Figs. 1.3,1.4 and 1.5, respectively.

The effect of nonlinearity of the energy band structure on the respective EEMs has been clearly indicated. It appears that in the determination of the EEM, it is sufficient to take the two band model of Kane to explain the variation of the EEM over a wide range of thickness. The deviation from the three-band model of Kane is much less indicating that the complexity in the energy band model can be reduced to a large extent by considering only the two-band model of Kane. This is extremely important with respect to the numerical computation in device analyses performance where sufficient longer computation time affects the efficiency in characterizing the

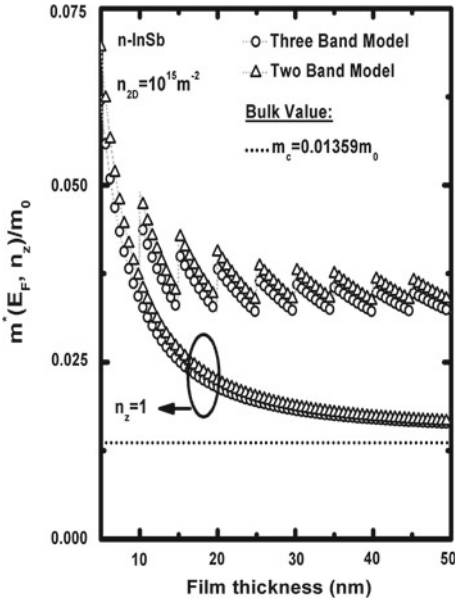

Fig. 1.4 Plot of EEM as function of film thickness for UFs of n-InSb for all the cases of Fig. 1.3

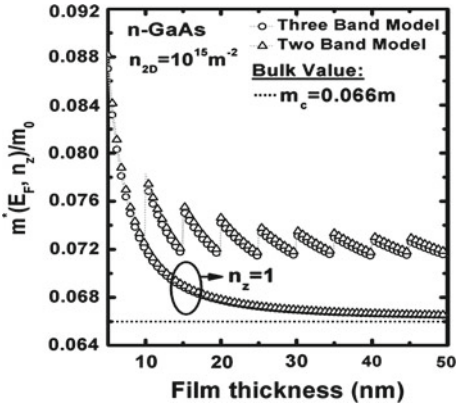

Fig. 1.5 Plot of the EEM as function of film thickness for UFs of n-GaAs for all the cases of Fig. 1.3

compact model with respect to the said materials. In all the Figs. 1.3, 1.4, 1.5, we have demonstrated the effect of two widely known models viz. the three and the two band models. Figures 1.6 and 1.7 exhibits the variation of the EEM with respect to the film thickness for the ternary and quaternary materials at same carrier degeneracy level. It appears that at an alloy composition $x = 0.3$, the EEM in both the cases tends to about 0.1 times the rest mass at film thickness of 5 nm. The effect of variation of EEM on the alloy composition for these two materials has been exhibited in Fig. 1.8.

The effect of increasing the alloy composition increases the EEM for the said two materials. For the purpose of comparison, we have also plotted the variation of

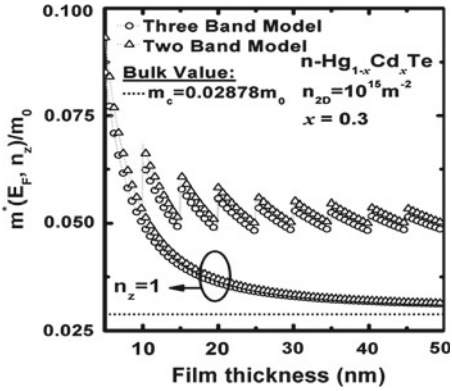

Fig. 1.6 Plot of the EEM as function of film thickness for UFs of n-$Hg_{0.3}Cd_{0.7}Te$ for all the cases of Fig. 1.3

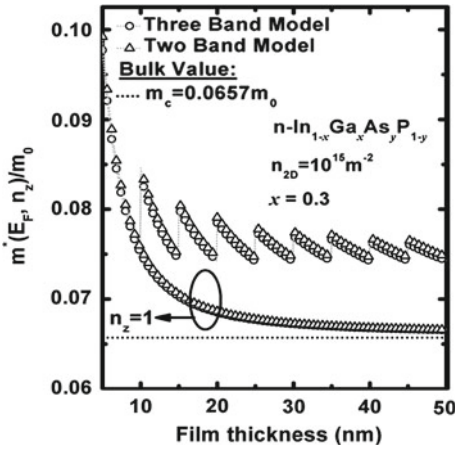

Fig. 1.7 Plot of the EEM as function of film thickness for UFs of n-$In_{1-x}Ga_xAs_yP_{1-y}$ for all the cases of Fig. 1.3

the bulk effective mass with the alloy composition. For the quaternary material, the difference between the two energy band models is not much, as can also be seen from Figs. 1.6 and 1.7. The increment in EEM is rather linear in case of InGaAsP than that of HgCdTe. This also exhibits the variation of the electron mobility in these systems as the alloy composition changes. It appears that with increase in x, the mobility falls down assuming a constant relaxation rate.

The effect of carrier degeneracy on the EEM in nonlinear optical, III-V, ternary and quaternary materials have been exhibited in Figs. 1.9, 1.10, 1.11, 1.12, 1.13, 1.14, 1.15. It appears that the EEM for all the aforementioned materials at 10 nm film thickness are almost invariant below sub 10^{15} m^{-2}. The effect of inclusion of both the higher order subbands and the lowest subband has been exhibited. From all the curves, it appears that the EEM bears almost exponential relation with the carrier degeneracy. This notion comes straightforward from the carrier concentration relation (1.27).

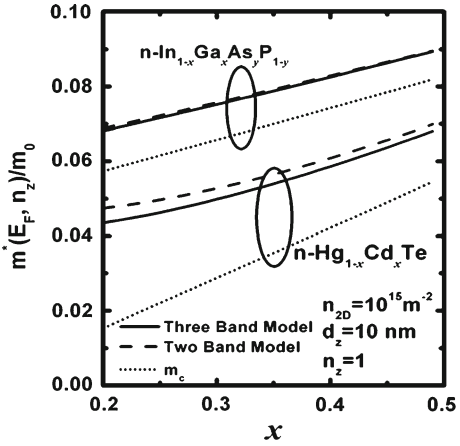

Fig. 1.8 Plot of the EEM at the lowest subband as function of alloy composition in UFs of n-$Hg_{1-x}Cd_x$ Te and n-$In_{1-x}Ga_xAs_yP_{1-y}$ for the three and the two band models of Kane respectively

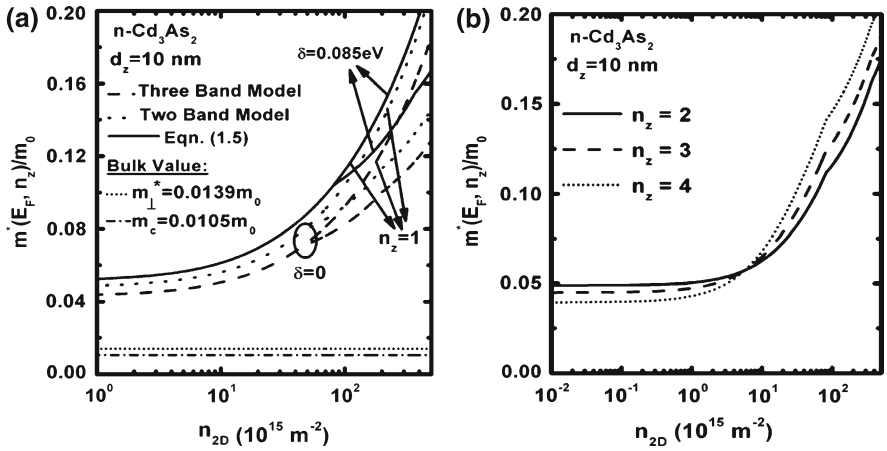

Fig. 1.9 **a** Plot of the EEM as function of surface electron concentration in UFs of n-Cd_3As_2. The plots for three- and two-band models of Kane have also been exhibited in which, $m_{\perp}^{*} = 0.0139m_0$ and $m_c = \frac{1}{2}\left(m_{11}^{*} + m_{\perp}^{*}\right)m_0 = 0.0105m_0$ are the corresponding bulk values. **b** Plot of the EEM as function of surface electron concentration in UFs of n-Cd_3As_2 at different subband levels for all cases of Fig. 1.9

The variation of the EEM in II-VI materials like p-CdS has been exhibited in Figs. 1.16 and 1.17 as functions of film thickness and Fermi energy respectively. In these two figures, instead of obtaining the Fermi energy from the corresponding carrier statistics, we have followed the opposite route, i.e., what values of the Fermi energy makes the EEM to be very low or very high. A corresponding concentration of that order can then be evaluated. A decision of this kind aids a good amount of estimation in the optimization. Using this approach, we estimate that the EEM can

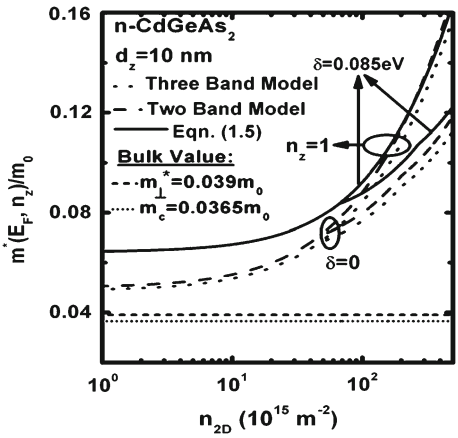

Fig. 1.10 Plot of the EEM as function of surface electron concentration in UFs of n-$CdGeAs_2$ for all the cases of Fig. 1.9

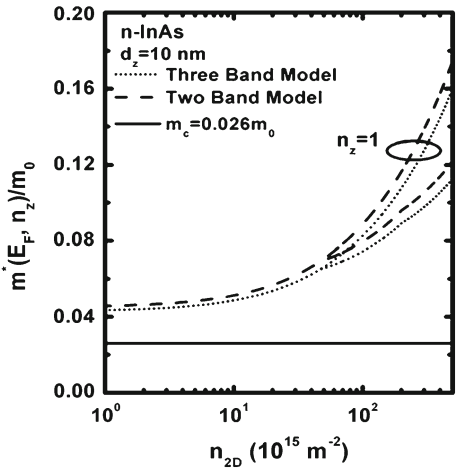

Fig. 1.11 Plot of the EEM as function of surface electron concentration in UFs of n-InAs

soar up to 0.77 times rest mass in the higher valley, while for the lower valley, it may plunge upto about 0.55 times rest mass.

The effect of valley degeneracy as we see from these two curves expresses much in understanding the electron transport direction.

It appears from the two curves that the channel oriented along the lower valley direction will most probably result in an increased value of current due to the low EEM. It would have been of much interest to figure out how the energy band gap at the two valleys changes with respect to the thickness and is left as an exercise to the reader.

Figures 1.18 and 1.19 exhibit the effect of film thickness and the carrier concentration on the EEM of UFs of Bismuth. The effect of increasing the carrier degeneracy has also been exhibited in Fig. 1.18. It appears that the EEM increases from its cor-

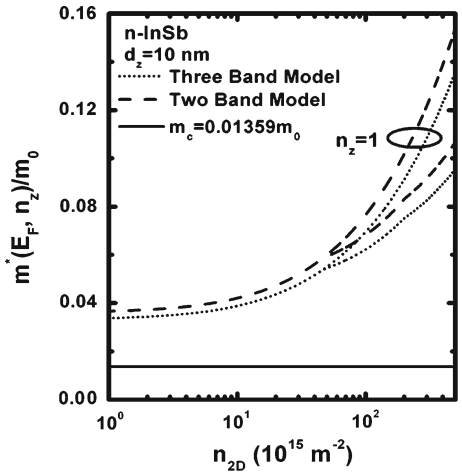

Fig. 1.12 Plot of the EEM as function of surface electron concentration in UFs of n-InSb

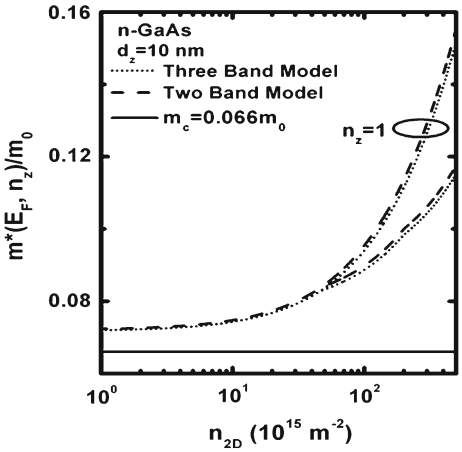

Fig. 1.13 Plot of the EEM as function of surface electron concentration in UFs of n-GaAs

responding bulk value sharply at the 5 nm film thickness implying a tremendous decrease in the carrier mobility.

Figure 1.19 exhibits the effect of different energy band model of Bi on EEM for a varying surface electron concentration. It appears that at the lowest subband energy level, there is almost no difference between the Mc Clure and Cohen model extracted EEM, however there is a significant change in the Hybrid and Lax ellipsoidal model. Figures 1.20, 1.21, and 1.22 exhibit the variation of the EEM at the lowest subband level for QWs of IV-VI, strained InSb and Ge. The effective mass in IV-VI materials exhibits strong variation for PbTe, an excellent thermoelectric material, whereas least for PbSnSe. It also appears that the EEM of PbTe is higher than that of PbSnSe and PbSnTe. With the advent of strained quantum effect devices, the analysis of EEM in strained quantum wells becomes very much important. It appears that the

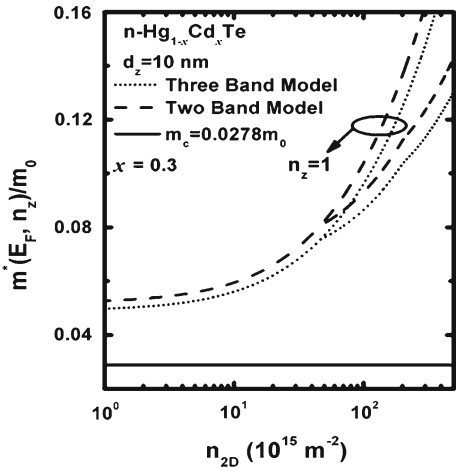

Fig. 1.14 Plot of the EEM as function of surface electron concentration in UFs of n-HgCdT

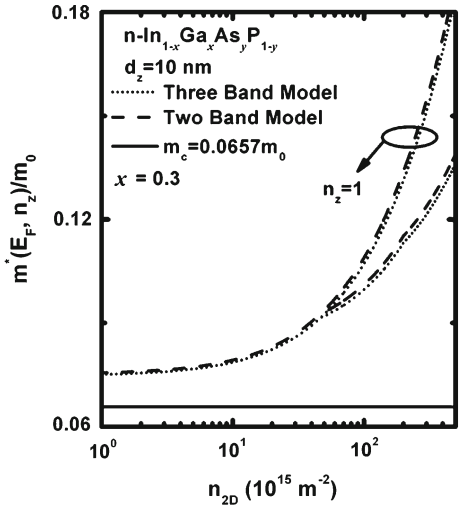

Fig. 1.15 Plot of the EEM as function of surface electron concentration in UFs of n-InGaAsP

compressive and tensile strain does not tend to modify the respective magnitude of the EEM in strained quantum wells of InSb. It should be noted that the EEM in Fig. 1.21 has been evaluated by considering the momentum matrix element $B_2 = 0.9\,\text{eVnm}$. This is a bulk value. However, an arbitrary increase in this geometry dependent parameter sufficiently reduces the EEM and thus finds extensive use in strained film transitors. In Chap. 8, we shall be presenting a much detailed explanation of the effect of uniaxial and biaxial strain on Si nanowires and the effect on energy band gap. The variation of the EEM in Ge has been exhibited in Fig. 1.22 as function of film thickness for the model of Cardona et al. The general trend of increase in the EEM has also been exhibited here at least 6 times the bulk value $\sqrt{m_1^* m_2^*}$ for three different carrier concentration levels.

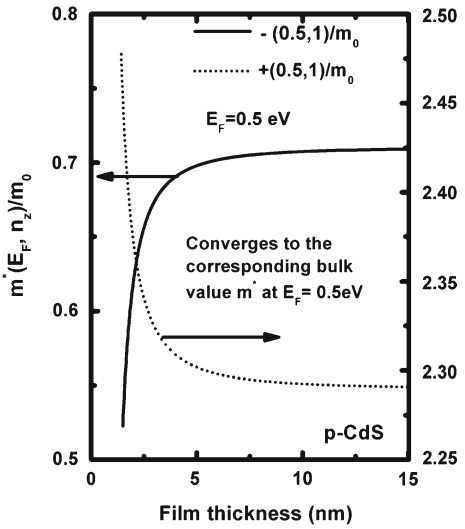

Fig. 1.16 Plot of the EEM as function of film thicknesss in UFs of p-CdS in two different conduction band valleys

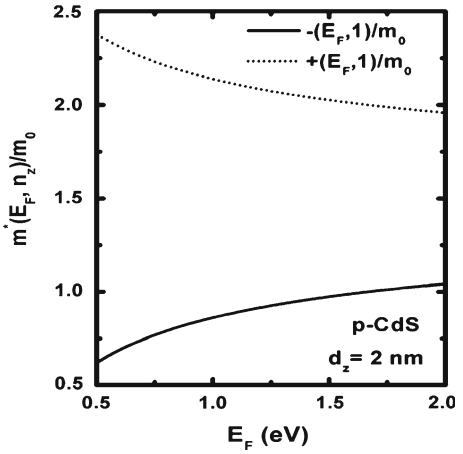

Fig. 1.17 Plot of the EEM as function of Fermi energy for all the cases of Fig. 1.16

We observe that considering the various subband levels, the EEM exhibits a step-functional decreasing dependence with increase in film thickness for UFs of all the single valley materials. The combined influence of the anisotropies of the energy band constants and the crystal-field splitting is to enhance the EEM as compared with the corresponding which is based on two band model of Kane in the whole range of thicknesses as considered in Fig. 1.1. The periodicity with respect to the film thickness is the same in both the cases and is invariant of the energy band constants.

The influence of quantum confinement is immediately apparent from Figs. 1.1, 1.2, 1.3, 1.4, 1.5, 1.6, 1.7 and 1.16, 1.18, 1.20, 1.21, 1.22 since the EEM depends

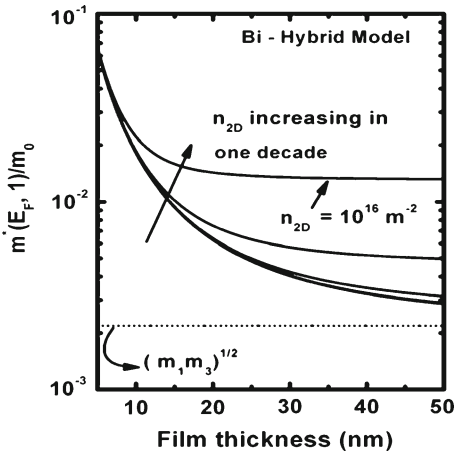

Fig. 1.18 Plot of the EEM as function of film thicknesss in UFs of Bismuth for different carrier concentration values using the Hybrid model

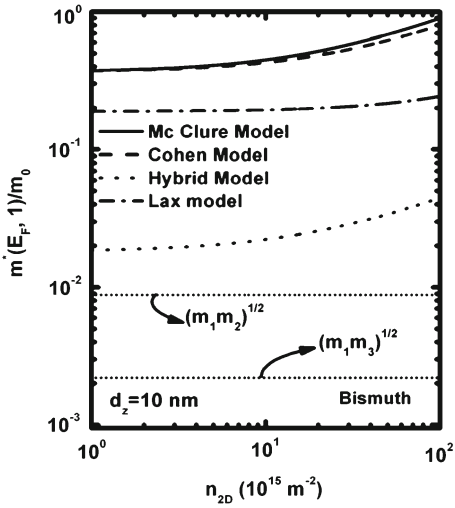

Fig. 1.19 Plot of the EEM at the lowest subband as function of surface electron coencentration in UFs of Bismuth using the Mc Clure, Cohen, Hybrid, and Lax energy band models

strongly on the thickness of the quantum-confined materials in contrast with the corresponding bulk specimens. The EEM changes with increasing carrier concentration suffering discontinuities with different numerical magnitudes. It appears from the aforementioned figures that the EEM exhibits spikes for particular values of film thickness which, in turn, depends on the particular band structure of the specific semiconductor. Moreover, the EEM from QWs of different compounds can be smaller than bulk specimens of the same materials having multi valley conduction band like in case of p-CdS, which is also a direct signature of quantum confinement. This effect of the discontinuity on the EEM will be less and less prominent with increasing film thickness. For bulk specimens of the same material, the EEM will be found to increase continuously with increasing electron degeneracy in a non-

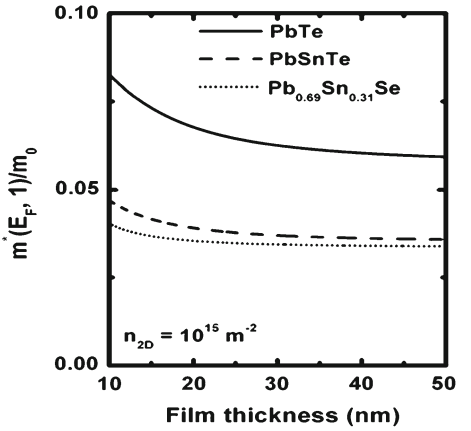

Fig. 1.20 Plot of the EEM at the lowest subband as function of film thickness in UFs of IV-VI materials

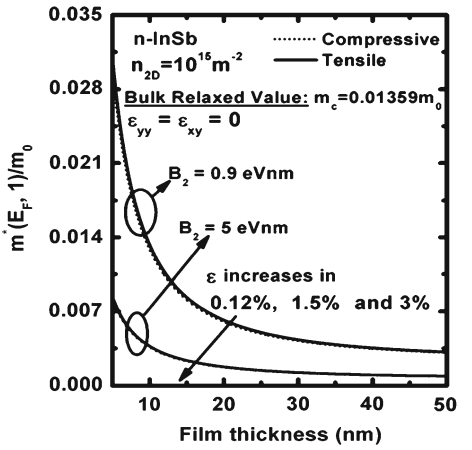

Fig. 1.21 Plot of the EEM at the lowest subband as function of film thickness in UFs of uniaxial strained InSb

oscillatory manner. The appearance of the discrete jumps in the respective figures is due to the redistribution of the electrons among the quantized energy levels when the size quantum number corresponding to the highest occupied level changes from one fixed value to the others.

With varying electron degeneracy, a change is reflected in the EEM through the redistribution of the electrons among the size-quantized levels. It may be noted that at the transition zone from one subband to another, the height of the peaks between any two subbands decreases with the increasing in the degree of quantum confinement and is clearly shown in the respective figures. It should be noted that although the EEM changes in various manners with all the variables as is evident from all the figures, the rates of variations are totally band-structure dependent.

It is imperative to state that the present investigation excludes the many-body, hot electron, broadening and the allied effects in the simplified theoretical formalism due to the absence of proper analytical techniques for including them for generalized

Table 1.1 The numerical values of the energy band constants of few materials

	Materials	Numerical values of the energy band constants
1	(a) The conduction electrons of n-cadmium germanium arsenide can be described by three types of band models	1. The values of the energy band constants in accordance with the generalized electron dispersion relation of nonlinear optical materials are as follows: $E_{g_0} = 0.57\,\text{eV}$, $\Delta_{\parallel} = 0.30\,\text{eV}$, $\Delta\perp = 0.36\,\text{eV}$, $m_{\parallel}^{*} = 0.034m_0$, $m_{\perp}^{*} = 0.039m_0$, $t = 4k$, $\delta = -0.21\,\text{eV}$, $g_v = 1$ [118, 119], $\varepsilon_{sc} = 18.4\varepsilon_0$ [120] (ε_{sc} and ε_0 are the permittivity of the semiconductor material and free space respectively) and W(electron affinity) = 4 eV [121, 122]
		2. In accordance with the three-band model of Kane the spectrum constants are given by $\Delta = \left(\Delta_{\parallel} + \Delta_{\perp}\right)/2 = 0.33\,\text{eV}$, $E_{g_0} = 0.57\,\text{eV}$, $m_c = \left(m_{\parallel}^{*} + m_{\perp}^{*}\right)/2 = 0.0365m_0$ and $\delta = 0\,\text{eV}$.
		3. In accordance with two-band model of Kane, the spectrum constants are given by $E_{g_0} = 0.57\,\text{eV}$ and $m_c = (m_{\parallel}^{*} + m_{\perp}^{*})/2 = 0.0365m_0$
	(b) The conduction electrons of n-cadmium arsenide can be described by three types of band models	1. The values of the energy band constants in accordance with the generalized electron dispersion relation of nonlinear optical materials are as follows $\left\|E_{g_0}\right\| = 0.095\,\text{eV}$, $\Delta_{\parallel} = 0.27\,\text{eV}$, $\Delta_{\perp} = 0.25\,\text{eV}$, $m_{\parallel}^{*} = 0.00697m_o$, $m_{\perp}^{*} = 0.013933m_0$, $T = 4K$, $\delta = 0.085\,\text{eV}$, $g_v = 1$ [118, 119] and $\varepsilon_{sc} = 16\varepsilon_0$ [121, 122]
		2. In accordance with the three-band model of Kane, the spectrum constants are given by $\Delta = (\Delta_{\parallel} + \Delta_{\perp})/2 = 0.26\,\text{eV}$, $\left\|E_{g_0}\right\| = 0.095\,\text{eV}$, $m_c = \left(m_{\parallel}^{*} + m_{\perp}^{*}\right)/2 = 0.0105m_0$ and $\delta = 0\,\text{eV}$
		3. In accordance with two-band model of Kane, the spectrum constants are given by $\left\|E_{g_0}\right\| = 0.095\,\text{eV}$, and $m_c = \left(m_{\parallel}^{*} + m_{\perp}^{*}\right)/2 = 0.0105m_0$
2	n-Indium arsenide	The values $E_{g_0} = 0.36\,\text{eV}$, $\Delta = 0.43\,\text{eV}$, $m_c = 0.026m_0$, $g_v = 1$, $\varepsilon_{sc} = 12.25\varepsilon_0$ [111] and $W = 5.06\,\text{eV}$ [123] are valid for three-band model of Kane
3	n-Gallium arsenide	The values $E_{g_0} = 1.55\,\text{eV}$, $\Delta = 0.35\,\text{eV}$, $m_c = 0.066m_0$, $g_v = 1$, $\varepsilon_{sc} = 12.9\varepsilon_0$ [111] and $W = 4.07\,\text{eV}$ [124] are valid for three-band model of Kane. The values $a_13 = -1.97 \times 10^{-37}\,\text{eV}m^4$ and $a_{15} = -2.3 \times 10^{-34}\,\text{eV}m^4$ [125] are valid for the Newson and Kurobe model [125]
4	n-Gallium aluminium arsenide	$E_{g_0} = (1.424 + 1.266x + 0.26x^2)\,\text{eV}$, $\Delta = (0.34 - 0.5x)\,\text{eV}$, $g_v = 1$, $m_c = (0.066 + 0.088x)m_0$, $\varepsilon_{sc} = [13.18 - 3.12x]\varepsilon_0$[1] and $W = (3.64 - 0.14x)\,\text{eV}$ [126]
5	n-Mercury cadmium telluride	$E_{g_0} = (-0.302 + 1.93x + 5.35 \times 10^{-4}(1 - 2x)T - 0.810x^2 + 0.832x^3)\,\text{eV}$, $\Delta = (0.63 + 0.24x - 0.27x^2)\,\text{eV}$, $m_c = 0.1m_0 Eg_0(\text{eV})^{-1}$, $g_v = 1$, $\varepsilon_{sc} = [20.262 - 14.812x + 5.22795x^2]\varepsilon_0$ [108] and $W = (4.23 - 0.183(E_{g_0} - 0.083))\,\text{eV}$ [127]
	n-Indium gallium arsenide	$E_{g_0} = (1.337 - 0.73y + 0.13y^2)\,\text{eV}$, $\delta = (0.114 + 0.26y - 0.22y^2)\,\text{eV}$

(continued)

Table 1.1 (continued)

	Materials	Numerical values of the energy band constants
6	Phosphide lattice matched to indium phosphide	$y = (0.1896-0.4052x)/(0.1896-0.0123x)$, $m_c = (0.08-0.039y)m_0$, $g_v = 1$, $\varepsilon_{sc} = [10.65+0.1320y]\varepsilon_0$ and [128] $W(x, y) = [5.06(1-x)y + 4.38(1-x)(1-y) + 3.64xy + 3.75\{x(1-y)\}]$eV
7	n-Indium antimonide	$E_{g_0} = 0.2352$ eV, $\Delta = 0.81$ eV, $m_c = 0.01359m_0$, $g_v = 1$, $\varepsilon_{sc} = 15.56\varepsilon_0$ [121, 122] and $W = 4.72$ eV [123]
8	n-Gallium antimonide	The values of $E_{g_0} = 0.81$ eV, $\Delta = 0.80$ eV, $p = 9.48 \times 10^{-10}$ eVm, $\bar{\zeta}_0 = -2.1$, $\bar{\nu}_0 = -1.49$, $\bar{\omega} = 0.42$, $g_v = 1$ [129] and [130] are valid for the model of Seiler et al. [129]
9	n-Cadmium sulphide	$m^*_{\parallel} = 0.7m_0$, $m^*_{\perp} = 1.5m_0$, $C_0 = 1.4\times10^{-8}$ eVm, $g_v = 1$ [121, 122], $\varepsilon_{sc} = 15.5\varepsilon_0$ [131] and $W = 4.5$ eV [123]
10	n-Lead telluride	The values $m_1^- = 0.070m_0$, $m_1^- = 0.54m_0$, $m_1^+ = 0.010m_0$, $m_1^+ = 1.4m_0$, $P_{\parallel} = 141$ meVnm, $P_{\perp} = 486$ meVnm, $E_{g_0} = 190meV$, $g_v = 4$ [121, 122], $\varepsilon_{sc} = 33\varepsilon_0$ [121, 122, 132] and $W = 4.6$ eV [133] are valid for the Dimmock model [134]. The values $m_1 = 0.0239m_0$,$m_2 = 0.024m_0$, $m'_2 = 0.31m_0$, $m_3 = 0.24m_0$ [135] are valid for the Cohen model [136–141].
11	Stressed n-indium antimonide	The values $m_c = 0.01359m_0$, $E_{g_0} = 0.081$ eV, $B_2 = 9 \times 10^{-10}$ eVm, $C_1 = 3$ eV, $C_2 = 2$ eV, $\bar{a}_0 = -10$ eV, $\bar{b}_0 = -1.7$ eV, $\bar{d}_0 = -4.4$ eV, $S_{xx} = 0.6\times10^{-3}(kbar)^{-1}$, $S_{yy} = 0.42\times10^{-3}(kbar)^{-1}$, $S_{zz} = 0.39 \times 10^{-3}(kbar)^{-1}$, $S_{xy} = 0.5 \times 10^{-3}(kbar)^{-1}$, $\varepsilon_{xx} = \sigma S_{xx}$, $\varepsilon_{yy} = \sigma Syy$, $\varepsilon_{zz} = \sigma S_{zz}$, $\varepsilon_{xy} = \sigma Sxy$, σ is the stress in kilobar, $g_v = 1$ [142] are valid for the model of Seiler et al. [142]
12	Bismuth	$E_{g_0} = 0.0153$ eV, $m_1 = 0.00194m_0$, $m_2 = 0.313m_0$, $m_3 = 0.00246m_0$, $m'_2 = 0.36m_0$, $g_v = 3$ [143, 144], $M_2 = 1.25m_0$, $M'_2 = 0.36m_0$ [145, 146] and $W = 4.34$ eV.
13	Mercury telluride	$m^*_v = 0.028m_0$, $g_v = 1$, $\varepsilon_{\infty} = 15.2\varepsilon_0$ [147] and $W = 5.5$ eV [148]
14	Platinum antimonide	For valence bands, along <100> direction, $\bar{\lambda}_0 = (0.02/4)$ eV, $\bar{l} = (-0.32/4)$ eV, $\bar{\nu} = (0.39/4)$ eV, $\bar{n} = (-0.65/4)$ eV, $\bar{a} = 0.643$ nm, $I = 0.30(\text{eV})^2$, $\bar{\delta}_0 = 0.02$ eV, $g_v = 6$ [151], $\varepsilon_{sc} = 30\varepsilon_0$ [149] and $\phi_w \approx 3.0$ eV [150, 151] For conduction bands, along <111> direction, $g_v = 8$ [149, 151], $\bar{\lambda}_0 = (0.33/4)$ eV, $\bar{l} = (1.09/4)$ eV, $\bar{\nu} = (0.17/4)$ eV and $\bar{n} = (0.22/4)$ eV
15	n-Gallium phosphide	$m^*_{\parallel} = 0.92m_0$, $m^*_{\perp} = 0.25m_0$, $k_0 = 1.7 \times 10^{15}m^{-1}$, $\lvert V_G\rvert = 0.21$ eV, $g_v = 6$ [152] and $W = 3.75$ eV [123]
16	Germanium	$E_{g_0} = 0.785$ eV, $m^*_{\parallel} = 1.57m_0$, $m^*_{\perp} = 0.0807m_0$ [123] and $W = 4.14$ eV [153],$g_v = 4$
17	Tellurium	The values $\psi_1 = 6.7 \times 10^{-16}meVm^2$, $\psi_2 = 4.2 \times 10^{-16}meVm^2$, $\psi_3 = 6 \times 10^{-8}$ meVm and $\psi_4 = (3.6 \times 10^{-8}$ meVm) [154–158] are valid for the model of Bouat et al. [154–158]

(continued)

Table 1.1 (continued)

	Materials	Numerical values of the energy band constants
18	Graphite	The values $\bar{\Delta} = -0.0002\,\text{eV}$, $\bar{\gamma}_1 = 0.392\,\text{eV}$, $\bar{\gamma}_5 = 0.194\,\text{eV}$, $c_6 = 0.674\,\text{nm}$, $\bar{\gamma}_2 = -0.019\,\text{eV}$, $a_6 = 0.246nm$, $\bar{\gamma}_0 = 3\,\text{eV}$, $\bar{\gamma}_4 = 0.193\,\text{eV}$, $\bar{\gamma}_3 = 0.21\,\text{eV}$ [159–163] and $W = 4.6\,\text{eV}$ [164–167] are valid for the model of Brandt et al. [159–163]
19	Lead germanium telluride	The values $g_v = 4$ [168] and $\phi_w \approx 6\,\text{eV}$ [169, 170] are valid for the model of Vassilev [208] as given by (R.1.18)
20	Cadmium antimonide	The values $a_1 = -32.3 \times 10^{-20}\,\text{eVm}^2$, $b_1 = -60.7 \times 10^{-20}\,\text{eVm}^2$, $a_2 = -16.3 \times 10^{-20}\,\text{eVm}^2$, $b_2 = -24.4 \times 10^{-20}\,\text{eVm}^2$, $a_3 = -91.9 \times 10^{-20}\,\text{eVm}^2$, $b_3 = -105 \times 10^{-20}\text{eVm}^2 A = 2.92 \times 10^{-10}\,\text{eVm}$, $B = -3.47 \times 10^{-10}\,\text{eVm}$, $G_3 = 1.3 \times 10^{-10}\,\text{eVm}$, $\Delta_3 = 0.070eV$ [171] and $\phi_w \approx 2\,\text{eV}$ [172–175]
21	Cadmium diphosphide	The values $\beta_1 = 8.6 \times 10^{-21}\,\text{eVm}^2$, $\beta_2 = 1.8 \times 10^{-21}\,\text{eVm}^2$, $\beta_4 = 0.0825\,\text{eV}$, $\beta_5 = -1.9 \times 10^{-19}\,\text{eVm}^2$ [176–183] and $\phi_w \approx 5\,\text{eV}$ [184] are valid for the model of Chuiko [190]
22	Zinc diphosphide	The values $\beta_1 = 8.7 \times 10^{-21}\,\text{eVm}^2$, $\beta_2 = 1.9 \times 10^{-21}\,\text{eVm}^2$, $\beta_4 = 0.0875\,\text{eV}$, $\beta_5 = -1.9 \times 10^{-19}\,\text{eVm}^2$ [176–183] and $W \approx 3.9\,\text{eV}$ [184] are valid for the model of Chuiko [190]
23	Bismuth telluride	The values $E_{g_0} = 0.145\,\text{eV}$, $\bar{\alpha}_{11} = 4.9$, $\bar{\alpha}_{22} = 5.92$, $\bar{\alpha}_{33} = 9.5$, $\bar{\alpha}_{23} = 4.22$, $g_v = 6$ [185–188] and $\phi_w = 5.3\,\text{eV}$ [189]
24	Carbon nanotube	The values $a_c = 0.144\,\text{nm}$ [190], $t_c = 2.7\,\text{eV}$ [191, 192], $\bar{r}_0 = 0.7nm$ [193] and $W = 3.2\,\text{eV}$ [96] are valid for graphene band structure realization of carbon nanotube [195]
25	Antimony	The values $\alpha_{11} = 16.7$, $\alpha_{22} = 5.98$, $\alpha_{33} = 11.61$, $\alpha_{23} = 7.54$ [195–197] and $W = 4.63\,\text{eV}$ are valid for the model of Ketterson [195–197]
26	Zinc selenide	$m_{c2} = 0.16m_0$, $\Delta = 0.42\,\text{eV}$, $E_{g_{02}} = 2.82\,\text{eV}$ [153] and $W = 3.2\,\text{eV}$ [198–200]
27	Lead selenide	$m_t^- = 0.23m_0$, $m_l^- = 0.32m_0$, $m_t^+ = 0.115m_0$, $m_l^+ = 0.303m_0$, $P_\parallel \approx 138\,\text{meVnm}$, $P_\perp = 471\,\text{meVnm}$, $E_{g_0} = 0.28\,\text{eV}$ [201], $\varepsilon_{sc} = 21.0\varepsilon_0$ [153] and $W = 4.2\,\text{eV}$ [202–206]

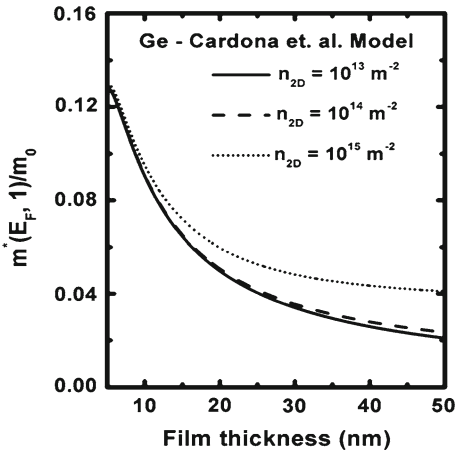

Fig. 1.22 Plot of the EEM at the lowest subband as function of film thickness in UFs of Ge

systems as considered here. We have also approximated the variation of value of the work function from its bulk value in the present system. Our simplified approach will be appropriate for the purpose of comparison when the methods of tackling the formidable problems after inclusion of the said effects for the generalized systems emerge. The results of this simplified approach get transformed to the well-known formulation of the EEM for wide gap materials having parabolic energy bands. This indirect test not only exhibits the mathematical compatibility of the formulation but also shows the fact that this simple analysis is a more generalized one, since one can obtain the corresponding results for materials having parabolic energy bands under certain limiting conditions from the present derivation. For the purpose of computer simulations for obtaining the plots of EEM versus various external variables, we have taken very low temperatures since the quantization effects are basically low temperature phenomena together with the fact that the temperature dependence of all the energy band constants of all the semiconductors and their nanostructures as considered in this chapter are not available in the literature. Our results as formulated in this chapter are valid for finite temperatures and are useful in comparing the results for temperature variations of EEM after the availability of the temperature dependences of such constants of various dispersion relations in this context. It is worth noting that the nature of the curves of EEM with various physical variables based on our simplified formulations as presented here would be useful to analyze the experimental results when they materialize. The inclusion of the said effects would certainly increase the accuracy of the results although the qualitative features of EEM would not change in the presence of the aforementioned effects.

It can be noted that on the basis of the dispersion relations of the various quantized structures as discussed above the low field carrier mobility, drive currents in field effect transistors, Fowler Nordhiem field current, the Debye screening length, the plasma frequency, the activity coefficient, the carrier contribution to the elastic constants, the diffusion coefficient of minority carriers, the third-order nonlinear optical

susceptibility, the heat capacity, the dia and paramagnetic susceptibilities and the various important DC/AC transport coefficients can be probed for all types of UFs as considered here. Thus, our theoretical formulation comprises the dispersion relation-dependent properties of various technologically important quantum-confined semiconductors having different band structures. We have not considered other types of compounds in order to keep the presentation concise and succinct. With different sets of energy band parameters, one gets different numerical values of the EEM. The nature of variations of the EEM as shown here would be similar for the other types of materials and the simplified analysis of this chapter exhibits the basic qualitative features of the EEM. The reader can also explore the EEM for the leftover 2D materials to enjoy the intricate computer programming and the 2D physics in this context. It may be noted that the basic aim of this chapter is not solely to demonstrate the influence of quantum confinement on the EEM for a wide class of quantized materials but also to formulate the appropriate carrier statistics in the most generalized form, since the transport and other phenomena in modern nano-structured devices having different band structures and the derivation of the expressions of many important carrier properties are based on the temperature-dependent carrier statistics in such systems.

For the purpose of condensed presentation, the carrier statistics and the EEM in different materials as considered in this chapter have been presented in Table 1.2.

1.4 Open Research Problems

The problems under these sections of this monograph are by far the most important part and a few open research problems from this chapter till the end are being presented. The numerical values of the energy band constants for various semiconductors are given in Table 1.1 for the related computer simulations.

R.1.1. Investigate the effective acceleration mass (EAM), density-of-state effective mass (DEM), concentration effective mass (CEM), conductivity effective mass (CoEM), Faraday rotation effective mass (FREM), and Optical effective mass (OEM) from all the bulk semiconductors whose respective dispersion relations of the carriers are given in this chapter.

R.1.2. Repeat R.1.1 for the bulk semiconductors whose respective dispersion relations of the carriers in the absence of any field are given below:

(a) The electron dispersion law in n-GaP can be written as [237]

$$E = \frac{\hbar^2 k_s^2}{2m_{||}^*} + \frac{\hbar^2 k_s^2}{2m_{\perp}^*} \mp \frac{\overline{\Delta}}{2} \pm \left[\left(\frac{\overline{\Delta}}{2}\right)^2 + P_1 k_z^2 + D_1 k_x^2 k_y^2\right]^{1/2} \tag{R1.1}$$

Table 1.2 The EEM and the electron statistics in ultrathin films of nonparabolic semiconductors

Type of materials	EEM	The electron statistics
1. Non-linear optical semiconductors	$m^*(E_{Fs},n_z)=\left(\frac{\hbar^2}{2}\right)[\psi_2(E_{Fs})]^{-2}\left[\psi_2(E_{Fs})\left\{\{\psi_1(E_{Fs})\}'-\{\psi_3(E_{Fs})\}'\left(\frac{n_z\pi}{d_z}\right)^2\right\}-\left\{\psi_1(E_{Fs})-\psi_3(E_{Fs})\left(\frac{n_z\pi}{d_z}\right)^2\right\}\{\psi_2(E_{Fs})\}'\right]$ (1.5)	$n_{2D}=\frac{g_v}{2\pi}\sum_{n_x=1}^{n_{xmax}}[T_{51}(E_{Fs},n_z)+T_{52}(E_{Fs},n_z)]$ (1.9)
2. III-V semiconductors i.		
(a) Three band model of Kane	$m^*(E_{Fs})=m_c\{I_{11}(E_{Fs})\}'$ (1.12)	$n_{2D}=\frac{m_c g_v}{\pi\hbar^2}\sum_{n_z=1}^{n_{zmax}}[T_{53}(E_{Fs},n_z)+T_{54}(E_{Fs},n_z)]$ (1.15)
(b) Two band model of Kane	$m^*(E_{Fs})=m_c(1+2\alpha E_{Fs})$ (1.18)	$n_{2D}=\frac{m_c k_B T g_v}{\pi\hbar^2}\sum_{n_z=1}^{n_{zmax}}\left[(1+2\alpha E_{n_{z_3}}F_0(\eta_{n_1})+2\alpha k_B T F_1(\eta_{n_1})\right]$ (1.21)
(c) Parabolic energy bands	$m^*(E_{Fs})=m_c$ (1.26)	
ii. Stillman et al.	$m^*(E_{Fs})=m_c\{I_{12}(E_{Fs})\}'$ (1.31)	$n_{2DT}=\frac{m_c k_b T g_v}{\pi\hbar^2}\sum_{n_z=1}^{n_{zmax}}F_0(\eta_{n_2})$ (1.27)
iii. Palik et al.	$m^*(E_{Fs})=m_c\{I_{13}(E_{Fs})\}'$ (1.38)	$n_{2D}=\frac{m_c g_v}{\pi\hbar^2}\sum_{n_z=1}^{n_{zmax}}\left[T_{55}(E_{Fs},n_z)+T_{56}(E_{Fs},n_z)\right]$ (1.34) $n_{2D}=\frac{m_c g_v}{\pi\hbar^2}\sum_{n_z=1}^{n_{zmax}}\left[T_{57}(E_{Fs},n_z)+T_{58}(E_{Fs},n_z)\right]$ (1.41)
3. II-VI semiconductors	$m^*(E_{Fs},n_z)=m_\perp^*\left[1\mp\frac{(\bar{\lambda}_o)}{\left[(\bar{\lambda}_o)^2-4a_o'b_o'\left(\frac{n_z\pi}{d_z}\right)^2+4a_o'E_{Fs}\right]^{1/2}}\right]$ (1.44)	$n_{2D}=\frac{g_v m_\perp^*}{\pi\hbar^2}\sum_{n_z=1}^{n_{z\max}}\left(E_{Fs}-E_{n_{z_5}}+\left(\bar{\lambda}\right)^2 m_\perp^*\hbar^{-2}\right)$ (1.48)

(continued)

Table 1.2 (continued)

Type of materials	EEM	The electron statistics
4. Bismuth		
i. McClure and Choi model	$m^*(E_{Fs}, n_z) = \left(\frac{2\hbar^2}{3\pi\sqrt{p_1}}\right)[R_3(E, n_z)]\Big\|_{E=E_{Fs}}$ (1.54)	$n_{2D}(E) = \left(\frac{2g_v}{3\pi^2\sqrt{p_1}}\right)\sum_{n_z=1}^{n_{max}}[\theta_1(E_{Fs}, n_z) + \theta_2(E_{Fs}, n_z)$ (1.57)
ii. Hybrid model	$m^*(E_{Fs}, n_y) = [\sqrt{m_1 m_3}]t'_{29}(E, n_y)$ (1.61)	$n_{2D}(E) = \frac{g_v\sqrt{m_1}m_3}{\pi\hbar^2}\sum_{n_y=1}^{n_{ymax}}\left[t_{29}(E_{Fs}, n_y) + t_{30}(E_{Fs}, n_y)\right]$ (1.64)
iii. Cohen model	$m^*(E_{Fs}, n_z) = \left(\frac{2\hbar^2}{3\pi\sqrt{p_1}}\right)\left[R_4(E, n_z)\right]\Big\|_{E=E_{Fs}}$ (1.68)	$n_{2D} = \left(\frac{2g_v}{3\pi^2\sqrt{p_1}}\right)\sum_{n_z=1}^{n_{zmax}}\left[\theta_3(E_{Fs}, n_z) + \theta_4(E_{Fs}, n_z)\right]$ (1.70)
iv. Lax model	$m^*(E_{Fs}) = \sqrt{m_1 m_2}(1 + 2\alpha E_{Fs})$ (1.73)	$n_{2D} = \frac{g_v\sqrt{m_1 m_2}k_B T}{\pi\hbar^2} \times \sum_{n_z=1}^{n_{zmax}}\left[(1 + 2\alpha E_{n_z 8})F_0(\eta_{y2}) + 2\alpha k_B T F_1(\eta_{y2})\right]$ (1.76)
v. Ellipsoidal parabolic model	$m^*(E_{Fs}) = \left(\sqrt{m_1 m_2}\right)$ (1.78)	$n_{2D} = \left[\frac{k_B T g_v\sqrt{m_1 m_2}}{\pi\hbar^2}\right]\sum_{n_z=1}^{n_{zmax}}F_0(\eta_{y_3})$ (1.81)
5. IV-VI semiconductors	$m^*(E, n_z) = \frac{\hbar^2}{2}[\theta_5(E, n_z)]\Big\|_{E=E_{Fs}}$ (1.94)	$n_{2D} = \frac{g_v}{2\pi}\sum_{n_z=1}^{n_{zmax}}[T_{59}(E_{Fs}, n_z) + T_{60}(E_{Fs}, n_z)]$ (1.97)
6. Stressed materials	$m^*(E_{Fs}, n_z) = \frac{\hbar^2}{2}[\theta_6(E, n_z)]\Big\|_{E=E_{Fs}}$ (1.101)	$n_{2D} = \frac{g_v}{2\pi}\sum_{n_z=1}^{n_{zmax}}[T_{61}(E_{Fs}, n_z) + T_{62}(E_{Fs}, n_z)]$ (1.104)

Table 1.2 (continued)

Type of materials	EEM	The electron statistics
7. Tellurium	$m^*(E_{Fs},n_z)=\frac{\hbar^2}{2}\left[t'_{40}(E,n_z)\right]\Big\vert_{E=E_{Fs}}$ (1.107)	$n_{2D}=\frac{g_v}{\pi}\sum_{n_z=1}^{n_{zmax}}[t_{40}(E_{Fs},n_z)+t_{41}(E_{Fs},n_z)]$ (1.110)
8. n-GaP	$m^*(E_{Fs},n_z)=\frac{\hbar^2}{2}t'_{42}(E_{Fs},n_z)$ (1.115)	$n_{2D}=\frac{g_v}{4\pi a^2}\sum_{n_z=1}^{n_{zmax}}\left[t_{42}(E_{Fs},n_z)+t_{43}(E_{Fs},n_z)\right]$ (1.117)
9. n type $PtSb_2$	$m^*(E_{Fs},n_z)=\frac{\hbar^2}{4A_9}t'_{44}(E_{Fs},n_z)$ (1.123)	$n_{2D}=\frac{g_v}{4\pi A_9}\sum_{n_z=1}^{n_{zmax}}[t_{44}(E_{Fs},n_z)+t_{45}(E_{Fs},n_z)]$ (1.126)
10. Bi_2Te_3	$m^*(E_{Fs})=\frac{m_0(1+2\overline{\alpha}E_{Fs})}{\sqrt{\overline{\alpha}_{22}\overline{\alpha}_{33}-4\overline{\alpha}_{23}^2}}$ (1.130)	$n_{2D}=\frac{k_BTg_v}{\pi\hbar^2}\left(\frac{m_0}{\sqrt{\overline{\alpha}_{22}\overline{\alpha}_{33}-4\overline{\alpha}_{23}{}^2}}\right)\sum_{n_z=1}^{n_{zmax}}[(1+2\alpha E_{n_z15})F_0(\eta_{n_n15})+2\alpha k_BTF_1(\eta_{n15})]$ (1.133)
11. n- Ge:		
i. Model by Cardona et al.	$m^*(E_{Fs},n_z)\equiv\sqrt{m_1^*m_2^*}\times\left[(1+2\alpha E_{Fs})-(2\alpha)\frac{\hbar^2}{2m_3^*}\left(\frac{n_z\pi}{d_z}\right)^2\right]$ (1.138)	$n_{2D}=\frac{4\sqrt{m_1^*m_2^*}k_BT}{\pi\hbar^2}\sum_{n_z=1}^{n_{zmax}}\times\left[(A_1(n_z)+2\alpha E_{n_z16})F_0(E_{n_z16})+2\alpha k_BTF_1(E_{n_z16})\right]$ (1.142)
ii. Model by Wang and Ressler	$m^*(E_{Fs,n_z})\equiv\sqrt{m_1^*m_2^*}\left[\{I_1(E_{Fs},n_z)\}'\right]$ (1.147)	$n_{2D}=\frac{4\sqrt{m_1^*m_2^*}}{\pi\hbar^2}\sum_{n_z=1}^{n_{zmax}}[t_{46}(E_{Fs},n_z)+t_{47}(E_{Fs},n_z)]$ (1.151)
12. n- GaSb	$m^*(E_{Fs})=m_c\{I_{36}(E_{Fs})\}'$ (1.155)	$n_{2D}=\left(\frac{m_cg_v}{\pi\hbar^2}\right)\sum_{n_z=1}^{n_{zmax}}[t_{55}(E_{Fs},n_z)+t_{56}(E_{Fs},n_z)]$ (1.158)

where, $\overline{\Delta} = 335\,\text{meV}$, $P_1 = 2 \times 10^{-10}\text{eVm}$, $D_1 = p_1 a_1$ and $a_1 = 5.4 \times 10^{-10}\text{m}$.

(b) In addition to the Cohen model, the dispersion relation for the conduction electrons for IV-VI semiconductors can also be described by the models of Bangert et al. [238] and Foley et al. [239], respectively.

(i) In accordance with Bangert et al. [238], the dispersion relation is given by

$$\Gamma(E) = F_1(E)k_s^2 + F_2(E)k_z^2 \tag{R1.2}$$

where, $\Gamma(E) = 2E$, $F_1(E) = \frac{R_1^2}{E+E_g} + \frac{S_1^2}{E+\Delta_c'} + \frac{Q_1^2}{E+E_g}$, $F_2(E) = \frac{2C_5^2}{E+E_g} + \frac{(S_1+Q_1)^2}{E+\Delta_c''}$ $R_1^2 = 2.3\times10^{-19}(\text{eVm})^2$, $C_5^2 = 0.83\times10^{-19}(\text{eVm})^2$, $Q_1^2 = 1.3R_1^2$, $S_1^2 = 4.6R_1^2$, $\Delta_c' = 3.07\,\text{eV}$, $\Delta_c'' = 3.28\,\text{eV}$ and $g_v = 4$. It may be noted that under the substitution $S_1 = 0$, $Q_1 = 0$, $R_1^2 \equiv \frac{\hbar^2 E_g}{m_\perp^*}$, $C_5^2 \equiv \frac{\hbar^2 E_g}{m_{\shortparallel}^*}$, (R1.2) assumes the form $E(1+\alpha E) = \frac{\hbar^2 k_s^2}{2m_\perp^*} + \frac{\hbar^2 k_z^2}{2m_\shortparallel^*}$ which is the simplified Lax model.

(ii) The carrier energy spectrum of IV-VI semiconductors in accordance with Foley et al. [239] can be written as

$$E + \frac{E_g}{2} = E_-(k) + \left[\left[E_+(k) + \frac{E_g}{2}\right]^2 + P_\perp^2 k_s^2 + P_\shortparallel^2 k_z^2\right]^{1/2} \tag{R1.3}$$

where, $E_+(k) = \frac{\hbar^2 k_s^2}{2m_\perp^+} + \frac{\hbar^2 k_z^2}{2m_\shortparallel^+}$, $E_-(k) = \frac{\hbar^2 k_s^2}{2m_\perp^-} + \frac{\hbar^2 k_z^2}{2m_\shortparallel^-}$ represents the contribution from the interaction of the conduction and the valance band edge states with the more distant bands and the free electron term, $\frac{1}{m_\perp^\pm} = \frac{1}{2}\left[\frac{1}{m_{tc}} \pm \frac{1}{m_{tc}}\right]$, $\frac{1}{m_\shortparallel^\pm} = \frac{1}{2}\left[\frac{1}{m_{lc}} \pm \frac{1}{m_{lv}}\right]$, For n-PbTe, $P_\perp = 4.61 \times 10^{-10}\,\text{eVm}$, $P_\shortparallel = 1.48 \times 10^{-10}\,\text{eVm}$, $\frac{m_0}{m_{tv}} = 10.36$, $\frac{m_0}{m_{tv}} = 0.75$, $\frac{m_0}{m_{tv}} = 11.36$, $\frac{m_0}{m_{lv}} = 1.20$ and $g_v = 4$.

(c) The hole energy spectrum of p-type zero-gap semiconductors (e.g. HgTe) is given by [240]

$$E = \frac{\hbar^2 k^2}{2m_v^*} + \frac{3e^2}{128\varepsilon_\infty}k - \left(\frac{2E_B}{\pi}\right)\ln\left|\frac{k}{k_0}\right| \tag{R1.4}$$

where m_v^* is the effective mass of the hole at the top of the valence band, ε_∞ is the semiconductor permittivity in the high frequency limit, $E_B \equiv \frac{m_0 e^2}{2\hbar^2\varepsilon_\infty^2}$ and $k_0 \equiv \frac{m_0 e^2}{\hbar^2\varepsilon_\infty}$.

(d) The conduction electrons of n-GaSb obey the following two dispersion relations:

(i) In accordance with the model of Seiler et al. [253]

$$E = \left[-\frac{E_g}{2} + \frac{E_g}{2}[1 + \alpha_4 k^2]^{1/2} + \frac{\bar{\varsigma}_0 \hbar^2 k^2}{2m_0} + \frac{\bar{\nu}_0 f_1(k)\hbar^2}{2m_0} \pm \frac{\bar{\omega}_0 f_2(k)\hbar^2}{2m_0} \right] \tag{R1.5}$$

where $\alpha_4 \equiv 4p^2(E_g + \frac{2}{3}\Delta)[E_g^2(E_g + \Delta)]^{-1}$, P is the isotropic momentum matrix element, $f_1(k) \equiv k^{-2}[k_x^2 k_y^2 + k_y^2 k_z^2 + k_z^2 k_x^2]$ represents the warping of the Fermi surface, $f_2(k) \equiv [\{k^2(k_x^2 k_y^2 + k_y^2 k_z^2 + k_z^2 k_x^2) - 9k_x^2 k_y^2 k_z^2\}^{1/2} k^{-1}]$ represents the inversion asymmetry splitting of the conduction band, and $\bar{\varsigma}_0$, $\bar{\nu}_0$, and $\bar{\omega}_0$ represent the constants of the electron spectrum in this case.

(ii) In accordance with the model of Zhang et al. [241]

$$E = [E_2^{(1)} + E_2^{(2)} K_{4,1}]k^2 + [E_4^{(1)} + E_4^{(2)} K_{4,1}]k^4 + k^6[E_6^{(1)} + E_6^{(2)} K_{4,1} + E_6^{(3)} K_{6,1}] \tag{R1.6}$$

where $K_{4,1} \equiv \frac{5}{4}\sqrt{21}\left[\frac{k_x^4 + k_y^4 + k_z^4}{k^4} - \frac{3}{5}\right]$,

$K_{6,1} \equiv \sqrt{\frac{639639}{32}}\left[\frac{k_x^2 k_y^2 k_z^2}{k^6} + \frac{1}{22}\left(\frac{k_x^4 + k_y^4 + k_z^4}{k^4} - \frac{3}{5}\right) - \frac{1}{105}\right]$, the coefficients are in eV, the values of k are $10\left(\frac{a}{2\pi}\right)$ times those of k in atomic units (α is the lattice constant), $E_2^{(1)} = 1.0239620$, $E_2^{(2)} = 0$, $E_4^{(1)} = -1.1320772$, $E_4^{(2)} = 0.05658$, $E_6^{(1)} = 1.1072073$, $E_6^{(2)} = -0.1134024$ and
$E_6^{(3)} = -0.0072275$.

(e) In addition to the well-known band models as discussed in this monograph, the conduction electrons of III-V semiconductors obey the following three dispersion relations:

(i) In accordance with the model of Rossler [242]

$$E = \frac{\hbar^2 k^2}{2m^*} + \bar{\alpha}_{10} k^4 + \bar{\beta}_{10}\left[k_x^2 k_y^2 + k_y^2 k_z^2 + k_z^2 k_x^2\right] \pm \bar{\gamma}_{10}\left[k^2(k_x^2 k_y^2 + k_y^2 k_z^2 + k_z^2 k_x^2) - 9k_x^2 k_y^2 k_z^2\right]^{1/2} \tag{R1.7}$$

where $\bar{\alpha}_{10} = \bar{\alpha}_{11} + \bar{\alpha}_{12} k$, $\bar{\beta}_{10} = \bar{\beta}_{11} + \bar{\beta}_{12} k$ and $\bar{\gamma}_{10} = \bar{\gamma}_{11} + \bar{\gamma}_{12} k$, in which, $\bar{\alpha}_{11} = -2132 \times 10^{-40}\,\text{eVm}^4$, $\bar{\alpha}_{12} = 9030 \times 10^{-50}\,\text{eVm}^5$, $\bar{\beta}_{11} = -2493 \times 10^{-40}\,\text{eVm}^4$, $\bar{\beta}_{12} = 12594 \times 10^{-50}\,\text{eVm}^5$, $\bar{\gamma}_{11} = 30 \times 10^{-30}\,\text{eVm}^3$ and $\bar{\gamma}_{12} = -154 \times 10^{-42}\,\text{eVm}^4$.

(ii) In accordance with Johnson and Dickey [243], the electron energy spectrum assumes the form

$$E = -\frac{E_g}{2} + \frac{\hbar^2 k^2}{2}\left[\frac{1}{m_0} + \frac{1}{m_{\gamma b}}\right] + \frac{E_g}{2}\left[1 + 4\frac{\hbar^2 k^2}{2m_c'}\frac{\bar{f}_1(E)}{E_g}\right]^{1/2} \tag{R1.8}$$

where, $\frac{m_0}{m_c'} \equiv P^2\left[\frac{\left(E_g+\frac{2\Delta}{3}\right)}{E_g(E_g+\Delta)}\right]$, $\bar{f}_1(E) \equiv \frac{(E_g)+\Delta)\left(E+E_g+\frac{2\Delta}{3}\right)}{\left(E_g+\frac{2\Delta}{3}\right)(E+E_g+\Delta)}$, $m_c' = 0.139m_0$ and $m_{\gamma b} = \left[\frac{1}{m_c'} - \frac{2}{m_0}\right]^{-1}$.

(iii) In accordance with Agafonov et al. [244], the electron energy spectrum can be written as

$$E = \frac{\bar{\eta} - E_g}{2}\left[1 - \frac{\hbar^2k^2}{2\bar{\eta}m^*}\left\{\frac{D\sqrt{3} - 3\bar{B}}{2\left(\frac{\hbar^2}{2m^*}\right)}\right\}\left[\frac{k_x^4 + k_y^4 + k_z^4}{k^4}\right]\right] \tag{R1.9}$$

where, $\bar{\eta} \equiv \left(E_g^2 + \frac{8}{3}P^2k^2\right)$ and $\bar{B} \equiv -21\frac{\bar{h}^2}{2m_0}$ and $D \equiv -40\left(\frac{\bar{h}^2}{2m_0}\right)$.

(f) The dispersion relation of the carriers in n-type $Pb_{1-x}Ga_x$Te with x=0.01 can be written [246] as

$$\left[E - 0.606k_s^2 - 0.0722k_z^2\right]\left[E + \bar{E}_g + 0.411k_s^2 + 0.0377k_z^2\right] = 0.23k_s^2 + 0.02k_z^2 \pm \left[0.06\bar{E}_g + 0.061k_s^2 + 0.0066k_z^2\right]k_s \tag{R1.10}$$

where, $\bar{E}_g(= 0.21\,\text{eV})$ is the energy gap for the transition point, the zero of the energy E is at the edge of the conduction band of the Γ point of the Brillouin zone and is measured positively upwards, $k_x, k_y,$ and k_z are in the units of $10^9\,\text{m}^{-1}$.

(g) The energy spectrum of the carriers in the two higher valence bands and the single lower valence band of Te can, respectively, be expressed as [245]

$$\bar{E} = A_{10}k_z^2 + B_{10}k_s^2 \pm \left[\Delta_{10}^2 + (\beta_{10}k_z)^2\right]^{1/2} \quad \text{and } \bar{E} = \Delta_{\parallel} + A_{10}k_z^2 + B_{10}k_s^2 \pm \beta_{10}k_z \tag{R1.11}$$

where $\bar{E}$ is the energy of the hole as measured from the top of the valence and within it, $A_{10} = 3.77 \times 10^{-19}\,\text{eVm}^2$, $B_{10} = 3.57 \times 10^{-19}\,\text{eVm}^2$, $\Delta_{10} = 0.628\,\text{eV}$, $(\beta_{10})^2 = 6 \times 10^-20(\text{eVm})^2$ and $\Delta_{\parallel} = 1004 \times 10^{-5}\,\text{eV}$ are the spectrum constants.

(h) The dispersion relation for the electrons in graphite can be written following Brandt [252] as

$$E = \frac{1}{2}[E_2 + E_3] \pm \left[\frac{1}{4}(E_2 - E_3)^2 + \eta_2^2k^2\right]^{1/2} \tag{R1.12}$$

where, $E_2 \equiv \bar{\Delta} - 2\bar{\gamma}_1\cos\phi_0 + 2\bar{\gamma}_5\cos^2\phi_0$, $\phi_0 \equiv \frac{c_6k_z}{2}$, $E_3 \equiv 2\bar{\gamma}_2\cos^2\phi_0$ and $\eta_2 \equiv \left(\frac{\sqrt{3}}{2}\right)a_6(\bar{\gamma}_0 + 2\bar{\gamma}_4\cos\phi_0)$ in which the band constants are $\bar{\Delta}, \bar{\gamma}_0, \bar{\gamma}_1, \bar{\gamma}_2, \bar{\gamma}_4, \bar{\gamma}_5, a_6$ and c_6 respectively.

(i) The dispersion relation of the conduction electrons in Antimony (Sb) in accordance with Ketterson [251] can be written as

$$2m_0E = \alpha_{11}P_x^2 + \alpha_{22}P_y^2 + \alpha_{33}P_z^2 + 2\alpha_{23}P_yP_z \tag{R1.13}$$

and

$$2m_0E = a_1P_x^2 + a_2P_y^2 + a_3P_z^2 + a_4P_yP_z \pm a_5P_xP_z \pm a_6P_xP_y \tag{R1.14}$$

where, $a_1 = \frac{1}{4}(\alpha_{11} + 3\alpha_{22}), a_2 = \frac{1}{4}(\alpha_{22} + 3\alpha_{11}), a_3 = \alpha_{33}, a_4 = \alpha_{33}, a_5 = \sqrt{3}$ and $a_6 = \sqrt{3}(\alpha_{22} - \alpha_{11})$ in which $\alpha_{11}, \alpha_{22}, \alpha_{33}$ and α_{23} are the system constants.

(j) The dispersion relation of the holes in p-InSb can be written in accordance with Cunningham [247] as

$$\bar{E} = c_4(1 + \gamma_4 f_4)k^2 \pm \frac{1}{3}[2\sqrt{2}\sqrt{c_4}\sqrt{16 + 5\gamma_4}\sqrt{E_4}g_4k] \tag{R1.15}$$

where $c_4 \equiv \frac{\hbar^2}{2m_0} + \theta_4, \theta_4 \equiv 4.7\frac{\hbar^2}{2m_0}, \gamma_4 \equiv \frac{b_4}{c_4}, b_4 \equiv \frac{3}{2}b_5 + 2\theta_4, b_5 \equiv 2.4\frac{\hbar^2}{2m_0}, f_4 \equiv \frac{1}{4}[\sin^2 2\theta + \sin^4\theta \sin^2 2\phi]$, θ is measured from the positive z-axis, ϕ is measured from positive x-axis, $g_4 \equiv \sin\theta\Big[\cos^2\theta + \frac{1}{4}sin^4\theta \sin^2 2\phi\Big]$ and $E_4 = 5 \times 10^{-4}$ eV.

(k) The energy spectrum of the valence bands of CuCl in accordance with Yekimov et al. [248] can be written as

$$E_h = (\gamma_6 - 2\gamma_7)\frac{\hbar^2k^2}{2m_0} \tag{R1.16}$$

and

$$E_{l,s} = (\gamma_6 + \gamma_7)\frac{\hbar^2k^2}{2m_0} - \frac{\Delta_1}{2} \pm \left[\frac{\Delta_1^2}{4} + \gamma_7\Delta_1\frac{\hbar^2k^2}{2m_0} + 9\left(\frac{\gamma_7\hbar^2k^2}{2m_0}\right)^2\right]^{1/2} \tag{R1.17}$$

where, $\gamma_6 = 0.53, \gamma_7 = 0.07, \Delta_1 = 70$ meV.

(l) In the presence of stress, χ_6 along <001> and <111> directions, the energy spectra of the holes in semiconductors having diamond structure valence bands can be respectively expressed following Roman [249] et al. as

$$E = A_6k^2 \pm \left[\bar{B}_7^2k^4 + \delta_6^2 + B_7\delta_6(2k_z^2 - k_s^2)\right]^{1/2} \tag{R1.18}$$

and

$$E = A_6 k^2 \pm \left[\bar{B}_7^2 k^4 + \delta_7^2 + \frac{D_6}{\sqrt{3}} \delta_7 (2k_z^2 - k_s^2) \right]^{1/2} \tag{R1.19}$$

where A_6, B_7, D_6, and C_6 are inverse mass band parameters in which $\delta_6 \equiv l_7(\bar{S}_{11} - \bar{S}_{12})\chi_6$, $\bar{S}_{ij}$ are the usual elastic compliance constants, $\bar{B}_7^2 \equiv \left(B_7^2 + \frac{c_6^2}{5} \right)$ and $\delta_7 \equiv \left(\frac{d_g S_{44}}{2\sqrt{3}} \right) \chi_6$. For gray tin, $d_g = -4.1\,\text{eV}$, $l_7 = -2.3\,\text{eV}$,
$A_6 = 19.2 \frac{\hbar^2}{2m_o}$, $B_7 = 26.3 \frac{\hbar^2}{2m_o}$, $D_6 = 31 \frac{\hbar^2}{2m_o}$ and $c_6^2 = -1112 \frac{\hbar^2}{2m_o}$.

(m) The dispersion relation of the carriers of cadmium and zinc diphosphides are given by [250]

$$E = \left[\beta_1 + \frac{\beta_2 \beta_3(k)}{8\beta_4} \right] k^2 \pm \left\{ \left[\beta_4 \beta_3(k) x \left(\beta_5 - \frac{\beta_2 \beta_3(k)}{8\beta_4} \right) k^2 \right] + 8\beta_4^2 \left(1 - \frac{\beta_3^2(k)}{4} \right) - \beta_2 \left(1 - \frac{\beta_3^2(k)}{4} \right) k^2 \right\}^{1/2} \tag{R1.20}$$

where $\beta_1, \beta_2, \beta_4$ and β_5 are system constants, and $\beta_3(k) = \frac{k_x^2 + k_y^2 - 2k_z^2}{k^2}$

R1.3. Investigate the EEM, EAM, DEM, CEM, CoEM, FREM, and OEM for ultrathin films, wires and dots of all the semiconductors as considered in R1.1 and R1.2, respectively.

R1.4. Investigate the same set of masses as defined in (R1.3) for bulk specimens of the heavily–doped semiconductors in the presences of Gaussian, exponential, Kane, Halperian, Lax and Bonch-Burevich types of Band tails [121, 121] for all systems whose unperturbed carrier energy spectra are defined in R1.1 and R1.2, respectively.

R1.5. Investigate the same set of masses as defined in (R1.3) for ultrathin films, wires, and dot of all the heavily doped semiconductors as considered in R1.4.

R1.6. Investigate the same set of masses as defined in (R1.3) for bulk specimens of the negative refractive index, organic, magnetic, and other advanced optical materials in the presence of an arbitrarily oriented alternating electric field.

R1.7. Investigate the same set of masses as defined in (R1.3) for ultrathin films, wires and dot of the negative refractive index, organic, magnetic and other advanced optical materials in the presence of an arbitrarily oriented alternating electric field.

R1.8. Investigate the same set of masses as defined in (R1.3) for the multiple ultrathin films, wires, and dots of semiconductors whose unperturbed carrier energy spectra are defined in R1.1, R1.2 and heavily doped semiconductors in the presences of Gaussian, exponential, Kane, Halperian, Lax, and Bonch-Burevich types of Band tails [121, 122] for all systems whose unperturbed carrier energy spectra are defined in the same problems respectively.

R1.9. Investigate the same set of masses as defined in (R1.3) for all the appropriate low-dimensional systems of this chapter in the presence of finite potential wells.

R1.10. Investigate the same set of masses as defined in (R1.3) for all the appropriate low-dimensional systems of this chapter in the presence of parabolic potential wells.

R1.11. Investigate the same set of masses as defined in (R1.3) for all the appropriate systems of this chapter forming quantum rings.

R1.12. Investigate the same set of masses as defined in (R1.3) for all the above appropriate problems in the presence of elliptical Hill and quantum square rings.

R1.13. Investigate the same set of masses as defined in (R1.3) for the appropriate accumulation layres for all the materials whose unperturbed carrier energy spectra are defined in R1.1 and R1.2, respectively.

R1.14. Investigate the same set of masses as defined in (R1.3) for parabolic cylindrical quantum dots in the presence of an arbitrarily oriented alternating electric field for all the materials whose unperturbed carrier energy spectra are defined in R1.1 and R1.2, respectively.

R1.15. Investigate the same set of masses as defined in (R1.3) for wedge shaped, cylindrical quantum dots of the negative refractive index, and other advanced optical materials in the presence of an arbitrarily oriented alternating electric field and non-uniform lightwaves.

R1.16. Investigate the same set of masses as defined in (R1.3) for triangular, cylindrical quantum dots of the negative refractive index, organic, magnetic and other advanced optical materials in the presence of an arbitrarily oriented alternating electric field in the presence of strain.

R1.17. Investigate the same set of masses as defined in (R1.3) for conical quantum dots of the negative refractive index, organic, magnetic, and other advanced optical materials in the presence of an arbitrarily oriented alternating electric field.

R1.18. (a) Investigate the same set of masses as defined in (R1.3) for conical quantum dots of the negative refractive index, organic, magnetic, and other advanced optical materials in the presence of an arbitrarily oriented alternating electric field considering many-body effects.
(b) Investigate all the appropriate problems of this chapter for a Dirac electron.
(c) Investigate all the appropriate problems of this chapter by including the many-body, image force, broadening and hot carrier effects respectively.

R1.19. Investigate all the appropriate problems of this chapter by removing all the mathematical approximations and establishing the respective appropriate uniqueness conditions.

References

1. S. Adachi, J. Appl. Phys. **58**, R11 (1985)
2. R. Dornhaus, G. Nimtz, *Springer Tracts in Modern Physics*, vol. 78 (Springer, Berlin, 1976), p. 1
3. W. Zawadzki, *Handbook of Semiconductor Physics*, vol. 1, ed. by W. Paul (North Holland, Amsterdam, 1982), p 719
4. I.M. Tsidilkovski, Cand. Thesis Leningrad University SSR (1955)
5. F.G. Bass, I.M. Tsidilkovski, Ivz. Acad. Nauk Azerb SSR **10**, 3 (1966)
6. B. Mitra, K.P. Ghatak, Phys. Scr. **40**, 776 (1989)
7. S.K. Biswas, A.R. Ghatak, A. Neogi, A. Sharma, S. Bhattacharya, K.P. Ghatak, Phys. E **36**, 163 (2007)
8. M. Mondal, S. Banik, K.P. Ghatak, J. Low Temp. Phys. **74**, 423 (1989)
9. K.P. Ghatak, S. Bhattacharya, H. Saikia, A. Sinha, J. Comp. Theor. Nanosci. **3**, 1 (2006)
10. K.P. Ghatak, S.N. Biswas, J. Vac. Sci. Tech. **7B**, 104 (1989)
11. P.K. Chakraborty, S. Choudhury, K.P. Ghatak, Phys. B **387**, 333 (2007)
12. S. Bhattacharya, S. Pahari, D.K. Basu, K.P. Ghatak, J. Comp. Theor. Nanosci. **3**, 280 (2006)
13. A. Sinha, A.K. Sharma, R. Barui, A.R. Ghatak, S. Bhattacharya, K.P. Ghatak, Phys. B **391**, 141 (2007)
14. S. Choudhury, L.J. Singh, K.P. Ghatak, Nanotechnology **15**, 180 (2004)
15. S. Chowdhary, L.J. Singh, K.P. Ghatak, Phys. B **B365**, 5 (2005)
16. P.K. Chakraborty, A. Sinha, S. Bhattacharya, K.P. Ghatak, Phys. B **390**, 325 (2007)
17. K.P. Ghatak, J.P. Banerjee, D. Bhattacharyya, Nanotechnology **7**, 110 (1996)
18. P.K. Chakraborty, B. Nag, K.P. Ghatak, J. Phys. Chem. Solids **64**, 2191 (2003)
19. K.P. Ghatak, J.P. Banerjee, B. Nag, J. Appl. Phys. **83**, 1420 (1998)
20. B. Nag, K.P. Ghatak, J. Phys. Chem. Solids **59**, 713 (1998)
21. P.K. Chakraborty, B. Nag, K.P. Ghatak, J. Phys. Chem. Solids **64**, 2191 (2003)
22. P.K. Chakraborty, K.P. Ghatak, Phys. Lett. **288**, 335 (2001)
23. P.K. Chakraborty, K.P. Ghatak, J. Phys. Chem. Sol. **62**, 1061 (2001)
24. P.K. Chakraborty, K.P. Ghatak, J. Phys. D Appl. Phys. **32**, 2438 (1999)
25. B. Nag, K.P. Ghatak, J. Phys. Chem. Solids **58**, 427 (1997)
26. K.P. Ghatak, D.K. Basu, B. Nag, J. Phys. Chem. Solids **58**, 133 (1997)
27. B. Nag, K.P. Ghatak, Nonlinear Opt. Quantum Opt. **19**, 1 (1998)
28. K.P. Ghatak, B. Nag, Nanostruct. Mat. **10**, 923 (1998)
29. K.P. Ghatak, B. Nag, D. Bhattacharyya, J. Low Temp. Phys. **14**, 1 (1995)
30. M. Mondal, K.P. Ghatak, Phys. Scr. **30**, 217 (1984)
31. M. Mondal, K.P. Ghatak, J. Magn. Magn. Mat. **62**, 115 (1986)
32. M. Mondal, K.P. Ghatak, Thin Solid Films **148**, 219 (1987)
33. K.P. Ghatak, A.K. Choudhury, S. Ghosh, A.N. Chakravarti, Appl. Phys. **23**, 241 (1980)
34. M. Mondal, N. Chattopadhyay, K.P. Ghatak, J. Low Temp, J. Low Temp. Phys. **73**, 321 (1988)
35. K.P. Ghatak, N. Chattopadhyay, M. Mondal, Appl. Phys. A **44**, 305 (1987)
36. B. Mitra, K.P. Ghatak, Phys. Lett. **135A**, 397 (1989)
37. B. Mitra, K.P. Ghatak, Solid State Electron. **32**, 810 (1989)
38. B. Mitra, K.P. Ghatak, Phys. Scr. **42**, 103 (1990)
39. K.P. Ghatak, M. Mondal, Z.F. Naturforschung **41A**, 821 (1986)
40. A.N. Chakravarti, A.K. Choudhury, K.P. Ghatak, S. Ghosh, A. Dhar, Appl. Phys. **25**, 105 (1981)
41. K.P. Ghatak, M. Mondal, Z.F. Phys. B **B69**, 471 (1988)
42. A.N. Chakravarti, K.P. Ghatak, K.K. Ghosh, S. Ghosh, A. Dhar, Z.F. Phys. B **47**, 149 (1982)
43. H.A. Lyden, Phys. Rev. **135**, A514 (1964)
44. E.D. Palik, G.B. Wright, in *Semiconductors and Semimetals*, ed. by R.K. Willardson, A.C. Beer, vol. 3. (Academic Press, New York, 1967), p. 421
45. H.L. Stomer, R. Dingle, A.C. Gossard, W. Wiegmann, M.D. Sturge, Solid State Commun. **29**, 705 (1979)

46. D.C. Rogers, J. Singleton, R.J. Nicholas, C.T. Foxon, in *High Magnetic Fields in Semiconductor Physics*, ed. by G. Landwehr, Springer Series in Solid-State Sciences, vol. 71. (Springer, Berlin, 1987), p. 223
47. M. Potemski, J.C. Maan, K. Pllog, G. Weimann, Solid State Commun. **75**, 185 (1990)
48. B.C. Cavenett, E.J. Pakulis, Phys. Rev. B **32**, 8449 (1985)
49. C. Wetzel, Al.L. Efros, A. Moll, B.K. Meyer, P. Omling, P. Sobkowicz. Phys. Rev. B **45**, 14052 (1992)
50. G. Hendorfer, M. Seto, H. Ruckser, W. Jantsch, M. Helm, G. Brunthaler, W. Jost, H. Obloh, K. Kohler, D.J. As, Phys. Rev. B **48**, 2328 (1993)
51. Q.X. Zhao, P.O. Holtz, B. Monemar, T. Lundstrom, J. Wallin, G. Landgren, Phys. Rev. B **48**(11), 890 (1983)
52. U. Ekenberg, Phys. Rev. B **36**, 6152 (1987)
53. H.I. Zhang, Phys. Rev. B **1**, 3450 (1970)
54. Y. Zhang, A. Mascarenhas, H.P. Xin, C.W. Tu, Phys. Rev. B **61**, 7479 (2000)
55. P.N. Hai, W.M. Chen, I.A. Buyanova, H.P. Xin, C.W. Tu, Appl. Phys. Lett. **77**, 1843 (2000)
56. J. Wu, W. Shan, W. Walukiewicz, K.M. Yu, J.W. Ager III, E.E. Haller, H.P. Xin, C.W. Tu, Phys. Rev. B **64**, 085320 (2001)
57. D.L. Young, D.L. Geisz, T.J. Coutts, Appl. Phys. Lett. **82**, 1236 (2003)
58. Y.J. Wang, X. Wei, Y. Zhang, A. Mascarenhas, H.P. Xin, Y.G. Hong, C.W. Tu, Appl. Phys. Lett. **82**, 4453 (2003)
59. F. Masia, A. Polimeni, G. Baldassarri Höger von Högersthal, M. Bissiri, M. Capizzi, P.J. Klar, W. Stolz, Appl. Phys. Lett. **82**, 4474 (2003)
60. A. Polimeni, G. Baldassarri Höger von Högersthal, F. Masia, A. Frova, M. Capizzi, S. Sanna, V. Fiorentini, P.J. Klar, W. Stolz, Phys. Rev. B **69**, 041201(R) (2004)
61. G. Baldassarri Höger von Högersthal, A. Polimeni, F. Masia, M. Bissiri, M. Capizzi, D. Gollub, M. Fischer, A. Forchel, Phys. Rev. B **67**, 233304 (2003)
62. M. Mondal, K.P. Ghatak, Phys. Lett. **131 A**, 529 (1988)
63. K.P. Ghatak, B. Mitra, Int. J. Electron. **72**, 541 (1992)
64. B. Mitra, A. Ghoshal, K.P. Ghatak, Nouvo Cimento D **12D**, 891 (1990)
65. K.P. Ghatak, S.N. Biswas, Nonlinear Opt. Quantum Opt. **4**, 347 (1993)
66. K.P. Ghatak, S.N. Biswas, Nonlinear Opt. Quantum Opt. **12**, 83 (1995)
67. V. Milanovic, D. Tjapkin, Phys. B and C **114**(3), 375(1982)
68. Z.S. Gribnikov, K. Hess, G.A. Kosinovsky, J. Appl. Phys. **7**(4), 1337 (1995)
69. M. Dyakonov, M.S. Shur, J. Appl. Phys. **84**(7), 3726 (1998)
70. K.P. Ghatak, A. Ghoshal, B. Mitra, Nouvo Cimento **14D**, 903 (1992)
71. K.P. Ghatak, A. Ghoshal, B. Mitra, Nouvo Cimento **13D**, 867 (1991)
72. B. Mitra, K.P. Ghatak, Solid State Electron. **32**, 177 (1989)
73. M. Mondal, N. Chattapadhyay, K.P. Ghatak, J. Low Temp. Phys. **66**, 131 (1987)
74. D.P. DiVincenzo, E.J. Mele, Phys. Rev. B **29**, 1685 (1984)
75. P. Perlin, E. Litwin-Staszewska, B. Suchanek, W. Knap, J. Camassel, T. Suski, R. Piotrzkowski, I. Grzegory, S. Porowski, E. Kaminska, J.C. Chervin, Appl. Phys. Lett. **68**, 1114 (1996)
76. G.E. Smith, Phys. Rev. Lett. **9**, 487 (1962)
77. D. Schneider, D. Rurup, A. Plichta, H.-U. Grubert, A. Schlachetzki, K. Hansen, Z. Phys. B **95**, 281 (1994)
78. F. Masia, G. Pettinari, A. Polimeni, M. Felici, A. Miriametro, M. Capizzi, A. Lindsay, S.B. Healy, E.P. O'Reilly, A. Cristofoli, G. Bais, M. Piccin, S. Rubini, F. Martelli, A. Franciosi, P.J. Klar, K. Volz, W. Stolz, Phys. Rev. B **73**, 073201 (2006)
79. V.K. Arora, H. Jeafarian, Phys. Rev. B **13**, 4457 (1976)
80. S.E. Ostapov, V.V. Zhikharevich, V.G. Deibuk, Semicond. Phys. Quantum Electron. Optoelectron. **9**, 29 (2006)
81. M.J. Aubin, L.G. Caron, J.-P. Jay- Gerin, Phys. Rev. B **15**, 3872 (1977)
82. S.L. Sewall, R.R. Cooney, P. Kambhampati, Appl. Phys. Lett. **94**, 243116 (2009)

83. K. Tanaka, N. Kotera, in *20th International Conference on Indium Phosphide and Related Materials*, Versailles, France, 25–29 May 2008, pp. 1–4
84. M. Singh, P.R. Wallace, S.D. Jog, J. Erushanov, J. Phys. Chem. Solids **45**, 409 (1984)
85. W. Zawadski, Adv. Phys. **23**, 435 (1974)
86. P.M. Petroff, A.C. Gossard, W. Wiegmann, Appl. Phys. Lett. **45**, 620 (1984)
87. J.M. Gaines, P.M. Petroff, H. Kroemar, R.J. Simes, R.S. Geels, J.H. English, J. Vac. Sci. Technol. B **6**, 1378 (1988)
88. J. Cilbert, P.M. Petroff, G.J. Dolan, S.J. Pearton, A.C. Gossard, J.H. English, Appl. Phys. Lett. **49**, 1275 (1986)
89. T. Fujui, H. Saito, Appl. Phys. Lett. **50**, 824 (1987)
90. H. Sasaki, Jpn. J. Appl. Phys. **19**, 94 (1980)
91. P.M. Petroff, A.C. Gossard, R.A. Logan, W. Weigmann, Appl. Phys. Lett. **41**, 635 (1982)
92. H. Temkin, G.J. Dolan, M.B. Panish, S.N.G. Chu, Appl. Phys. Lett. **50**, 413 (1988)
93. I. Miller, A. Miller, A. Shahar, U. Koren, P.J. Corvini, Appl. Phys. Lett. **54**, 188 (1989)
94. L.L. Chang, H. Esaki, C.A. Chang, L. Esaki, Phys. Rev. Lett. **38**, 1489 (1977)
95. K. Less, M.S. Shur, J.J. Drunnond, H. Morkoc, IEEE Trans. Electron. Devices **ED-30**, 07 (1983)
96. G. Bastard, *Wave Mechanics Applied to Semiconductor Heterostructures* (Halsted, Les Ulis, Les Editions de Physique, New York, 1988)
97. M.J. Kelly, *Low dimensional semiconductors: materials, physics, technology, devices* (Oxford University Press, Oxford, 1995)
98. C. Weisbuch, B. Vinter, *Quantum Semiconductor Structures* (Boston Academic Press, Boston, 1991)
99. N.T. Linch, Festkorperprobleme **23**, 27 (1985)
100. D.R. Sciferes, C. Lindstrom, R.D. Burnham, W. Streifer, T.L. Paoli, Electron. Lett. **19**, 170 (1983)
101. P.M. Solomon, Proc. IEEE **70**, 489 (1982)
102. T.E. Schlesinger, T. Kuech, Appl. Phys. Lett. **49**, 519 (1986)
103. D. Kasemet, C.S. Hong, N.B. Patel, P.D. Dapkus, Appl. Phys. Lett. **41**, 912 (1982)
104. K. Woodbridge, P. Blood, E.D. Pletcher, P.J. Hulyer, Appl. Phys. Lett. **45**, 16 (1984)
105. S. Tarucha, H.O. Okamoto, Appl. Phys. Lett. **45**, 16 (1984)
106. H. Heiblum, D.C. Thomas, C.M. Knoedler, M.I. Nathan, Appl. Phys. Lett. **47**, 1105 (1985)
107. O. Aina, M. Mattingly, F.Y. Juan, P.K. Bhattacharyya, Appl. Phys. Lett. **50**, 43 (1987)
108. I. Suemune, L.A. Coldren, IEEE J. Quant. Electron. **24**, 1178 (1988)
109. D.A.B. Miller, D.S. Chemla, T.C. Damen, J.H. Wood, A.C. Burrus, A.C. Gossard, W. Weigmann, IEEE J. Quant. Electron. **21**, 1462 (1985)
110. J.W. Rowe, J.L. Shay, Phys. Rev. B **3**, 451 (1973)
111. H. Kildal, Phys. Rev. B **10**, 5082 (1974)
112. J. Bodnar, in *Proceedings of the International Conference on Physics of Narrow-gap Semiconductors* (Polish Science Publishers, Warsaw, 1978)
113. G.P. Chuiko, N.N. Chuiko, Sov. Phys. Semicond. **15**, 739 (1981)
114. K.P. Ghatak, S.N. Biswas, Proc. SPIE **1484**, 149 (1991)
115. A. Rogalski, J. Alloys Comp. **371**, 53 (2004)
116. A. Baumgartner, A. Chaggar, A. Patanè, L. Eaves, M. Henini, Appl. Phys. Lett. **92**, 091121 (2008)
117. J. Devenson, R. Teissier, O. Cathabard, A.N. Baranov, Proc. SPIE **6909**, 69090U (2008)
118. B.S. Passmore, J. Wu, M.O. Manasreh, G.J. Salamo, Appl. Phys. Lett. **91**, 233508 (2007)
119. M. Mikhailova, N. Stoyanov, I. Andreev, B. Zhurtanov, S. Kizhaev, E. Kunitsyna, K. Salikhov, Y. Yakovlev, Proc. SPIE **6585**, 658526 (2007)
120. W. Kruppa, J.B. Boos, B.R. Bennett, N.A. Papanicolaou, D. Park, R. Bass, Electron. Lett. **42**, 688 (2006)
121. E.O. Kane, in *Semiconductors and Semimetals*, vol. 1, ed. by R.K. Willardson, A.C. Beer (Academic Press, New York, 1966), p. 75
122. B.R. Nag, *Electron Transport in Compound Semiconductors* (Springer, Heidelberg, 1980)

123. G.E. Stillman, C.M. Wolfe, J.O. Dimmock, in *Semiconductors and Semimetals*, vol. 12, ed. by R.K. Willardon, A.C. Beer (Academic Press, New York, 1977), p. 169
124. D.J. Newson, A. Karobe, Semicond. Sci. Tech. **3**, 786 (1988)
125. E.D. Palik, G.S. Picus, S. Teither, R.E. Wallis, Phys. Rev. **122**, 475 (1961)
126. P.Y. Lu, C.H. Wung, C.M. Williams, S.N.G. Chu, C.M. Stiles, Appl. Phys. Lett. **49**, 1372 (1986)
127. N.R. Taskar, I.B. Bhat, K.K. Prat, D. Terry, H. Ehasani, S.K. Ghandhi, J. Vac. Sci. Tech. **7A**, 281 (1989)
128. F. Koch, *Springer Series in Solid States Sciences* (Springer, Germany, 1984)
129. L.R. Tomasetta, H.D. Law, R.C. Eden, I. Reyhimy, K. Nakano, IEEE J. Quant. Electron. **14**, 800 (1978)
130. T. Yamato, K. Sakai, S. Akiba, Y. Suematsu, IEEE J. Quantum Electron. **14**, 95 (1978)
131. T.P. Pearsall, B.I. Miller, R.J. Capik, Appl. Phys. Lett. **28**, 499 (1976)
132. M.A. Washington, R.E. Nahory, M.A. Pollack, E.D. Beeke, Appl. Phys. Lett. **33**, 854 (1978)
133. M.I. Timmons, S.M. Bedair, R.J. Markunas, J.A. Hutchby, in *Proceedings of the 16th IEEE Photovoltaic Specialist Conference* (IEEE, San Diego, California 666, 1982)
134. J.A. Zapien, Y.K. Liu, Y.Y. Shan, H. Tang, C.S. Lee, S.T. Lee, Appl. Phys. Lett. **90**, 213114 (2007)
135. M. Park, Proc. SPIE **2524**, 142 (1995)
136. S.-G. Hur, E.T. -Kim, J. H. -Lee, G.H. -Kim, S.G. -Yoon, Electrochem. Solid-State Lett. **11**, H176 (2008)
137. H. Kroemer, Rev. Mod. Phys. **73**, 783 (2001)
138. T. Nguyen Duy, J. Meslage, G. Pichard, J. Crys. Growth **72**, 490 (1985)
139. T. Aramoto, F. Adurodija, Y. Nishiyama, T. Arita, A. Hanafusa, K. Omura, A. Morita, Solar Energy Mater. Solar Cells **75**, 211 (2003)
140. H.B. Barber, J. Electron. Mater. **25**, 1232 (1996)
141. S. Taniguchi, T. Hino, S. Itoh, K. Nakano, N. Nakayama, A. Ishibashi, M. Ikeda, Electron. Lett. **32**, 552 (1996)
142. J.J. Hopfield, J. Appl. Phys. **32**, 2277 (1961)
143. R.V. Belosludov, A.A. Farajian, H. Mizuseki, K. Miki, Y. Kawazoe, Phys. Rev. B **75**, 113411 (2007)
144. J. Heremans, C.M. Thrush, Y.-M Lin, S. Cronin, Z. Zhang, M.S. Dresselhaus, J.F. Mansfield, Phys. Rev. B **61**, 2921 (2000)
145. D. Shoenberg, Proc. R. Soc. (London) **170**, 341 (1939)
146. B. Abeles, S. Meiboom, Phys. Rev. **101**, 544 (1956)
147. B. Lax, J.G. Mavroides, H.J. Zieger, R.J. Keyes, Phys. Rev. Lett. **5**, 241 (1960)
148. Y.-H. Kao, Phys. Rev. **129**, 1122 (1963)
149. R.J. Dinger, A.W. Lawson, Phys. Rev. B **3**, 253 (1971)
150. J.F. Koch, J.D. Jensen, Phys. Rev. **184**, 643 (1969)
151. M.H. Cohen, Phys. Rev. **121**, 387 (1961)
152. S. Takaoka, H. Kawamura, K. Murase, S. Takano, Phys. Rev. B **13**, 1428 (1976)
153. J.W. McClure, K.H. Choi, Solid State Commun. **21**, 1015 (1977)
154. G.P. Agrawal, N.K. Dutta, *Semicond. Lasers* (Van Nostrand Reinhold, New York, 1993)
155. S. Chatterjee, U. Pal, Opt. Eng. (Bellingham), **32**, 2923 (1993)
156. T.K. Chaudhuri, Int. J. Energy Res. **16**, 481 (1992)
157. J.H. Dughaish, Phys. B **322**, 205 (2002)
158. C. Wood, Rep. Prog. Phys. **51**, 459 (1988)
159. K.-F. Hsu, S. Loo, F. Guo, W. Chen, J.S. Dyck, C. Uher, T. Hogan, E.K. Polychroniadis, M.G. Kanatzidis, Science **303**, 818 (2004)
160. J. Androulakis, K.F. Hsu, R. Pcionek, H. Kong, C. Uher, J.J. D'Angelo, A. Downey, T. Hogan, M.G. Kanatzidis, Adv. Mater. **18**, 1170 (2006)
161. P.F.P. Poudeu, J.D'Angelo, A.D. Downey, J.L. Short, T.P. Hogan, M.G. Kanatzidis, Angew. Chem. Int. Ed. **45**, 3835 (2006)

162. P.F. Poudeu, J. D'Angelo, H. Kong, A. Downey, J.L. Short, R. Pcionek, T.P. Hogan, C. Uher, M.G. Kanatzidis, J. Am. Chem. Soc. **128**, 14347 (2006)
163. J.R. Sootsman, R.J. Pcionek, H. Kong, C. Uher, M.G. Kanatzidis, Chem. Mater. **18**, 4993 (2006)
164. A.J. Mountvala, G. Abowitz, J. Am. Ceram. Soc. **48**, 651 (1965)
165. E.I. Rogacheva, I.M. Krivulkin, O.N. Nashchekina, AYu. Sipatov, V.A. Volobuev, M.S. Dresselhaus, Appl. Phys. Lett. **78**, 3238 (2001)
166. H.S. Lee, B. Cheong, T.S. Lee, K.S. Lee, W.M. Kim, J.W. Lee, S.H. Cho, J.Y. Huh, Appl. Phys. Lett. **85**, 2782 (2004)
167. K. Kishimoto, M. Tsukamoto, T. Koyanagi, J. Appl. Phys. **92**, 5331 (2002)
168. E.I. Rogacheva, O.N. Nashchekina, S.N. Grigorov, M.A. Us, M.S. Dresselhaus, S.B. Cronin, Nanotechnology **14**, 53 (2003)
169. E.I. Rogacheva, O.N. Nashchekina, A.V. Meriuts, S.G. Lyubchenko, M.S. Dresselhaus, G. Dresselhaus, Appl. Phys. Lett. **86**, 063103 (2005)
170. E.I. Rogacheva, S.N. Grigorov, O.N. Nashchekina, T.V. Tavrina, S.G. Lyubchenko, AYu. Sipatov, V.V. Volobuev, A.G. Fedorov, M.S. Dresselhaus, Thin Solid Bodies **493**, 41 (2005)
171. X. Qiu, Y. Lou, A.C.S. Samia, A. Devadoss, J.D. Burgess, S. Dayal, C. Burda, Angew. Chem. Int. Ed. **44**, 5855 (2005)
172. C. Wang, G. Zhang, S. Fan, Y. Li, J. Phys. Chem. Solids **62**, 1957 (2001)
173. B. Poudel, W.Z. Wang, D.Z. Wang, J.Y. Huang, Z.F. Ren, J. Nanosci. Nanotechnol. **6**, 1050 (2006)
174. B. Zhang, J. He, T.M. Tritt, Appl. Phys. Lett. **88**, 043119 (2006)
175. W. Heiss, H. Groiss, E. Kaufmann, G. Hesser, M. Böberl, G. Springholz, F. Schäffler, K. Koike, H. Harada, M. Yano, Appl. Phys. Lett. **88**, 192109 (2006)
176. B.A. Akimov, V.A. Bogoyavlenskiy, L.I. Ryabova, V.N. Vasil'kov, Phys. Rev. B **61**, 16045 (2000)
177. Ya. A. Ugai, A.M. Samoilov, M.K. Sharov, O.B. Yatsenko, B.A. Akimov, Inorg. Mater. **38**, 12 (2002)
178. Ya. A. Ugai, A.M. Samoilov, S.A. Buchnev, Yu. V. Synorov, M.K. Sharov, Inorg. Mater. **38**, 450 (2002)
179. A.M. Samoilov, S.A. Buchnev, YuV Synorov, B.L. Agapov, A.M. Khoviv. Inorg. Mater. **39**, 1132 (2003)
180. A.M. Samoilov, S.A. Buchnev, E.A. Dolgopolova, YuV Synorov, A.M. Khoviv, Inorg. Mater. **40**, 349 (2004)
181. H. Murakami, W. Hattori, R. Aoki, Phys. C **269**, 83 (1996)
182. H. Murakami, W. Hattori, Y. Mizomata, R. Aoki, Phys. C **273**, 41 (1996)
183. H. Murakami, R. Aoki, K. Sakai, Thin Solid Bodies **27**, 343 (1999)
184. B.A. Volkov, L.I. Ryabova, D.R. Khokhlov, Phys. Usp. **45**, 819 (2002), and references therein
185. F. Hüe, M. Hÿtch, H. Bender, F. Houdellier, A. Claverie, Phys. Rev. Lett. **100**, 156602 (2008)
186. S. Banerjee, K.A. Shore, C.J. Mitchell, J.L. Sly, M. Missous, IEE Proc. Circuits Devices Syst. **152**, 497 (2005)
187. M. Razeghi, A. Evans, S. Slivken, J.S. Yu, J.G. Zheng, V.P. Dravid, Proc. SPIE **5840**, 54 (2005)
188. R.A. Stradling, Semicond. Sci. Technol. **6**, C52 (1991)
189. P.K. Weimer, Proc. IEEE **52**, 608 (1964)
190. G. Ribakovs, A.A. Gundjian, IEEE J. Quant. Electron. **QE-14**, 42 (1978)
191. S.K. Dey, J. Vac. Sci. Technol. **10**, 227 (1973)
192. S.J. Lynch, Thin Solid Bodies **102**, 47 (1983)
193. V.V. Kudzin, V.S. Kulakov, D.R. Pape', S.V. Kulakov, V.V. Molotok, IEEE. Ultrason. Symp. **1**, 749 (1997)
194. F. Hatami, V. Lordi, J.S. Harris, H. Kostial, W.T. Masselink, J. Appl. Phys. **97**, 096106 (2005)
195. B.W. Wessels, J. Electrochem. Soc. **122**, 402 (1975)
196. D.W.L. Tolfree, J. Sci. Instrum. **41**, 788 (1964)
197. P.B. Hart, Proc. IEEE **61**, 880 (1973)

198. M.A. Hines, G.D. Scholes, Adv. Mater. **15**, 1844 (2003)
199. C.A. Wang, R.K. Huang, D.A. Shiau, M.K. Connors, P.G. Murphy, P.W. O'Brien, A.C. Anderson, D.M. DePoy, G. Nichols, M.N. Palmisiano, Appl. Phys. Lett. **83**, 1286 (2003)
200. C.W. Hitchcock, R.J. Gutmann, J.M. Borrego, I.B. Bhat, G.W. Charache, IEEE Trans. Electron. Devices **46**, 2154 (1999)
201. H.J. Goldsmid, R.W. Douglas, Br. J. Appl. Phys. **5**, 386 (1954)
202. F.D. Rosi, B. Abeles, R.V. Jensen, J. Phys. Chem. Sol. **10**, 191 (1959)
203. T.M. Tritt (ed.), *Semiconductors and Semimetals*, vol. 69, 70 and 71: Recent Trends in Thermoelectric Materials Research I, II and III (Academic Press, New York, 2000)
204. D.M. Rowe (ed.), *CRC Handbook of Thermoelectrics* (CRC Press, Boca Raton, 1995)
205. D.M. Rowe, C.M. Bhandari, *Modern Thermoelectrics* (Reston Publishing Company, Virginia, 1983)
206. D.M. Rowe (ed.), *Thermoelectrics Handbook: Macro to Nano* (CRC Press, Boca Raton, 2006)
207. H. Choi, M. Chang, M. Jo, S.J. Jung, H. Hwang, Electrochem. Solid-State Lett. **11**, H154 (2008)
208. S. Cova, M. Ghioni, A. Lacaita, C. Samori, F. Zappa, Appl. Opt. **35**, 1956 (1996)
209. H.W.H. Lee, B.R. Taylor, S.M. Kauzlarich, Nonlinear Optics: Materials, Fundamentals, and Applications (Technical Digest, 12, 2000)
210. E. Brundermann, U. Heugen, A. Bergner, R. Schiwon, G.W. Schwaab, S. Ebbinghaus, D.R. Chamberlin, E.E. Haller, M. Havenith, IN *29th International Conference on Infrared and Millimeter Waves and 12th International Conference on Terahertz, Electronics*, vol 283 (2004)
211. A.N. Baranov, T.I. Voronina, N.S. Zimogorova, L.M. Kauskaya, Y.P. Yakoviev, Sov. Phys. Semicond. **19**, 1676 (1985)
212. M. Yano, Y. Suzuki, T. Ishii, Y. Matsushima, M. Kimata, Jpn. J. Appl. Phys. **17**, 2091 (1978)
213. F.S. Yuang, Y.K. Su, N.Y. Li, Jpn. J. Appl. Phys. **30**, 207 (1991)
214. F.S. Yuang, Y.K. Su, N.Y. Li, K.J. Gan, J. Appl. Phys. **68**, 6383 (1990)
215. Y.K. Su, S.M. Chen, J. Appl. Phys. **73**, 8349 (1993)
216. S.K. Haywood, A.B. Henriques, N.J. Mason, R.J. Nicholas, P.J. Walker, Semicond. Sci. Technol. **3**, 315 (1988)
217. M. Abramowitz, I.A. Stegun, *Handbook of Mathematical Functions* (Dover Publications, New York, 1965)
218. J.S. Blakemore, *Semiconductor Statistics* (Dover Publications, New York, 1987)
219. K.P. Ghatak, S. Bhattacharya, S.K. Biswas, A. Dey, A.K. Dasgupta, Phys. Scr. **75**, 820 (2007)
220. K.P. Ghatak, S. Bhattachaya, D. De, *Einstein Relation in Compound Semiconductors and Nanostructures*, Springer Series in Material Sciences, vol. 116 (Springer, Germany, 2009)
221. J.O. Dimmock, in *The Physics of Semimetals and Narrowgap Semiconductors*, ed. by D.L. Carter, R.T. Bates (Pergamon Press, Oxford, 1971)
222. D.G. Seiler, B.D. Bajaj, A.E. Stephens, Phys. Rev. B **16**, 2822 (1977)
223. A.V. Germaneko, G.M. Minkov, Phys. Stat. Sol. (b) **184**, 9 (1994)
224. G.L. Bir, G.E. Pikus, *Symmetry and Strain -Induced effects in Semiconductors* (Nauka, Russia, 1972)
225. M. Mondal, K.P. Ghatak, Phys. Stat. Sol. (b) **135**, K21 (1986)
226. J. Bouat, J.C. Thuillier, Surf. Sci. **73**, 528 (1978)
227. G.J. Rees, Physics of Compounds, in *Proceedings of the 13th International Conference* ed. by F.G. Fumi (North Holland Company, 1976), p. 1166
228. P.R. Emtage, Phys. Rev. **138**, A246 (1965)
229. M. Stordeur, W. Kuhnberger, Phys. Stat. Sol. (b) **69**, 377 (1975)
230. D.R. Lovett, *Semimetals and Narrow-Bandgap Semiconductor* (Pion Limited, UK, 1977)
231. H. Kohler, Phys. Stat. Sol. (b) **74**, 591 (1976)
232. M. Cardona, W. Paul, H. Brooks Helv, Acta Phys. **33**, 329 (1960)
233. A.F. Gibson in *Proceeding of International School of Physics, ENRICO FERMI, course XIII*, ed. by R.A. Smith (Academic Press, New York, 1963), p. 171
234. C.C. Wang, N.W. Ressler, Phys. Rev. **2**, 1827 (1970)
235. M. Zalazny, Phys. B **124**, 352 (1984)

236. P.C. Mathur, S. Jain, Phys. Rev. **19**, 1359 (1979)
237. E.L. Ivchenko, G.E. Pikus Sov, Phys. Semicond. **13**, 579 (1979)
238. E. Bangert, P. Kastner, Phys. Stat. Sol (b) **61**, 503 (1974)
239. G.M.T. Foley, P.N. Langenberg, Phys. Rev. B **15B**, 4850 (1977)
240. V.I. Ivanov-Omskii, ASh Mekhtisev, S.A. Rustambekova, E.N. Ukraintsev, Phys. Stat. Sol. (b) **119**, 159 (1983)
241. H.I. Zhang, Phys. Rev. B **1**, 3450 (1970)
242. U. Rossler, Solid State Commun. **49**, 943 (1984)
243. J. Johnson, D.H. Dickey, Phys. Rev. **1**, 2676 (1970)
244. V.G. Agafonov, P.M. Valov, B.S. Ryvkin, I.D. Yarashetskin, Sov. Phys. Semiconduct. **12**, 1182 (1978)
245. L.A. Vassilev, Phys. State sol(b), **121**, 203 (1984)
246. N.S. Averkiev, V.M. Asnin, A.A. Bakun, A.M. Danishevskii, E.L. Ivchenko, G.E. Pikus, A.A. Rogachev, Sov. Phys. Semicond. **18**, (1984) pp. 379, 402
247. R.W. Cunningham, Phys. Rev. **167**, 761 (1968)
248. A.I. Yekimov, A.A. Onushchenko, A.G. Plyukhin, AI.L. Efros, J. Expt. Theor. Phys. **88**, 1490 (1985)
249. B.J. Roman, A.W. Ewald, Phys. Rev. **B5**, 3914 (1972)
250. G.P. Chuiko, Sov. Phys. Semiconduct. **19**(12), 1381 (1985)
251. J.B. Ketterson, Phys. Rev. **129**, 18 (1963)
252. N.B. Brandt, V.N. Davydov, V.A. Kulbachinskii, O.M. Nikitina, Sov. Phys. Sol. Stat. **29**, 1014 (1987)
253. D.G. Seiler, W.M. Beeker, L.M. Roth, Phys. Rev. **1**, 764 (1970)

http://www.springer.com/978-3-642-31247-2

Effective Electron Mass in Low-Dimensional Semiconductors

Bhattacharya, S.; Ghatak, K.P.

2013, XXIV, 536 p., Hardcover
ISBN: 978-3-642-31247-2